



**Pacific Northwest**  
NATIONAL LABORATORY

*Proudly Operated by Battelle Since 1965*

# Alternative Conceptual Models of the Subsurface at WMA C

March 2017

ML Rockhold  
ZF Zhang  
Y-J Bott



Prepared for the U.S. Department of Energy  
under Contract DE-AC05-76RL01830

## DISCLAIMER

This report was prepared as an account of work sponsored by an agency of the United States Government. Neither the United States Government nor any agency thereof, nor Battelle Memorial Institute, nor any of their employees, makes **any warranty, express or implied, or assumes any legal liability or responsibility for the accuracy, completeness, or usefulness of any information, apparatus, product, or process disclosed, or represents that its use would not infringe privately owned rights.** Reference herein to any specific commercial product, process, or service by trade name, trademark, manufacturer, or otherwise does not necessarily constitute or imply its endorsement, recommendation, or favoring by the United States Government or any agency thereof, or Battelle Memorial Institute. The views and opinions of authors expressed herein do not necessarily state or reflect those of the United States Government or any agency thereof.

PACIFIC NORTHWEST NATIONAL LABORATORY  
*operated by*  
BATTELLE  
*for the*  
UNITED STATES DEPARTMENT OF ENERGY  
*under Contract DE-AC05-76RL01830*

Printed in the United States of America

Available to DOE and DOE contractors from the  
Office of Scientific and Technical Information,  
P.O. Box 62, Oak Ridge, TN 37831-0062;  
ph: (865) 576-8401  
fax: (865) 576-5728  
email: [reports@adonis.osti.gov](mailto:reports@adonis.osti.gov)

Available to the public from the National Technical Information Service  
5301 Shawnee Rd., Alexandria, VA 22312  
ph: (800) 553-NTIS (6847)  
email: [orders@ntis.gov](mailto:orders@ntis.gov) <<http://www.ntis.gov/about/form.aspx>>  
Online ordering: <http://www.ntis.gov>



This document was printed on recycled paper.

(8/2010)

# **Alternative Conceptual Models of the Subsurface at WMA C**

ML Rockhold  
ZF Zhang  
Y-J Bott

March 2017

Prepared for  
the U.S. Department of Energy  
under Contract DE-AC05-76RL01830

Pacific Northwest National Laboratory  
Richland, Washington 99352



## Abstract

This report describes the development and application of alternative conceptual models that examine the effects of heterogeneity on water flow and Tc-99 transport in the subsurface for Waste Management Area (WMA) C. The heterogeneous models considered herein are alternatives to a base case model developed by the tank farm operations and closure contractor (WRPS) that is being used in a performance assessment (PA) of WMA C. The base case model uses an equivalent homogeneous medium (EHM) modeling approach in which effective parameters for equivalent homogeneous porous media are estimated for major hydro-stratigraphic units. The alternative models consider heterogeneity at smaller facies and model grid block scales.

The purpose of this report is to illustrate the potential impacts of heterogeneity and differences in interpretation of site characterization data on model parameterization and prediction of contaminant transport from past leaks and losses and residual tank waste releases in the subsurface for WMA C. Selected site characterization and monitoring data were used to develop the alternative conceptual models. The alternative models are consistent with available data, but differ in the types of data that are used, and how the data are used to infer model features and associated parameters. The alternative conceptual models were implemented with eSTOMP, a parallel version of the STOMP simulator. Simulations were performed using the alternative conceptual models and results were compared to simulation results generated using the EHM base case model.

Simulations of releases from tank waste residuals and past tank waste losses were performed using transport of Tc-99 from tank C-105, with Tc-99 being modeled as a conservative tracer. Simulation results generated using the EHM-based PA model, two stochastic realizations of a facies-based model, and one stochastic realization of a model developed using field-measured water content data, yield similar water content and saturation distributions. For tank residual simulations, predicted times for Tc-99 to reach peak concentrations in groundwater 100-m down-gradient of the WMA C fence-line are similar for all cases, ranging from year 3519 (1499 years after closure) for facies realization 003, to year 3692 (1672 years after closure) for the theta-based realization. Simulated peak concentrations range from 18.9 pCi/L for the theta-based realization, to 19.9 pCi/L for the EHM-based PA model. All cases yield predicted peak concentrations that are a factor of 45 or more below the maximum contaminant level (MCL) of 900 pCi/L for Tc-99 promulgated by the Environmental Protection Agency. For the past tank waste loss simulations, predicted times for Tc-99 to reach peak concentrations in groundwater 100-m down-gradient of the WMA C fence-line are also similar for all cases, ranging from year 2008 for facies realization 003 to year 2019 for the theta-based realization. Peak simulated concentrations ranged from 4690 pCi/L for the theta-based realization to 6850 pCi/L for the Facies003 case. All simulation cases yielded predicted peak concentrations that are a factor of 5.2 or more above the MCL for Tc-99.



## **Acknowledgments**

This work was performed in support of the Waste Management Area C Tank Closure Project led by Washington River Protection Solutions for the U.S. Department of Energy, Office of River Protection. We thank members of the PA modeling team: Bill McMahon (CHRPC) for providing STOMP input files for a WMA C base case and Arun Wahi (INTERA) for sharing his compilation of water content data from WMA C. We also thank Vicky Freedman (PNNL) for the technical review of this document, and Matt Wilburn (PNNL) for editorial assistance. Finally, we gratefully acknowledge Mike Connelly (TEC-GEO, Inc.) for providing a geologic framework model of WMA C and other supporting information, and Marcel Bergeron (WRPS) for his support of this work.



## Acronyms and Abbreviations

CHPRC	CH2M Hill Plateau Remediation Company
EHM	equivalent homogeneous medium
IDF	Integrated Disposal Facility
IFRC	Integrated Field Research Center
PA	performance assessment
PTF	pedotransfer function
SST	single-shell tank
WMA	Waste Management Area
WRPS	Washington River Protection Solutions



# Contents

Abstract.....	iii
Acknowledgments.....	v
Acronyms and Abbreviations .....	vii
Contents .....	ix
Figures .....	x
Tables.....	xii
1.0 Introduction .....	1.1
2.0 Engineered Features .....	2.1
3.0 Characterization and Monitoring Data .....	3.1
3.1 Physical Properties .....	3.3
3.1.1 Grain Size Distribution Data .....	3.3
3.1.2 Water Content Data.....	3.7
3.2 Hydraulic Properties.....	3.9
3.3 Geochemical Properties.....	3.10
4.0 Model Setup and Parameterization.....	4.1
4.1 Geologic Framework.....	4.1
4.2 Initial Conditions.....	4.3
4.3 Boundary Conditions.....	4.4
4.4 Source Terms .....	4.6
4.4.1 Considerations for Tank Waste Residual Releases .....	4.6
4.4.2 Considerations for Past Tank Waste Leaks and Losses .....	4.7
4.5 Parameterization.....	4.7
4.5.1 Pedotransfer Functions for Water Retention Parameters .....	4.7
4.5.2 Hydraulic Conductivity .....	4.9
4.5.3 Parameter Adjustments .....	4.10
4.5.4 Scaling.....	4.17
4.5.5 Parameterization of Facies Models .....	4.20
4.6 Overview of Conceptual Models.....	4.21
5.0 Simulation Results.....	5.1
5.1 Simulations of Releases from Tank Residuals .....	5.1
5.2 Simulations of Past Tank Waste Releases.....	5.5
6.0 Summary and Conclusions .....	6.1
7.0 References .....	7.1
Appendix A Geostatistical Analysis of Sediment Moisture Content Data from WMA C.....	A.1

# Figures

Figure 1.1. Map of the Hanford Site showing the location of the 200 East Area on the Central Plateau. ....	1.3
Figure 1.2. Locations of tank farms on Hanford’s Central Plateau (after Connelly et al. 2014) .....	1.4
Figure 2.1. Map showing placement of tanks, diversion boxes, pipelines, and a catch tank in the WMA C tank farm (after Connelly et al. 2014). ....	2.2
Figure 3.1. Map showing plan view outline of WMA C with some borehole, groundwater well, and dry well locations and lines of cross section (after Brown et al. 2006). ....	3.1
Figure 3.2. Generalized stratigraphic cross-sections through WMA C corresponding to the lines of cross-section shown in Figure 3.1 (after Brown et al. 2006). ....	3.2
Figure 3.3. Plan view (large rectangle) of the WMA C model domain showing outline of WMA C, tanks in both WMA C and in the A-AX tank farms (open circles), and borehole or well locations for which physical property data are available.....	3.3
Figure 3.4. Grain size distribution data for a sediment sample from the ROCSAN database. ....	3.4
Figure 3.5. Volumetric water content data from selected deep boreholes at WMA C. ....	3.8
Figure 3.6. Volumetric water content data from four boreholes at the AX tank farm. ....	3.9
Figure 3.7. Volumetric water content data from four boreholes at the A tank farm. ....	3.10
Figure 4.1. Stacked surfaces representing the tops of geologic units underlying WMA C (after Connelly et al. 2014). ....	4.2
Figure 4.2. Plan view of top of STOMP model domain showing spatial discretization of model grid, outlines of tanks in WMA C, A-AX tank farms, and points representing locations where grain size data are available.....	4.3
Figure 4.3. Aerial photograph of the area around WMA C and A–AX tank farms showing variable land surface conditions. ....	4.5
Figure 4.4. Correlation functions for grain size distribution metrics and van Genuchten (1980) model water retention parameters for sediment from the IDF, Sisson and Lu, and IFRC sites at Hanford. Coefficients of determination for the $\theta_s$ , $\theta_r$ , $\alpha$ , and $n$ regression relationships are 0.395, 0.322, 0.228, and 0.563.....	4.9
Figure 4.5. Analytical solution results for 1-D steady vertical flow using PTF-based hydraulic parameters (top), and adjusted parameters (bottom). Symbols represent data from Brown et al. (2006). The dashed line shows theoretical soil moisture tension results for zero flux conditions. ....	4.15
Figure 4.6. Water retention (WRC) and unsaturated hydraulic conductivity (K(h)) curves generated with parameters developed from PTFs using grain size distribution metrics, and parameters adjusted to provide better matches to water content and soil moisture tension data from Brown et al. (2006). Horizontal lines represent different recharge rates. ....	4.16
Figure 4.7. Reference water retention curve for unit H2 and scaled curves required to obtain the given values of water content at the reference soil moisture tension. ....	4.19
Figure 4.8. Soil moisture tension and water content profiles computed using a steady-state analytical solution and data from Brown et al. (2006). ....	4.20
Figure 4.9. Cutaway view showing material regions for the PA base case model (top) and one realization of a lithofacies model (bottom) for WMA C. ....	4.23

Figure 4.10. Zoomed image of one water content realization (001) used for parameterization of the WMA C model domain. The vertical elevation extent shown is 95-210 m. ....	4.24
Figure 5.1. Oblique cutaway views of moisture content distributions at year 2020 for the four conceptual models of WMA C tank residual. ....	5.1
Figure 5.2. Oblique cutaway views of the distributions of aqueous Tc-99 from C-105 at year 3280 for the four conceptual models of WMA C tank residual. ....	5.2
Figure 5.3. Oblique cutaway views of the distributions of aqueous Tc-99 from C-105 at year 3680 for the four conceptual models of WMA C tank residual. ....	5.3
Figure 5.4. Flux-averaged concentrations in the top 5 m of the unconfined aquifer at different locations along a plane located 100-m down-gradient of the WMA C fence line for the simulations of tank residuals. PoC refers to points of calculation used in RPP-ENV-58782, Rev A Draft.....	5.4
Figure 5.5. Oblique cutaway views of moisture content distributions at year 1980 for the four conceptual models of WMA C past tank releases. ....	5.6
Figure 5.6. Oblique cutaway views of the distributions of aqueous Tc-99 from C-105 at year 1980 for the four conceptual models of WMA C past tank releases. ....	5.7
Figure 5.7. Oblique cutaway views of the distributions of aqueous Tc-99 from C-105 at year 2020 for the four conceptual models of WMA C past tank releases. ....	5.8
Figure 5.8. Flux-averaged concentrations in the top 5 m of the unconfined aquifer at different locations along a plane located 100-m down-gradient of the WMA C fence line for the four conceptual models of WMA C past tank releases. PoC refers to points of calculation used in RPP-ENV-58782, Rev A draft. (Note that the distances in the direction parallel to the fence line of these PoCs are not the same as those used in the simulations of tank residual in Fig. 5.4). ....	5.9

## Tables

Table 3.1.	Summary of sediment samples with grain size data available from wells near WMA C .....	3.6
Table 3.2.	Average and median of geometric mean grain diameters $d_g$ (mm) and $\sigma_g$ values for different geologic units at WMA C. ....	3.7
Table 4.1.	PTF-based estimates of van Genuchten (1980) model water retention parameters, vertical saturated hydraulic conductivity, $K_{szz}$ , and pore-interaction term, $\ell_{zz}$ , for the major hydrostratigraphic units underlying WMA C, and adjusted parameter estimates fit to field data from Brown et al. (2006). ....	4.12
Table 4.2	Reference hydraulic parameters for water content-based parameterization of WMA C model .....	4.18
Table 4.3	Hydraulic parameters for facies-based parameterization of WMA C models .....	4.21
Table 5.1	Flux-averaged peak concentrations and arrival time in the top 5 m of the unconfined aquifer at different locations along a plane located 100-m down-gradient of the WMA C fence line for simulations of tank residuals. PoC refers to points of calculation used in RPP-ENV-58782, Rev A Draft. ....	5.5
Table 5.2	Flux-averaged peak concentrations and arrival time in the top 7.5 m of the unconfined aquifer at different locations along a plane located 100-m down-gradient of the WMA C fence line for simulations of past tank releases. PoC refers to points of calculation used in RPP-ENV-58782, Rev A Draft. (Note that the distances in the direction parallel to the fence line of these PoCs are not the same as those used in the simulations of tank residual in Table 5.1). ....	5.10

# 1.0 Introduction

WMA C is one of 12 tank farms within seven WMAs (A-AX, B-BX-BY, C, S-SX, T, TX-TY, and U) at Hanford (Figures 1.1 and 1.2). These WMAs contain 149 single-shell tanks (SSTs) and ancillary equipment that were built at the Hanford Site between 1943 and 1964. Mixed radioactive and chemical wastes resulting from nuclear weapons production and fuel fabrication activities are or were temporarily stored in these tanks. The SSTs have exceeded their design life and leaks have been documented for some of these tanks and ancillary equipment. Tank waste retrieval operations and transfer of some of the wastes to newer double-shell tanks has been performed. Waste retrieval operations are ongoing and a waste treatment plant is under construction. The treated and stabilized wastes will ultimately be disposed in a permanent disposal facility and the Hanford tank farms will eventually be closed.

Planning and permitting for closure of WMA C and other Hanford tanks farms requires performance assessments to evaluate the long-term impacts on human health and the environment. The performance assessment for WMA C is being used by the U.S. Department of Energy Office of River Protection to evaluate closure of WMA C under federal requirements, and forthcoming state-approved closure plans and permits in accordance with the Hanford Federal Facility Agreement and Consent Order Action Plan (Ecology et al. 1989, Appendix I). The scope of the final performance assessment for WMA C will include evaluation of human health and environmental impacts from radioactive and hazardous chemical and dangerous waste constituents contained in both residual wastes left in the tanks and ancillary equipment at closure, and contaminated soils impacted by past leaks and releases of wastes during historical operations of WMA C.

Performance and risk assessment for waste management decisions at Hanford require the development and application of numerical flow and transport models. These models must be parameterized based on available site characterization and monitoring data. Data sparsity and associated uncertainty have resulted in the use of models based primarily on major stratigraphy inferred from borehole geologic and geophysical logs. During previous WMA C workshops, questions were raised as to the possible impact of heterogeneity in the vadose zone on contaminant transport. While an EHM model, based on the distribution of soil texture and upscaled (effective) properties within previously recognized hydrogeologic units was employed for the base case analysis in the PA, some heterogeneous alternative model representations are in the process of being evaluated. The purpose of the work performed for this investigation was to determine if representing heterogeneity at finer scales within the vadose zone region of the modeled domains might produce results that are significantly different than those obtained for the PA base case analysis.

Support was provided during the PA scoping process on the agreed use of alternative models to represent and evaluate the effect of alternative conceptual model interpretations of various features seen in the subsurface on flow and contaminant transport at WMA C. As a result, multiple interpretations of available site characterization and monitoring data have been developed and are being evaluated by U.S. Department of Energy Office of River Protection and the tank farm operations and closure contractor, Washington River Protection Solutions (WRPS), as a part of the PA effort. This report documents the development and implementation of some alternative heterogeneous representations of the subsurface beneath WMA C.

Washington River Protection Solutions (WRPS) and support contractors recently completed a set of performance assessment calculations to evaluate potential human health and environment impacts associated with residual wastes remaining in the tanks after retrieval (RPP-ENV-58782 and RPP-ENV-58806), and from soils contaminated by past leaks (RPP-RPT-59197). The scope of the investigation described here was to develop three new heterogeneous conceptual and numerical models, based on borehole data obtained in the vicinity of WMA C. Hydraulic parameters were assigned to the models based on field-measured water content, geophysical logs, and textural data. Releases of Tc-99 from tank C-105 residuals after retrieval, and associated with past leaks were simulated. The results from these models were then compared to the results of similar simulations obtained using the model developed for the base case PA analysis. Although the alternative conceptual models described herein could potentially be used as selected sensitivity cases to support the WMA C performance assessment, the scope of this report was limited to development and parameterization of these alternative conceptual and numerical models, and applying them to simulation of hypothetical transport.

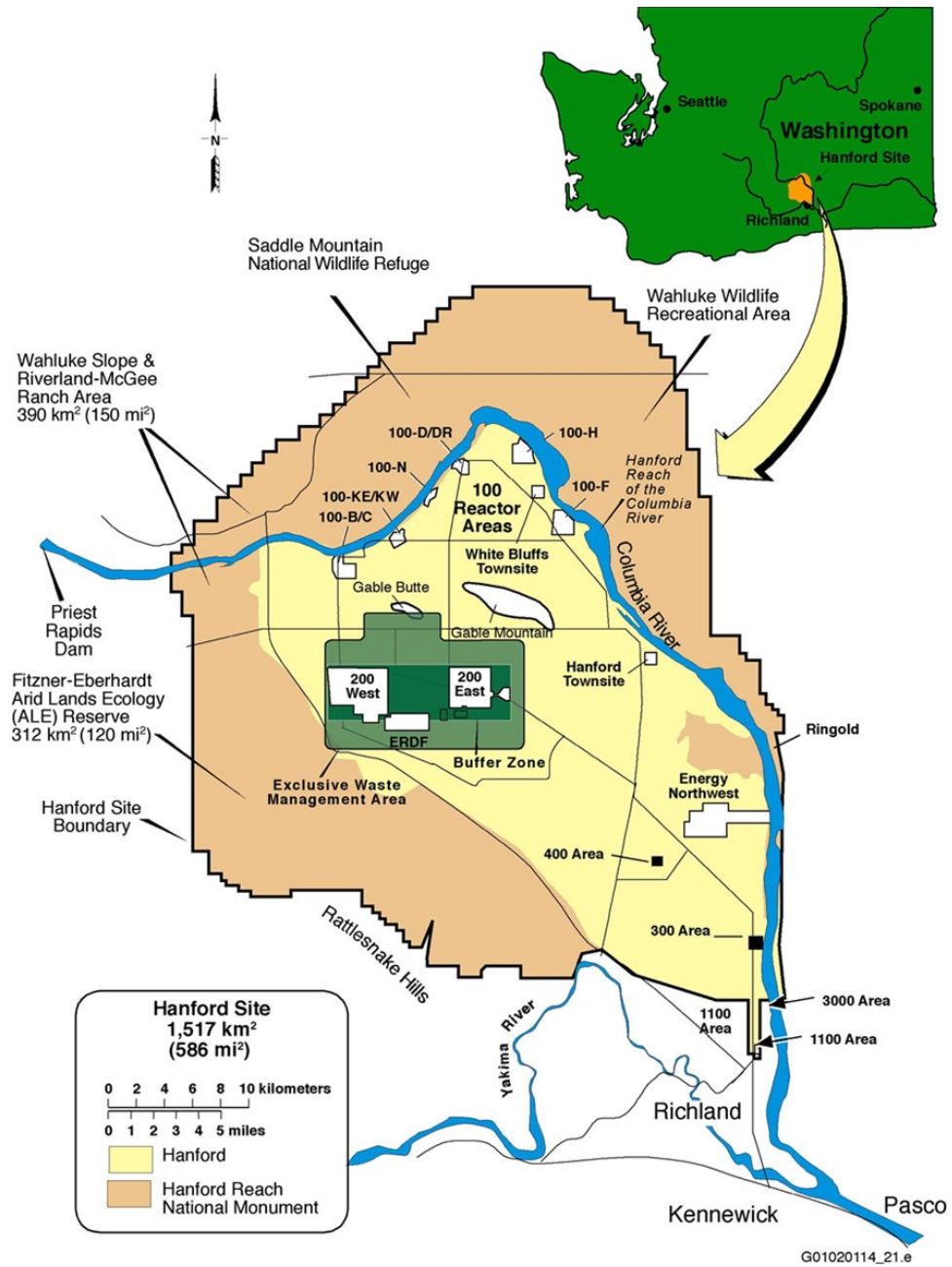


Figure 1.1. Map of the Hanford Site showing the location of the 200 East Area on the Central Plateau.

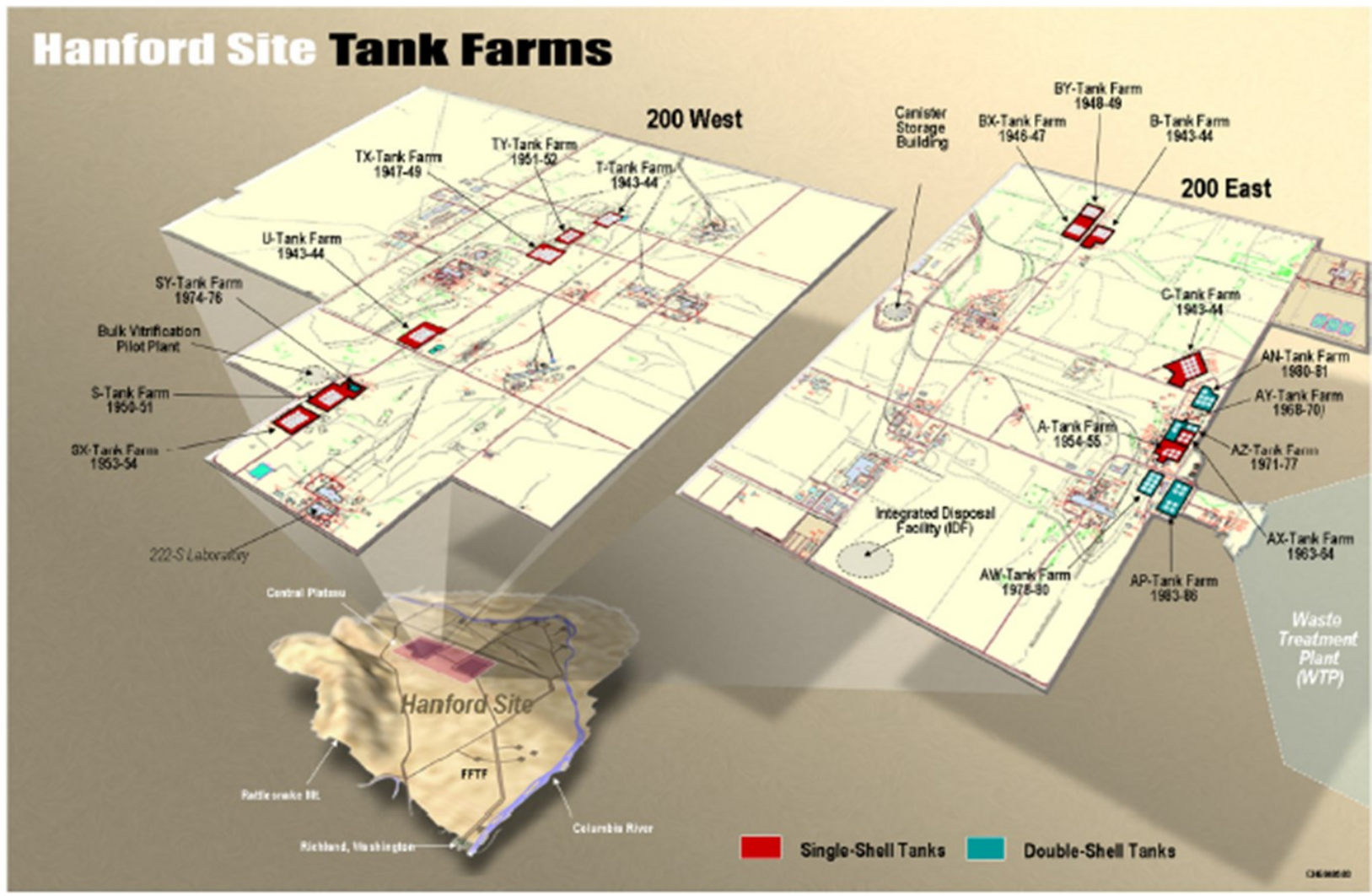
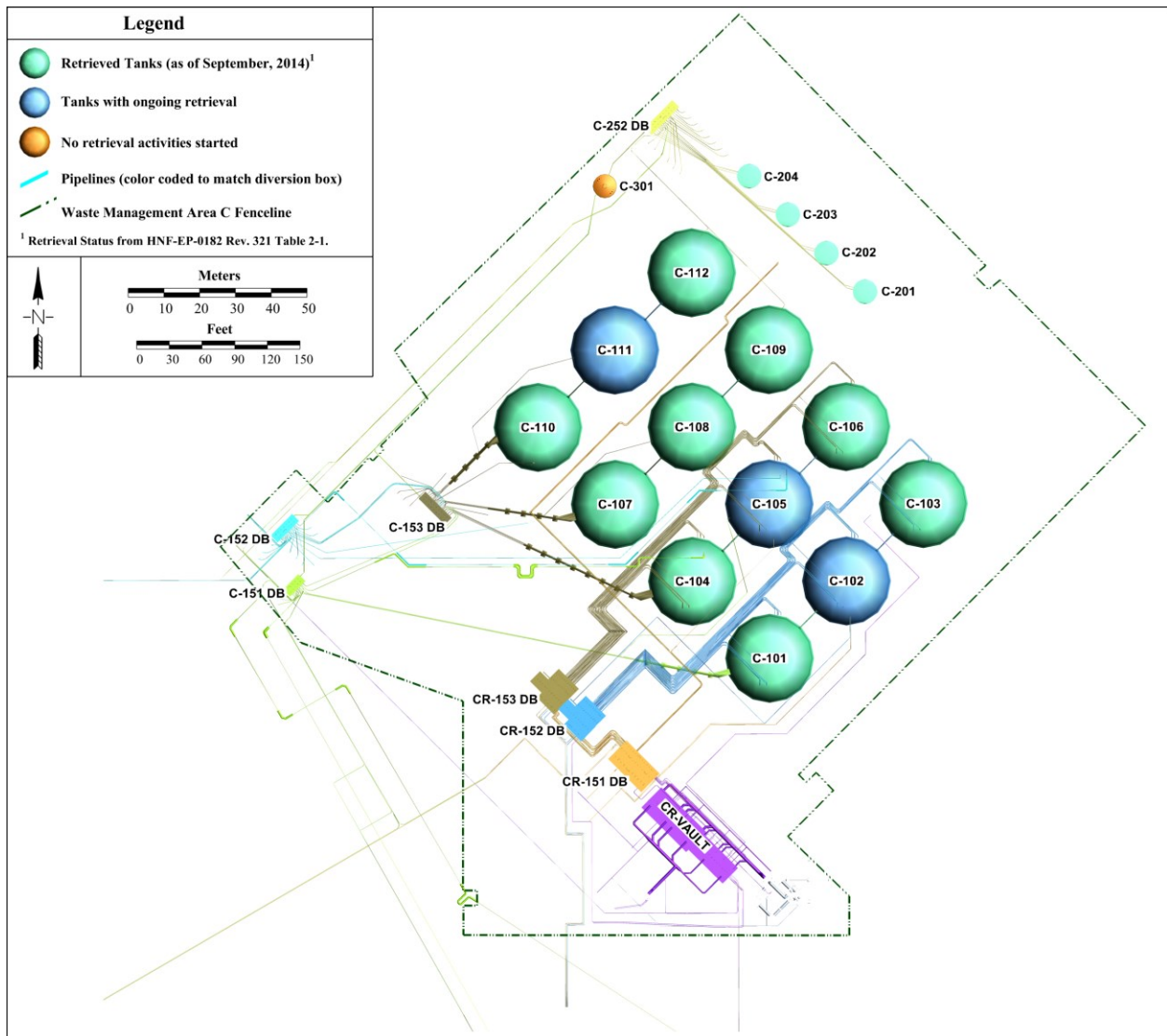


Figure 1.2. Locations of tank farms on Hanford’s Central Plateau (after Connelly et al. 2014)

## 2.0 Engineered Features

The WMA C contains twelve domed 100-series tanks that are all 23 m (75 ft) in diameter, have an operating depth of 5 m (15 ft), and each tank has an operating capacity of 1,892,700 L (530,000 gal). (Connelly et al. 2014). The tanks were constructed within a large pit that was later backfilled such that the tops of the tanks are covered with at least 2 m (~6.6 ft) of native sediment. The WMA C also contains four 200-series tanks that are all 6 m (20 ft) in diameter, have a 7.32-m (24-ft) operating depth, and each tank has an operating capacity of 208,000 L (55,000 gal) (Connelly et al. 2014). Figure 2.1 shows the locations of the SSTs, transfer lines, and other structures within WMA C. At the time the waste inventory was set for use in the WMA C PA, waste from the 13 tanks shown in green in Figure 2.1 had been retrieved, and retrieval was underway for the remaining 3 tanks shown in blue (Connelly et al. 2014). No retrieval activity has started yet for the catch tank (C-301) shown in orange in Figure 2.1.



**Figure 2.1.** Map showing placement of tanks, diversion boxes, pipelines, and a catch tank in the WMA C tank farm (after Connelly et al. 2014).

### 3.0 Characterization and Monitoring Data

Many thousands of boreholes and wells have been drilled and installed at the Hanford Site for both site characterization and groundwater monitoring (Ward et al. 2006; DOE 2013). Site characterization and monitoring at WMA C has included borehole geophysical measurements using spectral and/or total gamma and neutron moisture logging tools. Grab and core sampling have also been performed for physical property and geochemical characterization (Brown et al. 2006). Water content data have been collected for both site characterization and monitoring, for detection of tank leaks. A plan view of some of the local monitoring wells, groundwater wells, dry wells, and characterization borehole locations at WMA C is shown in Figure 3.1.

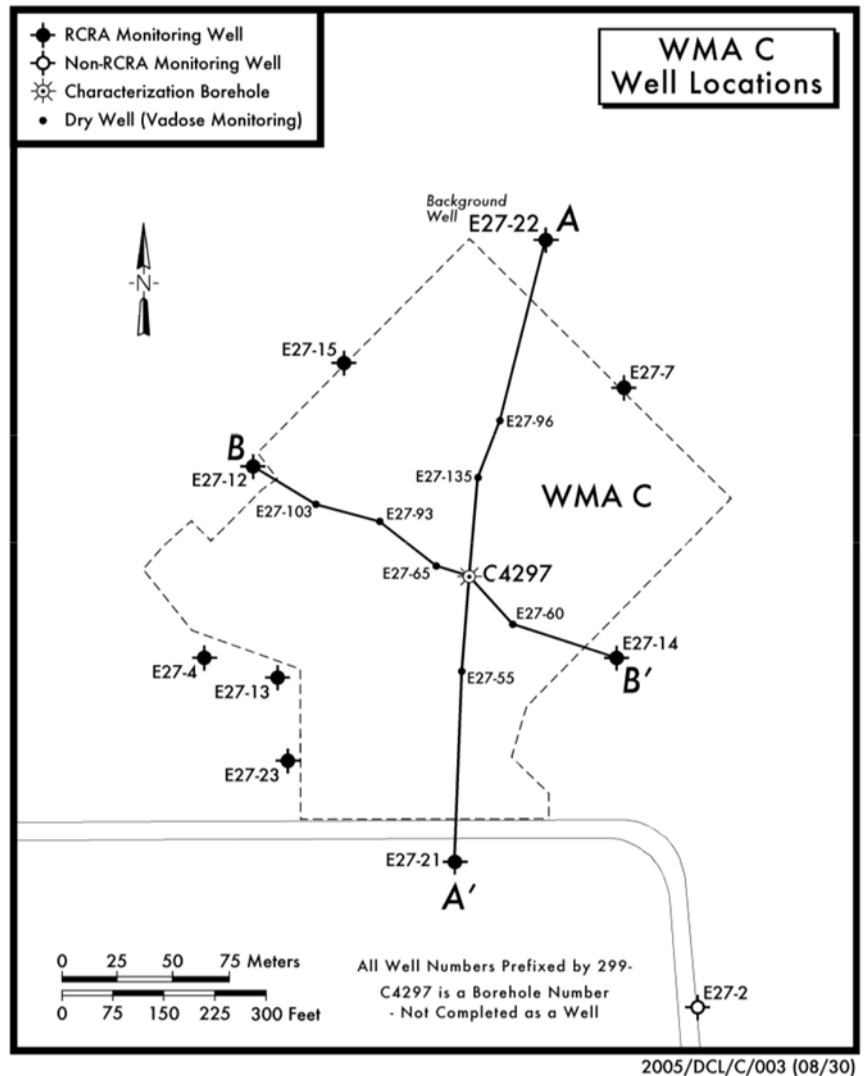


**Figure 3.1.** Map showing plan view outline of WMA C with some borehole, groundwater well, and dry well locations and lines of cross section (after Brown et al. 2006).

Generalized stratigraphic cross-sections are shown in Figure 3.2 that correspond with transects A-A' and B-B' of Figure 3.1. The stratigraphic nomenclature used for subsurface sediments at WMA C and elsewhere at Hanford is from DOE 2002.

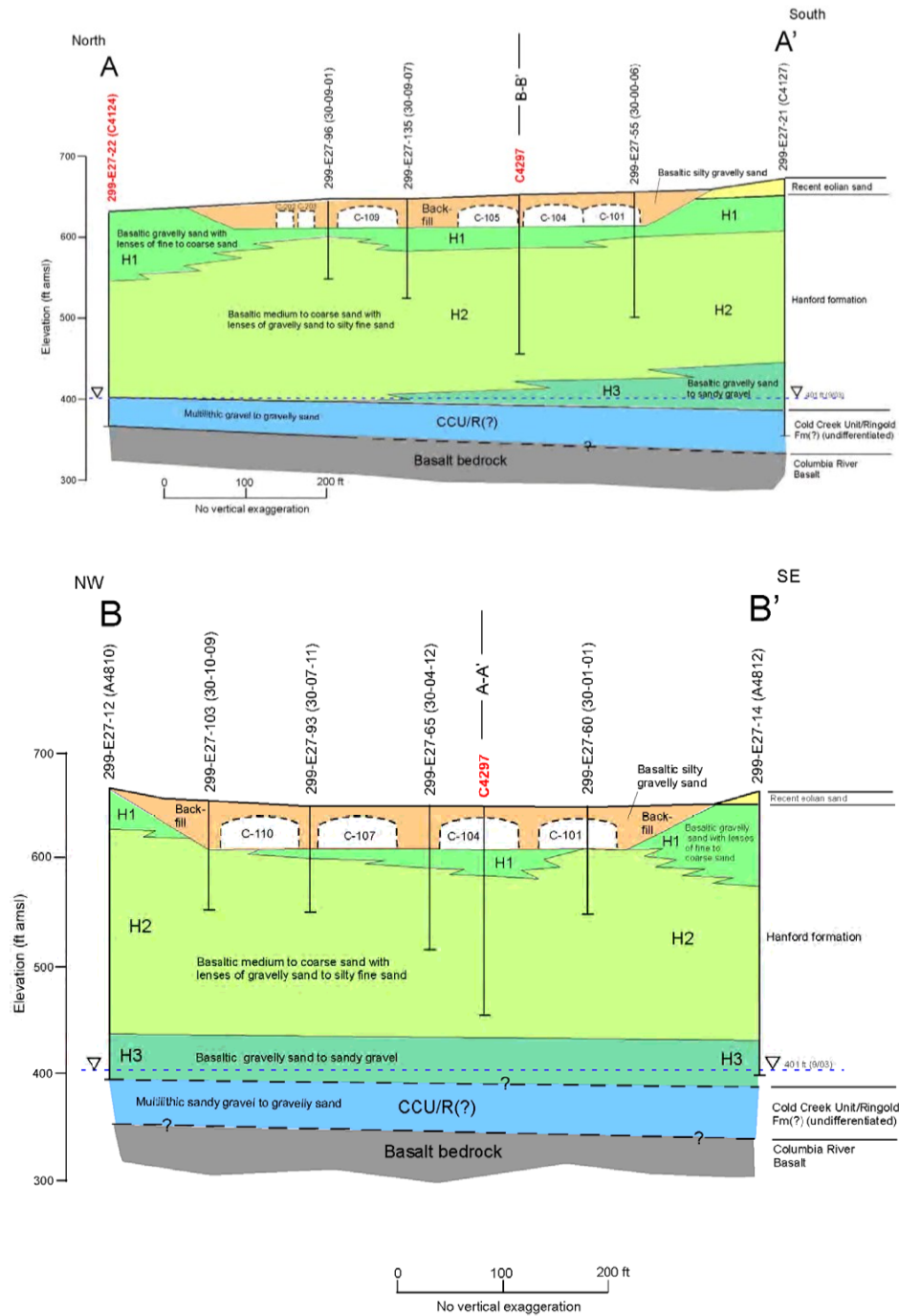


**Figure 3.2.** Generalized stratigraphic cross-sections through WMA C corresponding to the lines of cross-section shown in Figure 3.1 (after Brown et al. 2006).

### 3.1 Physical Properties

A plan view of a model domain being used for numerical simulations of subsurface flow and transport at WMA C is shown in Figure 3.3. Also shown are tank locations (open circles) and borehole or well locations for both WMA C and the A-AX tank farms, which are located on the edge of the WMA C model domain to the southeast. The borehole/well locations shown in Figure 3.3, and others that are not shown, have been used for geophysical logging and physical property measurements. Physical property measurements that are available for samples from WMA C and vicinity include grain size distribution data and volumetric water content data. These data sets are described in the following sections.

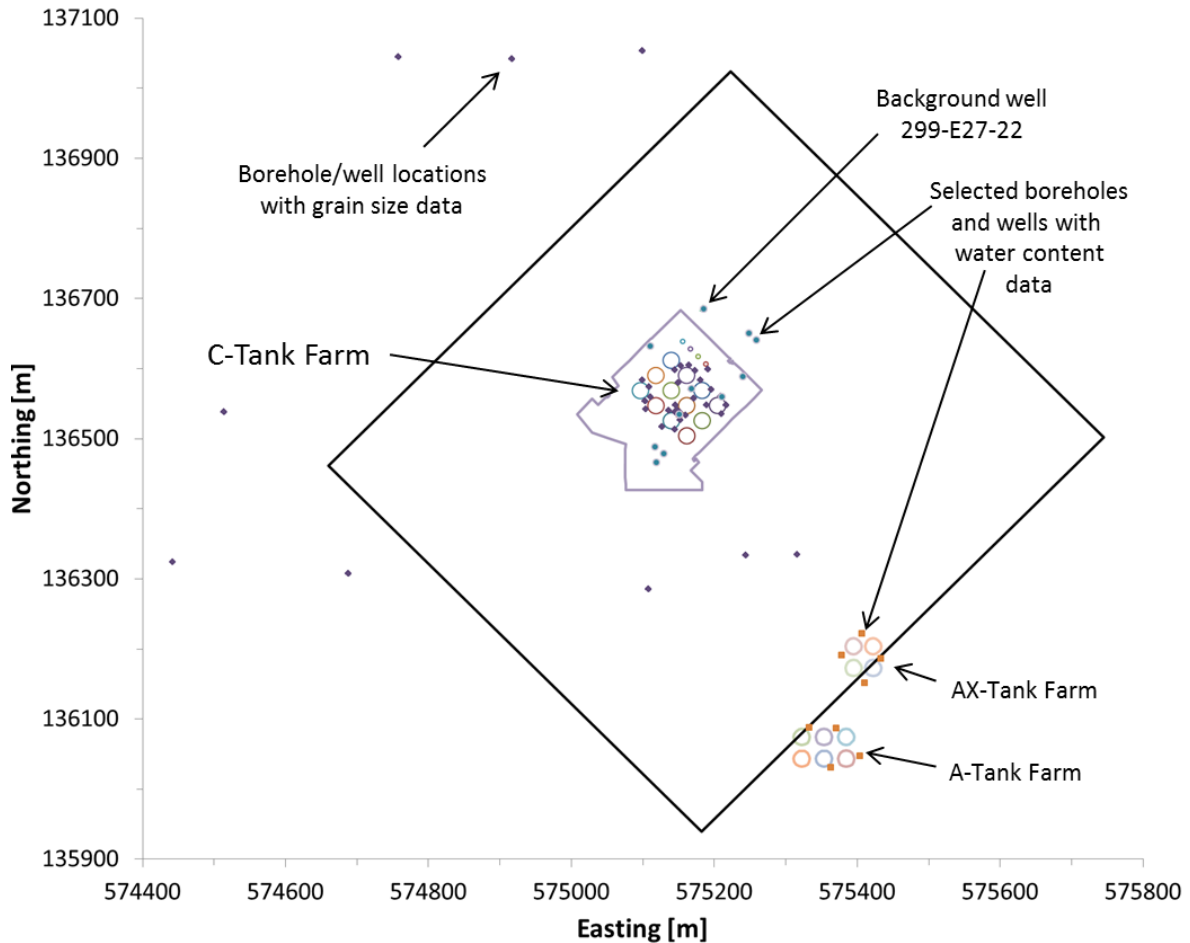


**Figure 3.3.** Plan view (large rectangle) of the WMA C model domain showing outline of WMA C, tanks in both WMA C and in the A-AX tank farms (open circles), and borehole or well locations for which physical property data are available.

#### 3.1.1 Grain Size Distribution Data

Detailed physical and geochemical property measurements were made on selected samples from two borehole/well locations near WMA C: well 299-E27-22 (C4124) and borehole C4297 (Brown et al. 2006). The physical property measurements included grain size distributions determined using wet sieve and hydrometer methods (Gee and Or 2002). In addition, dry sieve data are available from more than 800

sediment samples collected from other borehole/well locations in and around WMA C from the ROCSAN database, accessible from the Hanford Virtual Library. Figure 3.4 shows an example of grain size distribution data for a sediment samples from the ROCSAN database, and computed grain size distribution metrics.

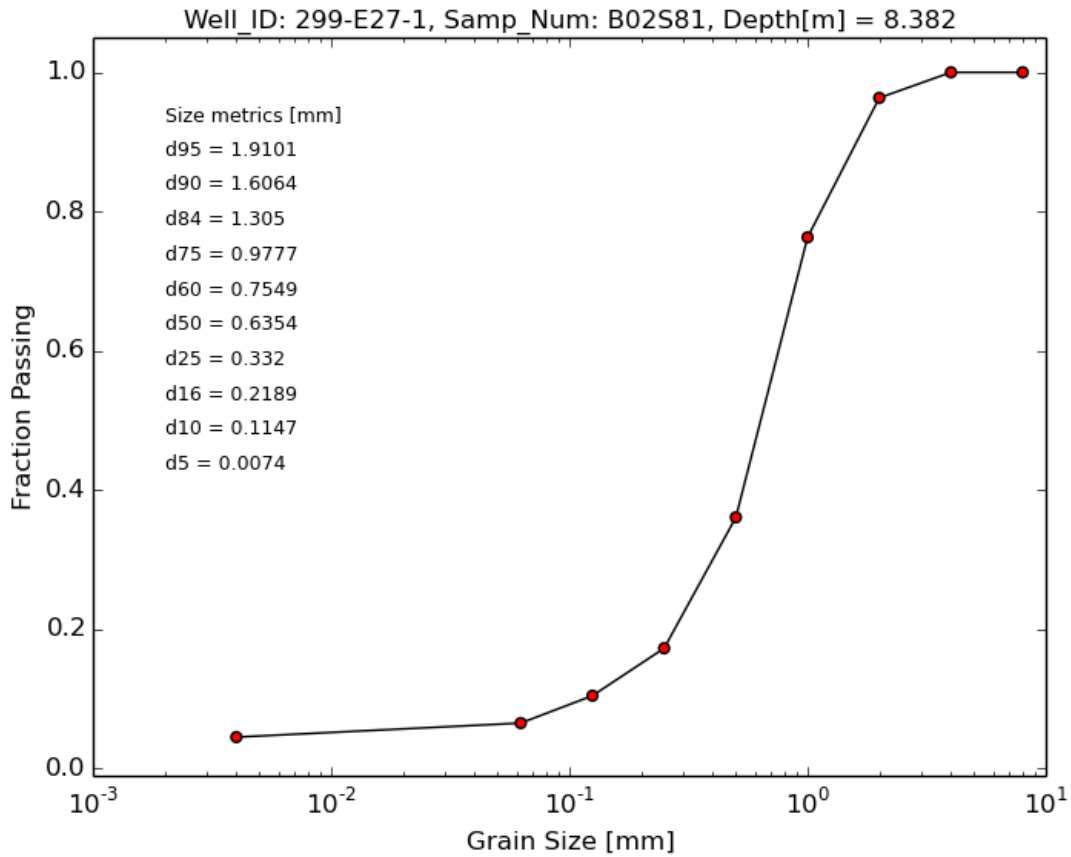


**Figure 3.4.** Grain size distribution data for a sediment sample from the ROCSAN database.

Two particular grain size distribution metrics are of interest here: the geometric mean grain diameter,  $d_g$ , and the geometric standard deviation,  $\sigma_g$ . Sediment grain-size distributions are often approximately log-normally distributed, in which case the entire distribution can be fully defined by  $d_g$  and  $\sigma_g$ . The cumulative distribution function,  $P$ , for a log-normal distribution representing the fraction of the total sediment mass that is smaller than size  $x$ , is defined as

$$P(< x) \equiv \int_0^x p(x') dx' = \frac{1}{2} \operatorname{erfc} \left\{ -\frac{1}{\sqrt{2}} \left[ \frac{\ln(x) - \mu}{\sigma} \right] \right\} \quad (3.1)$$

where  $p$  is the probability density function,  $\operatorname{erfc}$  is the complementary error function,  $\mu = \ln(d_g)$  and  $\sigma = \ln(\sigma_g)$ . Given values of  $\mu$  and  $\sigma$ , and any particular grain size ( $x$ ) representing, for example, the cutoff between sand and gravel (2 mm) or between silt and sand (0.063 mm) size classes, the cumulative distribution function can be used to estimate the mass fraction of the sediment that is smaller than a given

size. To estimate the size that corresponds to a particular mass fraction of grain sizes smaller than it (e.g.,  $d_{16}$ ,  $d_{60}$ ,  $d_{84}$ ), the inverse cumulative distribution function can be evaluated as

$$x(P) = \exp\left[\mu - \sqrt{2}\sigma \operatorname{erfc}^{-1}(2P)\right] \quad (3.2)$$

Given discrete grain size distribution data, such as that shown in Figure 3.4, the size metrics  $d_g$  and  $\sigma_g$  can be estimated by fitting a log-normal distribution function to the data. Alternatively,  $d_g$  and  $\sigma_g$  may be approximated from

$$d_g \cong \sqrt{d_{16} \cdot d_{84}} \quad (3.3)$$

$$\sigma_g \cong \sqrt{\frac{d_{84}}{d_{16}}} \quad (3.4)$$

Grain size distribution data from borehole and well locations depicted in Figure 3.1 were used to estimate the metrics  $d_g$  and  $\sigma_g$  for each sample. Table 3.1 lists the number of samples in each geologic unit. Where possible, the available sample data were grouped by geologic unit. The mean and median  $d_g$  and  $\sigma_g$  values for the four major geologic units depicted in Figure 3.2 (i.e., backfill, and Hanford formation units H1, H2 [grouped], and H3 [grouped]) are listed in Table 3.2.

The measures of central tendency for the subunits of the H2 unit are somewhat counter to the texture implied by their names, but this is likely a result of the very small sample sizes (see Table 3.1). The H3 unit is shown as being split into regions that are above (H3-Unsat) and below (H3-Sat) the water table, which lies at an elevation of  $\sim 121$  m. The sample sizes for the H3 subunits are also very small. Therefore the fine, coarse, and silt subunits of the Hanford H2 formation, and the saturated and unsaturated portions of the H3 unit were grouped to obtain estimates of central tendency for the  $d_g$  and  $\sigma_g$  metrics for the H2 and H3 units. Note that at WMA C H3 unit is an undifferentiated sequence of Hanford H3, Cold Creek, and Ringold gravely sands and sandy gravels.

**Table 3.1.** Summary of sediment samples with grain size data available from wells near WMA C<sup>1</sup>.

Borehole_ID	Well_Name	Unit_Code									Length of Sampled Interval [m]
		-99	1	2	3	4	5	6	7	8	
		Outside	Basalt	H3-Sat	H3-Unsat	H2 Silt	H2 Coarse	H2	H1	Backfill	
A4807	299-E27-1	58									102.108
A4808	299-E27-10	47									71.628
A4817	299-E27-8	51									76.2
A4818	299-E27-9	48									73.152
A6671	299-E27-3		4	13	6	4	10	29	6		108.204
A6672	299-E27-5	40									88.392
A6673	299-E27-6							10	10		28.956
A6690	299-E27-65							16	3	2	36.576
A6691	299-E27-66							19	1	2	38.1
A6692	299-E27-67							14	4	2	36.576
A6695	299-E27-70							12	6	2	35.052
A6697	299-E27-72							11	6	2	33.528
A6699	299-E27-74							4	10	2	24.384
A6700	299-E27-75							8	32	2	25.908
A6701	299-E27-76							3	3	1	21.336
A6703	299-E27-78							5	6	2	25.908
A6704	299-E27-79							9	3	2	25.908
A6705	299-E27-80							8	2	2	25.908
A6707	299-E27-82							8	4	2	25.908
A6708	299-E27-83							38	16	2	25.908
A6709	299-E27-84							5	6	2	25.908
A6710	299-E27-85								6	2	16.764
A6711	299-E27-86							6	6	2	25.908
A6716	299-E27-91							6		2	16.764
A6717	299-E27-92							56		2	25.908
A6718	299-E27-93							9	1	2	24.384
A6719	299-E27-94							6	6	2	25.908
A6721	299-E27-96							6	6	2	25.908
A6722	299-E27-97							6	6	2	25.908
A6724	299-E27-99							5	6	2	25.908
A6725	299-E27-100							4	7	2	25.908
A6726	299-E27-101							10	1	1	25.908
A6727	299-E27-102							10	2	2	25.908
A6735	299-E27-115								2	2	10.668
A6736	299-E27-116									1	0
A6737	299-E27-117									1	0
A6738	299-E27-118									2	4.572
A6739	299-E27-119									3	6.096
A6747	299-E27-127	7									10.668
A6776	299-E27-147								7		10.668
C4124	299-E27-22						6	7	5		60.198
Subtotal		251	4	13	6	4	16	330	179	59	

<sup>1</sup> Note that although grain size metrics were computed for four samples that were categorized as “basalt,” the region of the model domain that actually extends into basalt is inactive, so this information is not used. Note also that samples from 251 borehole or well locations outside of the domain of the WMA C geologic framework model (see unit code-99 in Table 3.1) could not be readily binned by geologic unit because no information on unit contacts was immediately available for locations outside of the modeled domain.

**Table 3.2.** Average and median of geometric mean grain diameters  $d_g$  (mm) and  $\sigma_g$  values for different geologic units at WMA C.

Unit_Code	Name	Grain Size Metrics				Grouped H2 and H3	
		Avg. $d_g$	Avg. $\sigma_g$	median $d_g$	median $\sigma_g$	median $d_g$	median $\sigma_g$
8	Backfill	0.71	3.98	0.70	3.46	0.70	3.46
7	H1	0.66	3.26	0.64	2.94	0.64	2.94
6	H2-Fine	0.53	2.93	0.48	2.83	0.47	2.83
5	H2-Coarse	0.42	4.44	0.40	3.27	0.47	2.83
4	H2-Silt	0.53	2.79	0.56	2.76	0.47	2.83
3	H3-Unsat	0.82	4.98	0.77	5.23	0.55	3.58
2	H3-Sat	0.56	3.66	0.40	2.83	0.55	3.58

### 3.1.2 Water Content Data

Water content data are available from many borehole/well locations in and around WMA C (see Appendix A). Water content data are also available from additional wells located around the A-AX tank farms, located southeast of WMA C. Much of the water content data for WMA C are from relatively shallow “dry wells” (cased well used for monitoring the vadose zone) located around the tanks. These dry wells, which typically only penetrate to a depth of 60 m or less below ground surface, have historically been used for leak detection monitoring, or for characterization of the shallow subsurface following a suspected tank loss or leak event. Therefore, some of the available water content data are clearly influenced by non-meteoric sources. Measurements from the dry wells at WMA C and the A-AX tank farms typically extend through the backfill into the underlying Hanford H1 unit and upper part of the Hanford H2 unit. Water content data are also available from WMA C for a number of deeper wells, some of which penetrate to depths of 75 to 80 m or more below ground surface, extending into the lower part of the Hanford H2 unit and possibly into the upper part of the Hanford H3 unit (Figure 3.1). Geostatistical analysis and kriging results for water content data are provided in Appendix A. A subset of the water content data was used for model parameterization in an attempt to reduce the influence of data affected by water line leaks, as described in Section 4 and Appendix A.

Water content data from selected boreholes from WMA C are shown in Figure 3.5. Backfill materials are generally found at elevations above ~185 to 190 m, and in this area the Hanford H1 unit is found at elevations between ~174 and 185 m. Water content values in the backfill materials are typically larger than those found in underlying units, with the exception of isolated spikes of higher water content that are found throughout the Hanford H2 unit at all well locations. These higher water content spikes in the H2 unit, which range from ~15% to 27% by volume, are indicative of finer-grained sand and silt lenses that retain more moisture relative to the coarser surrounding materials. In some places, the spikes of higher water content also correspond with the interfaces between major hydro-geologic units that have been identified from borehole geologic and geophysical logs.

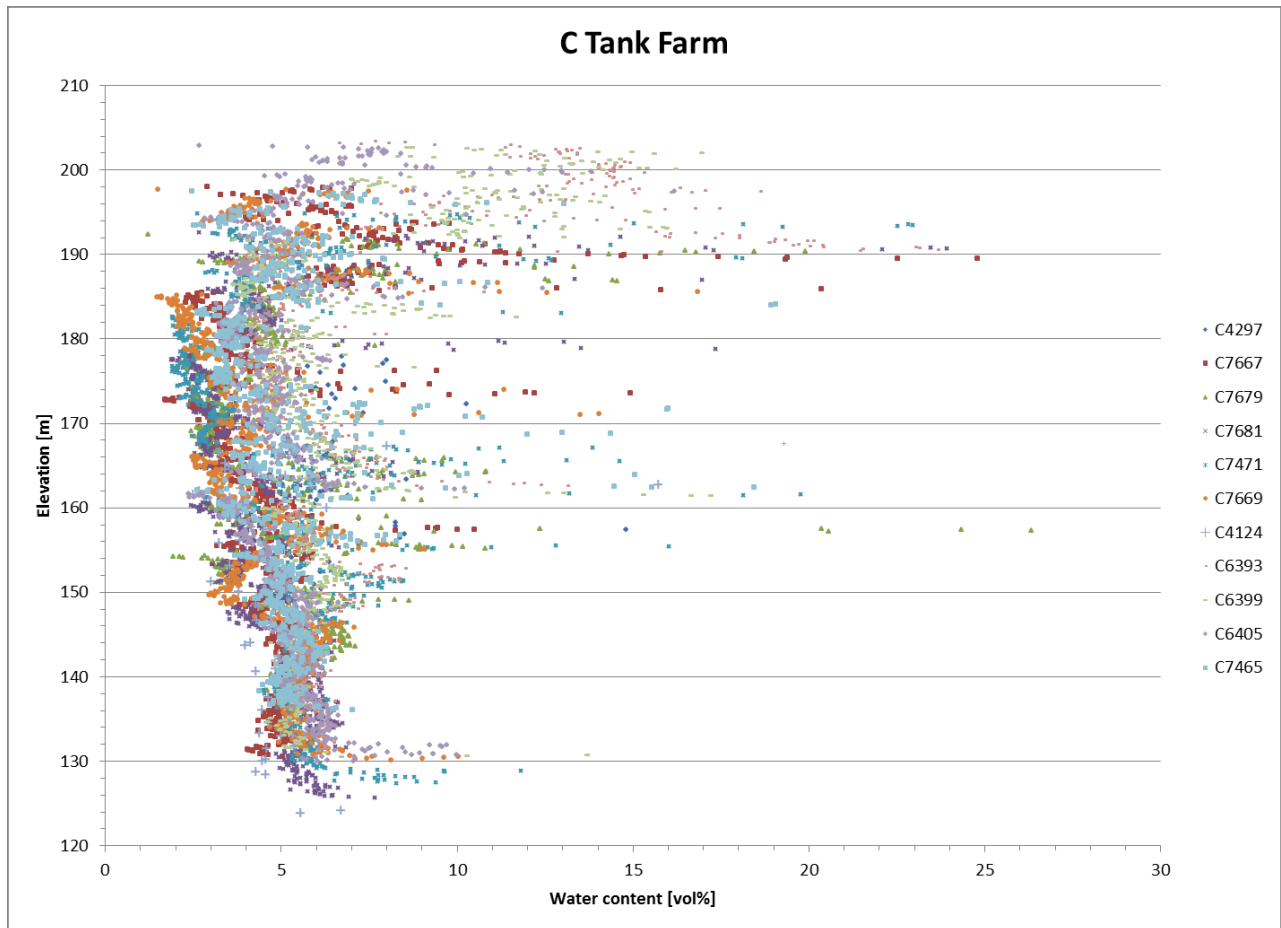


**Figure 3.5.** Volumetric water content data from selected deep boreholes at WMA C.

The Hanford H2 unit lies at elevations between ~148 and ~174 m, and the Hanford H3 units lie below ~148 m. As shown in Figure 3.5, the upper part of the Hanford H3 unit shows less variability in water content than the overlying or underlying materials, ranging from ~4% to 7% by volume. This reduced variability in water contents suggests that this part of the Hanford H3 unit is more uniform in texture than other parts of the sediment profile at these well locations.

Figure 3.6 shows water content data from four boreholes located in the AX tank farm. Backfill materials lie above an elevation of ~192 m and the Hanford H1 unit is found between elevations of ~172 to 178 and ~192 m. The range of variability in water content values within the Hanford H1 unit at the AX tank farm is very similar to that found within the upper H3 unit at the C tank farm. This similarity suggests that the sediments of the Hanford H1 unit and upper part of the Hanford H3 unit may have similar textures. The lower water content values seen in the H1 unit at WMA C relative to those seen in the H1 unit at the AX tank farm suggest that the H1 unit may be somewhat coarser at WMA C than at the AX tank farm. This observation is consistent with expectations since the A-AX tank farm area is downstream of WMA C when cataclysmic flood events occurred that deposited the Hanford formation sediments (Bjornstad, 2006).

Figure 3.7 shows water content data from four boreholes in the A tank farm, located just southwest of the AX tank farm. The water content profiles for the A tank farm are very similar to those seen at the AX

tank farm. The water contents in the backfill at the A tank farm are somewhat smaller than those at the AX tank farm. Note that leaks have been documented from at least two tanks in the A tank farm, but none of the tanks in the AX tank farm are known to have leaked.

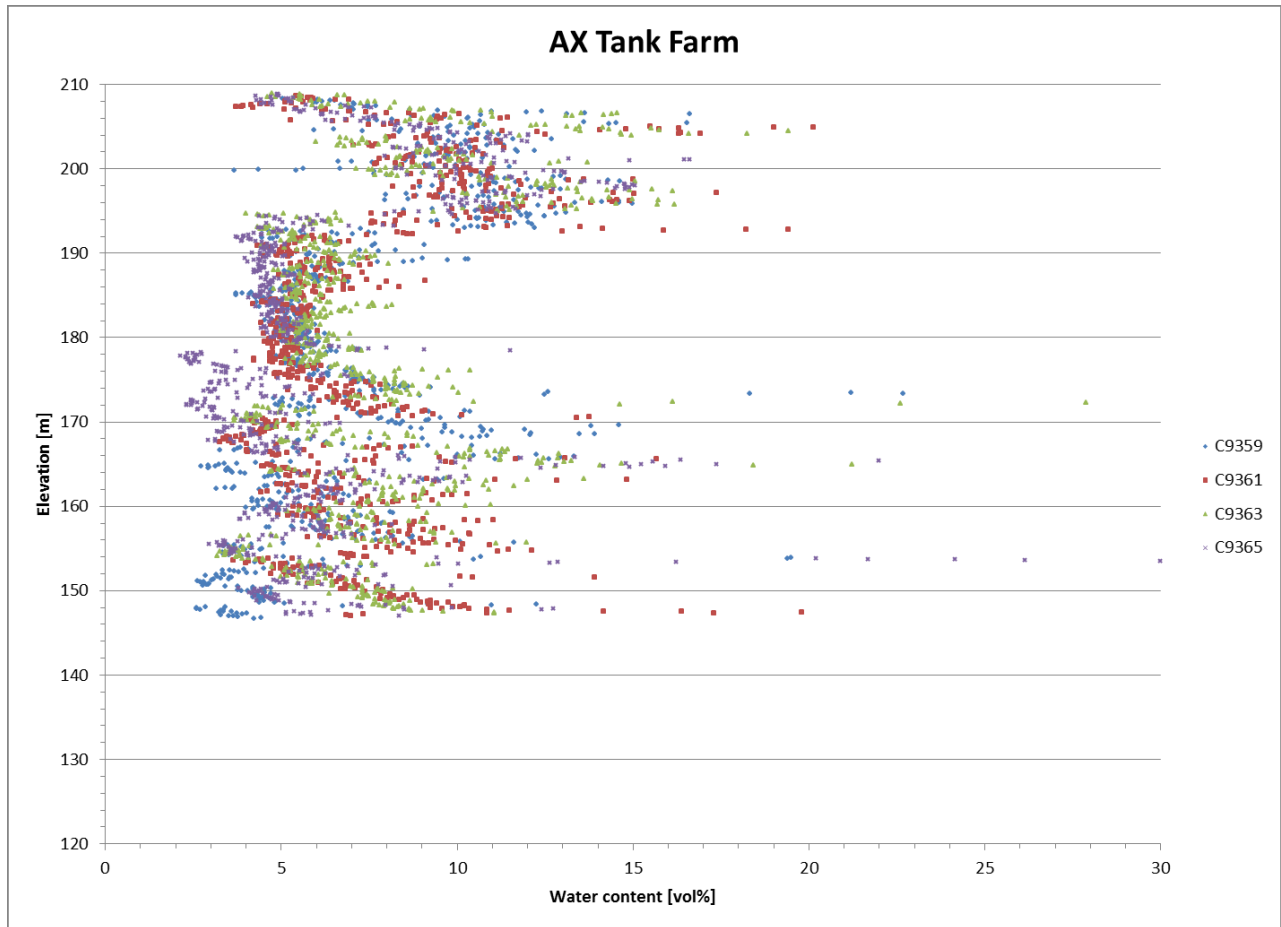


**Figure 3.6.** Volumetric water content data from four boreholes at the AX tank farm.

## 3.2 Hydraulic Properties

Hydraulic property measurements for Hanford sediments have historically been performed on selected repacked samples or intact cores for determination of saturated hydraulic conductivity and water retention characteristics (Bergeron et al. 1987; Rockhold et al. 1988, 1993). More recently, hydraulic parameters have been estimated for core samples using inverse modeling with data from multistep outflow experiments (Schaap et al. 2003; Khaleel 2004, Rockhold et al. 2013). Unfortunately, no site-specific hydraulic property data are available from core or sediment samples collected from WMA C.

Although no local hydraulic property data are available for WMA C, detailed hydraulic property characterization data and parameters are available for 63 samples from the Sisson and Lu site (Sisson and Lu 1984; Fayer et al. 1995; Schaap et al. 2003; Rockhold et al. 2010) and for 44 samples from the Integrated Disposal Facility (IDF) site (Khaleel 2004; Rockhold et al. 2015). Both of these sites are located at the southern end of the 200 East Area. Hydraulic property data and parameters for Hanford sediments are also available in several other compilations of physical and hydraulic properties (Rockhold

et al. 1988; Connelly et al. 1992; Khaleel and Freeman 1995; Rockhold et al. 2013). Some approaches for estimating hydraulic parameters from surrogate data for WMA C are described in Section 4.

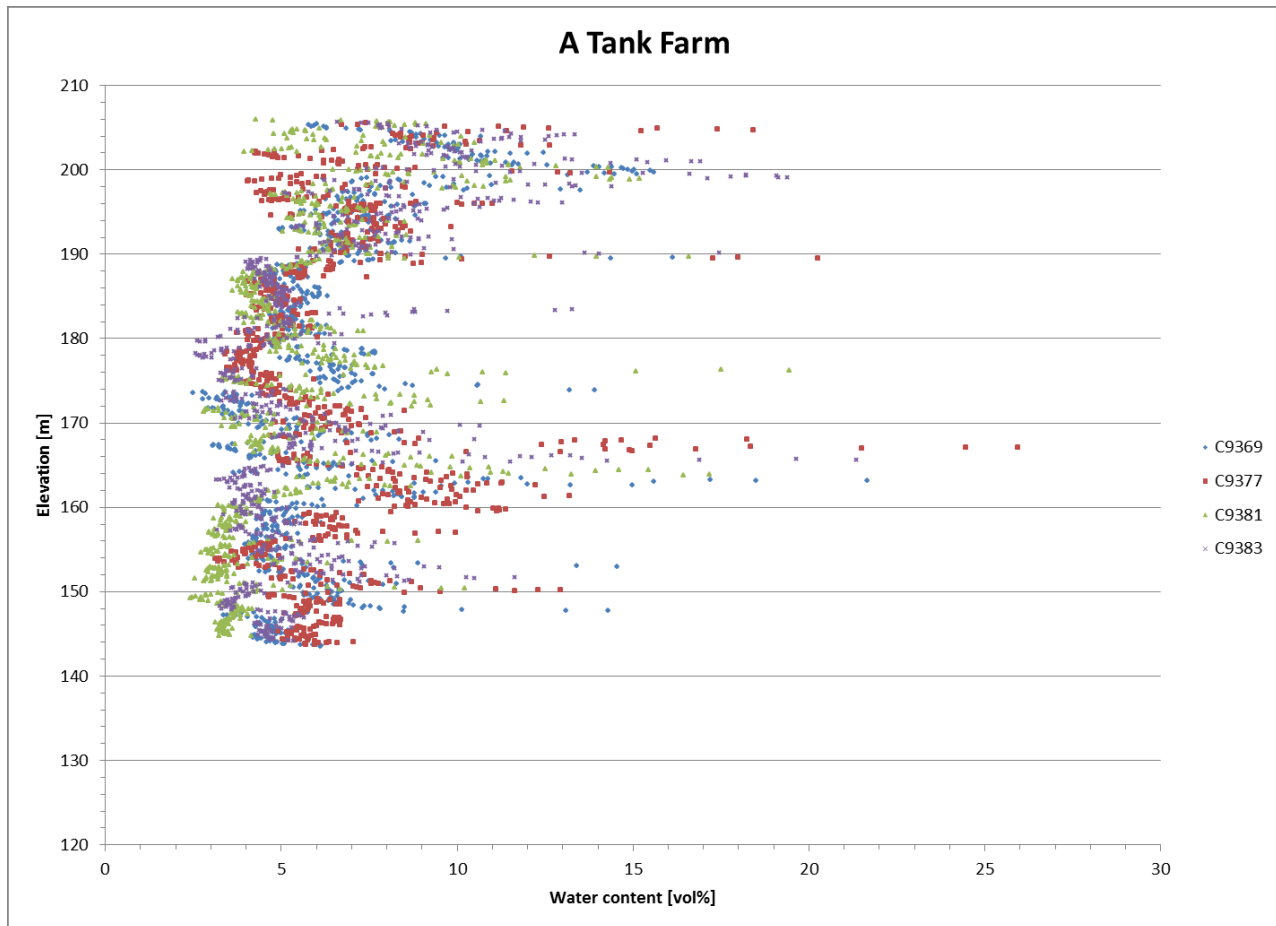


Figure 3.7. Volumetric water content data from four boreholes at the A tank farm.

### 3.3 Geochemical Properties

Geochemical measurements on select grab and core samples have included batch and leach tests to determine concentrations of major and trace ions and radionuclides, and to determine sorption-related parameters (Brown et al. 2004). This type of geochemical characterization data for borehole C4297 was used to estimate the vertical extent of tank waste loss or leak events associated with the C-105 tank at WMA C. Geochemical and electrical conductivity data from a “background” well, 299-E27-22 (C4124), which is outside the fence line of WMA C, provided evidence that this well may have actually been impacted by nonradioactive waste stream. No geochemical data are used directly for the work reported in this document, but such data is critical for assessment of past tank waste leaks and losses at WMA C.

## 4.0 Model Setup and Parameterization

The purpose of the modeling assessment in this report is to compare results generated by different conceptual models of material property and associated parameter distributions for the subsurface of WMA C. STOMP model input files representing a PA base case conceptual model developed employing an equivalent homogeneous model (EHM) approach were obtained from WRPS and subcontractor personnel from CH2M Hill Plateau Remediation Company (CHPRC). The alternative conceptual models described in this report and in Hou et al. (2015) used the same model grid and upper boundary conditions used in the PA base case model provided by WRPS.

WRPS has supported the development of both facies-based models (Hou et al. 2015) and water content based models (this report) of WMA C. The facies-based models were developed using a stochastic indicator simulation method, conditioned on clustered spectral gamma log data (Hou et al. 2015). The water content based method, described here, uses a stochastic Gaussian simulation method, conditioned on field measured water content data. In the facies based models, the material types are generated for each grid block. In the water content based model, the hydraulic properties are generated for each grid block. Assigning material types and/or properties on a cell-by-cell basis for the model grid is intended to capture more of the local heterogeneities that manifest larger scale flow and transport behavior.

### 4.1 Geologic Framework

A geologic framework model was developed for the entire 200 East groundwater aggregate area of the Hanford Site by Connelly et al. (1992). Since that time, more detailed local models have been developed for individual operable units and waste management areas, including WMA C. Connelly et al. (2014, pp. 3-1 and 3-2) describe the major geologic units that have been identified within WMA C. These are, from top to bottom: Hanford H1 Unit, Hanford H2 Sand Unit, Hanford H2 Coarse Gravelly Sand Unit, Hanford H2 Silt Unit, Undifferentiated Hanford H3 Gravels, Cold Creek, and Ringold Units, and Columbia River Basalt. The Hanford H1 unit is overlain in places by backfill sediments. In the vicinity of WMA C the Hanford H3 Gravels, Cold Creek Unit, and Ringold Formation Units tend to be discontinuous and difficult to distinguish from one another, so they are grouped as one undifferentiated unit. The PA base case model referenced here was developed from Alternative Geologic Model 1 of Connelly et al. (2014).

Alternative Geologic Model 1 was developed by interpolating the so-called “picks” or “tops,” determined from borehole geologic and geophysical logs, to a triangular mesh using kriging. The resulting surfaces, shown in Figure 4.1, represent the tops of each major geologic unit. These surfaces were evaluated to determine the material types for assignment to cell centroids of the model grid. Further details on the borehole and well data and methods used to develop the geologic framework model are described by Connelly et al. (2014). The elevation extent of the numerical flow and transport model that was discretized based on these surfaces ranging from 95 to 210 m. Grid cells lying above ground surface and below the top of the basalt were assigned to be inactive (the non-computational grid cells within the model gridded domain).

Within the PA base case model, groundwater flow is assumed to be from the northwest to southeast. The simulation domain (Figure 4.2) was set up so that the X direction is aligned with the groundwater

flow direction. In the following, the convention of the STOMP simulator will be used to refer to the directions of the simulation domain. Figure 4.2 shows a plan view of the WMA C model grid with the outlines of the 200-series (larger diameter) and 100-series (smaller diameter) tanks. Also shown are the outlines of the tanks in the A-AX tank farms. The dark symbols in Figure 4.2 represent the locations of wells whose numbers begin with 299-E27 from which grain size distribution data are available from the Hanford Virtual Library. Selected borehole and well locations with water content data are also shown.

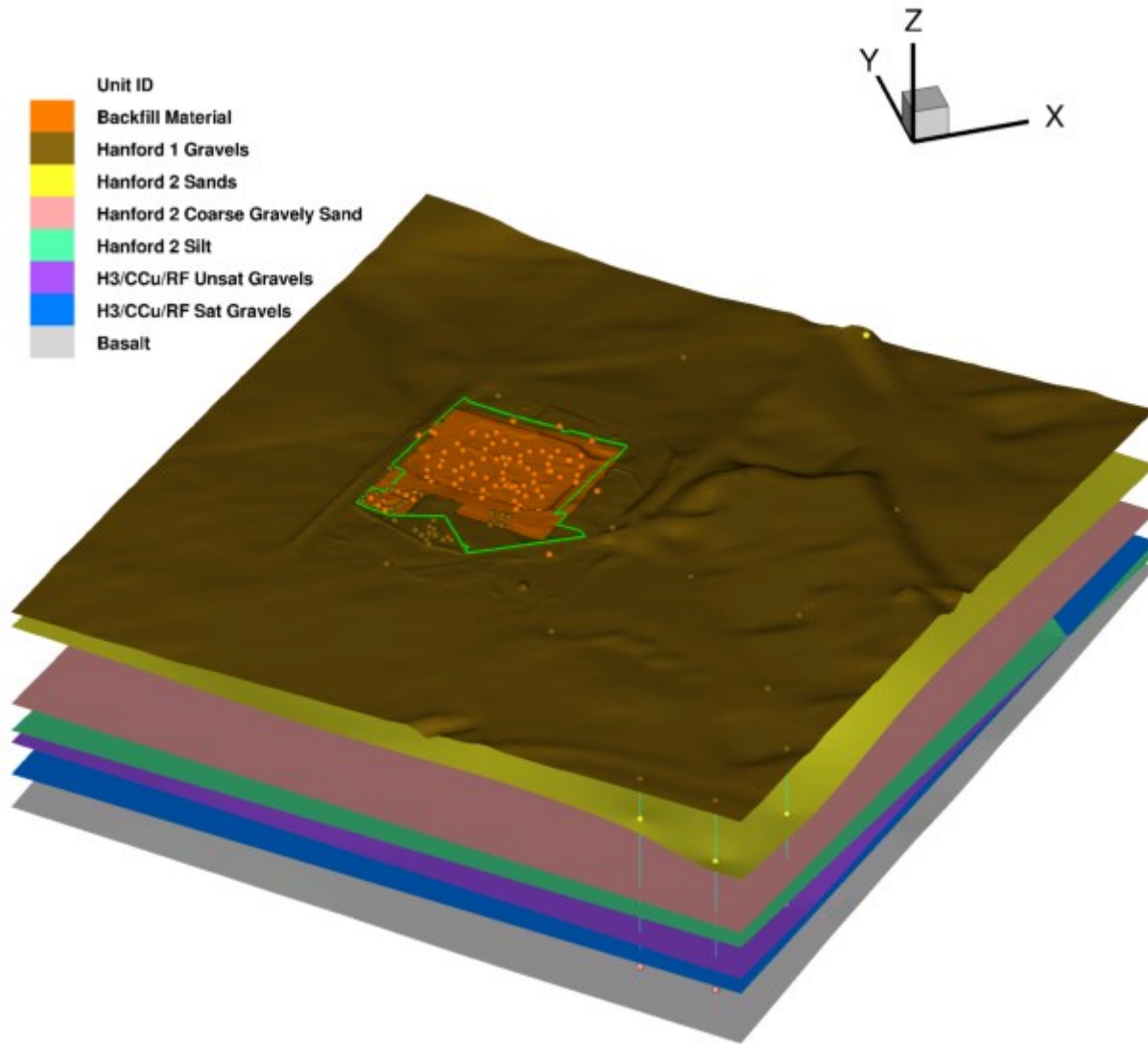


**Figure 4.1.** Stacked surfaces representing the tops of geologic units underlying WMA C (after Connelly et al. 2014).



### 4.3 Boundary Conditions

Boundary conditions are needed for the upper (ground surface) and lateral boundaries of the WMA C model domain. Any model grid block below the top of the basalt is treated as inactive, so the interface between the undifferentiated H3/CCu/RF units and the basalt at the bottom of the domain is effectively a no-flow boundary. The northwest and southeast sides of the simulation domain were assigned as linked-list “XYZ seepage face” boundary conditions with base pressures that correspond to the position of the water table. In STOMP this is a dynamic boundary condition in which cell faces below the water table are assigned aqueous pressures that depends on their elevation, and cell faces above the water table are assigned no-flow boundary conditions. The southwest and northeast sides were assigned zero flux boundary conditions. Groundwater flows from west to east with a hydraulic gradient of  $\sim 2.0E-5$ . For the tank residual simulations, a water table elevation of 119.5 m was specified along the west side and a water table elevation of 119.485m was specified along the east side. For the past tank leak/loss simulations, a water table elevation of 122.25 m was specified along the west side and a water table elevation of 122.235 m was specified along the east side. This boundary condition setup differs from the conditions specified by WRPS, which used a combination of Neumann (specified flux) and Dirichlet (specified pressure) boundary conditions to achieve a similar hydraulic gradient.

Figure 4.3 is an aerial photograph of the area around WMA C and the A-AX tank farms showing variable land surface conditions. Recharge rates from meteoric sources are known to depend on climate (atmospheric forcing), sediment type, and vegetation (Fayer and Szecsody 2004). Figure 4.3 clearly depicts the areas around WMA C and the A-AX tank farms that have been disturbed by excavations and roads. The tanks were emplaced after excavating large pits, which disturbed the natural layering of the sediments. The tank farms also have gravel-covered surfaces and are maintained free of vegetation to prevent plant roots from accessing radioactive materials. This condition maximizes the net infiltration or recharge rates (Gee et al. 1992; 2007).

Other areas exist outside the tank farms, where sediments appear to be relatively undisturbed and native shrub-steppe vegetation exists, so recharge rates are expected to be spatially variable over the larger area of the model domain. The range of recharge values used here and in the calculations performed for the PA by WRPS is based on observations from field water balance study locations at Hanford. Lysimeter studies and modeling results suggest recharge rates range from  $\sim 10$  to  $100$  mm/yr for gravel-covered surfaces devoid of vegetation (Fayer and Szecsody 2004). Recharge rates are lower for undisturbed areas with native shrub-steppe vegetation, with estimates ranging from  $0$  to  $\sim 3.5$  mm/yr. Fayer and Szecsody (2004) report recharge rate estimates based on the chloride mass balance method of  $0.24$  mm/yr and  $0.62$  mm/yr for two boreholes/wells ( C3177/299-E24-21 and C3826/299-E15-22, respectively) located near the IDF site.



## 4.4 Source Terms

Different considerations were required for development of source terms for the tank waste residual and past tank waste release simulations. These considerations are described as follows.

### 4.4.1 Considerations for Tank Waste Residual Releases

For the tank waste residuals simulation cases, three separate source regions were defined in the STOMP input for the PA base case model, one each for the C-105 tank, the C-203 tank, and one for pipelines. Each tank source was defined by a specific set of several grid blocks approximating the tank's general location in the model domain. The source release model for the pipelines is quite different from the tanks. Instead of modeling discrete source terms, a single source area reflective of the approximate areal distribution of the waste transfer pipelines is considered. This is the assessed area of the tank farm where pipelines are generally present. The estimated residual inventory is uniformly spread over this area. Unlike tanks, the pipelines are assumed not to be filled with grout at closure, and due to limited information on the condition of the pipeline material, the pipeline walls are assumed to be absent (i.e., no structural integrity). Therefore, both advective and diffusive releases are considered from the pipelines. Only the transport results associated with source term for C-105 are evaluated in this report. The other source terms are mentioned here so that reader is aware that a more comprehensive treatment of contaminant sources at WMA C is being addressed in the PA effort.

For the purpose of developing a source release model for tanks, the residual waste volume in tanks is conceptualized to be present as a thin layer at the base of the tank. The estimated residual waste volume is assumed to be spread across the circular tank dish bottom area. At closure, the tanks are assumed to be filled with grout. While the tank is intact, it will divert any water that infiltrates through the surface cover. In the PA base case model, the tank is assumed to remain intact for the entire period of analysis. Therefore, the transport mechanism for release of contaminants from the residual tank waste to the underlying vadose zone is primarily diffusive. The dissolved concentration of contaminants in the residual waste pore volume is controlled by the waste characteristics, such as waste form degradation and dissolution of solubility controlling mineral phases. For technetium-99, a matrix-degradation-rate-based empirical release model based on the results of the Single-Pass Flow-through experiments conducted on C-103, C-202, and C-203 tank residual waste. The experimental setup and analyses results are presented in PNNL-20616, "Contaminant Release from Hanford Tank Residual Waste – Results of Single-Pass Flow-Through Tests" and in Cantrell et al. 2013.

The presence of continuous water connections is assumed across the grout and concrete layers at the base of the tank for the diffusive transport to occur in the aqueous phase. As a result, the residual waste layer is conceptualized to overlie the 0.05-m (2-in.)-thick grout layer that is underlain by the 0.15-m (6-in.)-thick base slab concrete layer. The source term model represents the shortest possible vertical diffusive transport path length from residual waste layer to outside of the tank, which is the combined thickness of grout and base slab concrete layer of 0.2 m (8 in.). The diffusive area is taken to be the base area of the tank. The aqueous concentration of contaminants in the residual waste provides the upstream boundary concentration for diffusive transport with a zero concentration boundary being applied in the far-field (at the water table depth). A linear sorption isotherm (using a  $K_d$  approach) is also considered for determining sorption within the grout and concrete layer for various contaminants as they undergo diffusive (and advective) transport through the tank. For technetium-99, the  $k_d$  was set to 1 ml/g.

Specific details of the conceptual and mathematical models of source terms and associated model parameterization used in the PA for tank waste residuals are provided Section 6.2.1 and 6.3.1 of the RPP-ENV-58782, Rev. 0.

#### **4.4.2 Considerations for Past Tank Waste Leaks and Losses**

The source terms used to approximate the past tank waste leaks and losses at WMA Care input directly in STOMP input files as a constituent mass and associated water volume into the STOMP model at nodes representing the estimated location and duration of the occurrence of the leak. The specific details of the constituent masses, leak volumes, and durations associated with past waste leaks and releases are provided in Section 2.1 of RPP-RPT-59197, Rev. 0.

### **4.5 Parameterization**

As noted previously, no hydraulic property data are available for WMA C. Therefore, pedotransfer functions were developed to provide initial estimates of model parameters for the water content based model. The pedotransfer function-based parameter estimates were subsequently adjusted to yield results more consistent with data from Brown et al. (2006). Adjusted parameters were used with a scaling procedure to estimate spatially-distributed model parameters from the stochastic conditional simulation results for water content. These steps are described in the following subsections.

#### **4.5.1 Pedotransfer Functions for Water Retention Parameters**

Pedotransfer function (PTFs) are empirical correlation functions that relate hydraulic or other types of parameters to more easily measured, less expensive, and usually more prevalent surrogate data, such as average grain size and bulk density, among others (Pachepsky and Rawls, 2004). PTFs have also been developed using other grain size distribution metrics, including  $d_g$  and  $\sigma_g$  (Campbell 1974; Ward et al. 2006). PTFs tend to be site-specific, but Campbell (1974) suggested that the use of  $d_g$  and  $\sigma_g$  might allow for development of PTFs with broader applicability. Several alternative approaches have also been used for estimating water retention parameters from bulk density and grain size distribution data (Arya and Paris 1981; Arya et al. 1999).

Campbell (1974) demonstrated the use of the grain size metrics  $d_g$  and  $\sigma_g$  in estimating hydraulic parameters for soils. Ward et al. (2006) suggested that the ratio  $d_g/\sigma_g$ , which was referred to as the Fredle index (Lotspeich and Everest 1981), can be used to estimate hydraulic parameters and other types of parameters including specific surface area, cation-exchange capacity, and dispersivity. Although strong correlations were shown for Brooks and Corey (1964) type hydraulic parameters, Ward's correlations were developed using averages for 11 textural classes that are commonly used to categorize agricultural soils. Averaging the samples for each texture class, and then regressing the results for the class averages, significantly reduces the variability of the results relative to what would be obtained using data from individual samples. Agricultural soils also typically have much finer texture than most of the sediments found at Hanford. Exploratory analysis using data sets from the Sisson and Lu and IDF sites in the 200 East Area, and the Integrated Field Research Center (IFRC) site in the 300 Area at Hanford indicated that several other grain size distribution metrics, or combinations of metrics, are more well-correlated with

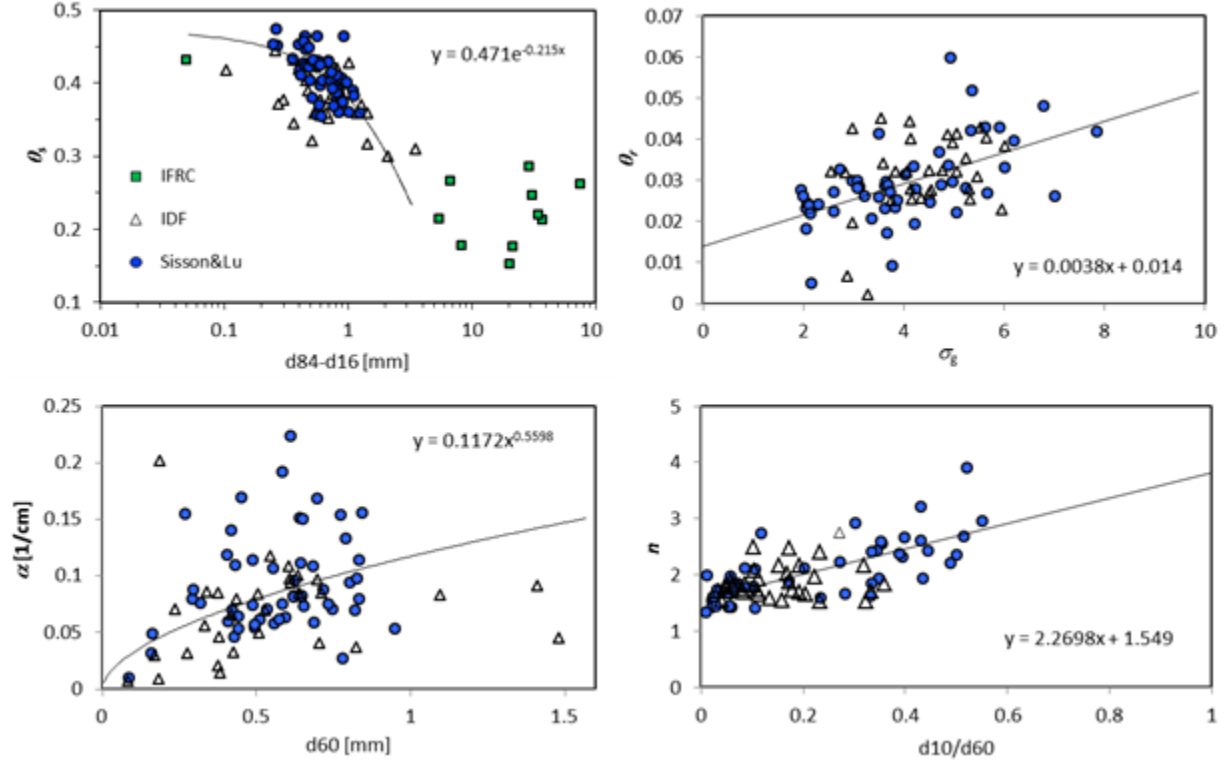
hydraulic parameters than is the Fredde index for these data sets. Using  $d_{16}$  as the effective grain diameter increases predicted  $K_s$  values by a factor of  $\sim 2$  relative to using  $d_{10}$ .

Figure 4.4 shows regression relationships for various grain size metrics and van Genuchten (1980) model water retention parameters. The  $\theta_s$  parameters shown in the upper left panel of are assumed to be equivalent to sample porosity. It is well known that porosity decreases as sediments become more poorly sorted (Yu and Standish, 1991). The difference between the  $d_{84}$  and  $d_{16}$  size metrics was found to be more strongly correlated with porosity than any other metric or combination of metrics evaluated, including  $\sigma_g$  for these Hanford sediment samples. The porosity values shown for the IFRC sediments represent mostly very coarse (gravel- and cobble-dominated) and poorly sorted sediments from the Hanford formation in the 300 Area, with the exception of one high-porosity sample from the Ringold U4 (silt) unit. It is assumed that some of the variability in porosity values for the IFRC site, and elsewhere, is affected by disturbance from sampling these unconsolidated and predominantly coarse sediments. The exponential function shown in Figure 4.4 appears to provide reasonable first estimates of porosity for a relatively wide range of sediment textures. The use of a lower truncation limit (e.g.,  $\sim 0.2$ ) is advised to prevent estimation of unrealistically low values of porosity for very poorly sorted sediments; i.e.,  $\theta_s = \max \{0.2, 0.471 \cdot \exp[-0.215 \cdot (d_{84} - d_{16})]\}$ . Note that the maximum porosity estimate that would be obtained from this equation is 0.471, which is close to the theoretical maximum of 0.476 that could be obtained for a cubic packing of uniform spheres (Bear 1971). Higher porosities are possible, however, for materials with non-spherical or angular particle shapes (e.g., silts and clays).

The other regression relationships in Figure 4.4 show considerable scatter, which is typical of PTFs, but they are assumed to provide reasonable first estimates of water retention parameters when only grain size distribution data are available. The residual water content,  $\theta_r$ , typically shows a relatively small range of variability, but increases in value as the sediment become more poorly sorted. The  $n$  parameter also typically has a relatively small range of variability relative to other parameters. The regression equation shown in Figure 4.4 for  $n$  indicates that as  $d_{10}/d_{60}$  (the reciprocal of the *uniformity coefficient*) approaches unity,  $n$  approaches a value of  $\sim 4$ . Larger  $n$  values have been fit for very uniform sands used in laboratory studies (Schroth et al. 1996), but it is rare to see  $n$  values greater than 4 in field-textured Hanford sediments (Khaleel and Freeman 1995). The regression relationship for the  $\alpha$  parameter shows more scatter. In the parametrization method described later in this report,  $\alpha$  parameters are scaled from reference values so that the resulting hydraulic parameters are consistent with field-measured water content and soil moisture tension data. It should be noted that although the data shown in Figure 4.4 show considerable scatter, when water retention data from many different samples are pooled and fit to estimate van Genuchten (1980) model parameters for use in equivalent homogeneous medium (EHM) representations of porous media (cf. Figures 3 and 5 of Khaleel and Freeman, 1995), such as that used for the base case PA model of WMA C, or parameters for tensorial pore connectivity-tortuosity models (cf. Figures 6.6 and 6.7 of Rockhold et al. 2015), there is typically also a lot of scatter in the water retention data.

An alternative to using PTFs for estimating hydraulic parameters at sites where no hydraulic property data are available would be to use a catalog of soil properties that contains both grain size distribution data and hydraulic parameters for the same sediment samples. Khaleel and Freeman (1995) developed such a database for soil samples evaluated in the 200 Areas of Hanford. Their reported grain size distribution data consist of mass fractions of sediment in five different size classes: gravel, coarse sand, fine sand, silt, and clay. These mass distribution data could be fit or interpolated to estimate size metrics

of interest, and then these metrics could be searched for the closest matches. The hydraulic parameters for the sample with the closest matched grain size distribution metrics could then simply be assigned to the sediment sample of interest. The use of regression-based PTFs is more compact, but both approaches are viable.



**Figure 4.4.** Correlation functions for grain size distribution metrics and van Genuchten (1980) model water retention parameters for sediment from the IDF, Sisson and Lu, and IFRC sites at Hanford. Coefficients of determination for the  $\theta_s$ ,  $\theta_t$ ,  $\alpha$ , and  $n$  regression relationships are 0.395, 0.322, 0.228, and 0.563.

#### 4.5.2 Hydraulic Conductivity

In addition to water retention parameters, estimates of the saturated hydraulic conductivity,  $K_s$ , are needed. The well-known Kozeny-Carman equation (Bear 1974) was used to estimate  $K_s$ :

$$K_s [cm / s] = \frac{\rho_w g}{\mu_w} \frac{d_{eff}^2}{180} \frac{\phi^3}{(1-\phi)^2} \quad (4.1)$$

where  $\rho_w$  is the density of water [0.9991 g/cm<sup>3</sup>],  $g$  is a gravitational constant [981 cm<sup>2</sup>/s] and  $\mu_w$  is the dynamic viscosity of water [0.011 g/(cm s)]. Porosities were estimated for use with the Kozeny-Carman equation using  $\theta_s$  values generated from the regression equation shown in Figure 4.4 (or adjusted values), and using  $d_{10}$  as the effective grain diameter. Comparisons of experimentally determined values of  $K_s$  with those estimated using equation 4.1 indicate that  $d_{eff}$  is closer to  $d_{10}$  or  $d_{16}$  than to  $d_g$ . Using  $d_{16}$  as the effective grain diameter increases predicted  $K_s$  values by a factor of ~2 relative to using  $d_{10}$ .

For sediments in the vadose zone,  $K_s$  is often assumed to be isotropic, but unsaturated hydraulic conductivity is well known to exhibit saturation-dependent anisotropy. Anisotropy ( $K_{xx}/K_{zz}$  or  $K_{yy}/K_{zz}$ ) increases as water content decreases and soil moisture tension increases. Saturation-dependent anisotropy can be estimated using the Polmann model (Polmann 1990; Khaleel 2004) or the tensorial connectivity-tortuosity (TCT) model (Zhang et al. 2003; Rockhold et al. 2015). The Polmann model was used for the EHM base case model developed for the PA effort. The TCT model was used for the alternative conceptual models described here. Both models effectively accomplish the same goal of generating soil moisture tension-dependent anisotropy, but the TCT model is considered to be more parsimonious (Rockhold et al. 2015). The Polmann and TCT models are usually used only with EHM-type models, for which small scale heterogeneities are not explicitly represented. The TCT model was also used here for both the facies and water content based models because the model grid block sizes are relatively large compared to the scale of some heterogeneities and to the scale of core and grab samples and geophysical logging measurements that form the basis for site characterization.

### 4.5.3 Parameter Adjustments

The regression relationships shown in Figure 4.4 can provide estimates of hydraulic parameters at the core sample scale, since the hydraulic properties used in the regressions were determined at that scale. However, to estimate parameters that are representative of larger scales, some type of upscaling is usually required. The PTF-based parameter estimates were used in conjunction with field-measured water content data and estimates of soil moisture tension measured on borehole samples to generate initial estimates of hydraulic parameters for the model grid block scale. It is expected that the resulting heterogeneity in hydraulic parameters at the grid block scale, which are conditioned on field measured water content, will manifest behavior that is similar to that observed at larger field scales. However, the PTF-based parameter estimates were subsequently revised to produce water content results that are more consistent with the data from Brown et al. (2006).

The median values of the  $d_g$  and  $\sigma_g$  parameters shown in Table 3.2 were used with the regression relationships shown in Figure 4.4 to estimate van Genuchten (1980) model water retention function parameters for each major hydrostratigraphic unit. The parameter estimates are shown in Table 4.1 under the headings “PTF.” Also shown are parameters that were adjusted (“Adj.”) to better fit the data from Brown et al. (2006) using an analytical solution for 1-D steady vertical water flow (Rockhold et al. 1997). However, no attempt was made to optimize model parameters owing to uncertainty in the reported values of soil moisture tension from Brown et al. 2006. The data and analytical solution results are shown in Figure 4.5. The  $K_s$  values in Table 4.1 were estimated with the Kozeny-Carman equation using the PTF-predicted and adjusted porosities and with  $d_{10}$  as the effective grain diameter.

Calculations were performed with the analytical solution technique for a recharge rate of 3.5 mm/yr, which was assumed to be representative of relatively undisturbed conditions, and for a recharge rate of 100 mm/yr, which may be representative of the range of higher recharge rates for disturbed areas, including the un-vegetated, gravel-covered, backfilled region surrounding the tanks (Fayer and Szecsody 2004). The results from the analytical solution are compared in Figure 4.5 with water content and soil moisture tension data from samples collected from borehole C4297, and well 299-E27-22 (C4124) from Brown et al. (2006). Borehole C4297 was located immediately adjacent to tank C-105, inside the WMA C fence line, and well 299-E27-22 is located just outside the fence line. The data from these two locations show that conditions are wetter inside the tank farm.

Gravimetric water contents rather than volumetric water contents were reported by Brown et al. (2006). The gravimetric data were converted to volumetric water content by multiplying by bulk density values that were estimated using the PTF-based or adjusted porosity estimates and an assumed particle density of  $2.72 \text{ g/cm}^3$ . This particle density is the average of 14 particle densities measured for sediment samples from well 299-E25-234, which is located within the former Grout Treatment Facility landfill (Rockhold et al. 1993; Table A.2), located to the southeast of WMA C. If porosity estimates were adjusted,  $K_s$  estimates were also recomputed using the Kozeny-Carman equation.

No property estimates were needed for unit H3 for this comparison with the data of Brown et al. (2006) because C4297 is relatively shallow and the H3 unit was not encountered at that location. The Cold Creek/Ringold Formation sediments were encountered at an elevation of  $\sim 123 \text{ m}$  in 299-E27-22, but the water table is located at an elevation of  $\sim 121 \text{ m}$ , so this small section of the lower units was assumed to be the same as the H2 unit at this location. The nature of the contact between the H2 unit and the H3 unit and other units found at similar depths such as the Cold Creek (CCu) and Ringold Formation (R), and the sparsity of data is such that these lower units tend to be grouped (i.e., interpreted as an undifferentiated H3/CCu/R unit) for vadose zone and groundwater flow and transport modeling at WMA C. Based on the available water content data from both WMA C and the A- AX tank farms, and the initial PTF-based estimates of hydraulic parameters, the hydraulic properties of the H3 unit are assumed to be very similar to the H1 unit.

Most of the PTF-based parameter estimates shown in Table 4.1 are within the range of reported parameter estimates for similar materials at the IDF site (Rockhold et al. 2015). The adjustments required to get better fits to the field data are relatively small for most of the parameters, but again no attempt was made to optimize parameters. However, the estimated upscaled value of  $\theta_s = 0.174$  for the gravel sequence at the IDF site (Rockhold et al. 2013) is significantly lower than the PTF-based estimates of porosity for the H1 (0.33) and H3 (0.32) units. The data for samples with high gravel content that were used to represent the IDF site in Khaleel (2004) were not actually from the IDF site, because no data from the H3 unit were available for IDF. The gravel samples used to represent the gravelly sequence at IDF were actually from the 100 and 300 Areas (Rockhold et al. 2015). It may be of interest to note that the estimated porosity (or saturated water content) values for the upper and lower “gravel” units of the Hanford formation reported by Connelly et al. 1992 and Rockhold et al. 1988 (mean  $\theta_s = 0.358$ ) are more similar to the PTF-based porosity estimates than to those estimated for the IDF site. Nevertheless, the lower adjusted values of  $\theta_s$  used here provide reasonable parameter estimates, within the range of measured values for gravel-dominated sediments at Hanford.

The estimated upscaled values of  $n$  for the sand ( $n = 1.698$ ) and gravel ( $n = 1.271$ ) sequences at the IDF site are also significantly less than the PTF-based estimates for the  $n$  parameter for WMA C sediments shown in Table 4.1. This difference is in part a consequence of upscaling to determine effective parameters for IDF. The  $n$  parameters that were adjusted to get better fits to the WMA C field data are more similar to the values obtained from fitting of IDF core water retention data to estimate effective parameters for that site.

**Table 4.1.** PTF-based estimates of van Genuchten (1980) model water retention parameters, vertical saturated hydraulic conductivity,  $K_{szz}$ , and pore-interaction term,  $\ell_{zz}$ , for the major hydrostratigraphic units underlying WMA C, and adjusted parameter estimates fit to field data from Brown et al. (2006).

Unit	Parameter											
	$\theta_s$		$\theta_r$		$\alpha$ [1/cm]		$n$		$K_{szz}$ §[cm/s]		$\ell_{zz}$	
	PTF	Adj.	PTF	Adj.	PTF	Adj.	PTF	Adj.	PTF	Adj.	PTF	Adj.
Backfill	0.293	- <sup>†</sup>	0.027	-	0.114	-	1.887	1.74	5.07E-3	-	0.5	0.1
H1	0.330	0.2	0.025	-	0.106	0.12	1.983	1.60	1.03E-2	1.60e-3	0.5	-1.2
H2	0.367	-	0.025	-	0.089	0.14	2.009	1.80	9.40E-3	-	0.5	-0.2
H3	0.320	N/A	0.028	N/A	0.100	N/A	1.870	N/A	4.00E-3	N/A	0.5	N/A

<sup>†</sup> “-” indicates that no parameter adjustments were made.  
<sup>§</sup>  $K_s$  estimate from Kozeny-Carman equation using  $d_{10}$  as the effective grain diameter. Estimated  $K_s$  increases by factor of ~2x using  $d_{16}$  as the effective diameter.  
N/A indicates not applicable because no other information was available for the H3 unit in Brown et al. 2006.

The  $\ell_{zz}$  parameter in Table 4.1 is a pore interaction term in the Mualem (1976) unsaturated hydraulic conductivity model that is often assumed to equal 0.5 as a default. The value 0.5 is an average determined by Mualem (1976) for the samples that he analyzed. Significant adjustments to this default value were required to get better matches to the data from Brown et al. 2006. A wide range of  $\ell$  parameters have actually been reported in the literature (Rockhold et al. 2015; Table 6.2) but a value of  $\ell=0.5$  is typically assumed if no data on unsaturated hydraulic conductivity are available. Rockhold et al. (2015) also discuss the use of tensorial pore interaction terms for representing anisotropy in unsaturated hydraulic conductivity.

Different average values of hydraulic parameters for WMA C site materials would likely be obtained if PTF-based estimates were made for each individual sediment sample, and if those estimates of hydraulic parameters were then averaged. Another alternative would be to generate discrete water retention and unsaturated hydraulic conductivity values using the PTF-based hydraulic parameter estimates for individual samples, and then simultaneously fit the discrete hydraulic property values to estimate effective parameters, similar to the approach used to estimate van Genuchten (1980) model parameters for use with EHM-type models. The approach taken depends on how the parameter estimates will be used. The parameter adjustments made to achieve better correspondence between calculated and observed water content and soil moisture tension data with the analytical solution essentially constitute a form of upscaling, to estimate effective parameters for the sediment profile under assumed vertical flow conditions.

The measured water content data from inside and outside the tank farm are similar but water content values inside the tank farm are larger. Lower soil moisture tension values also occur inside the tank farm, which is consistent with the higher water contents (Brown et al. 2006). The difference in soil moisture tensions inside and outside the tank farm could potentially create a driving force for lateral flow away from the tank farm. However, as shown in Figure 4.5, the differences in the soil moisture tension profiles decrease with depth, suggesting that the localized higher water contents and a potential lateral flow component diminishes with depth such that a more uniform areal distribution of flux at depth would be expected. Brown et al. (2006) also discussed evidence that suggests the background well (299-E27-22) had been affected by a non-radioactive waste stream.

The soil moisture tension data shown in Figure 4.5 exhibit significant short-range variability, some of which may be experimental error associated with the filter paper method that was used to generate the data (Brown et al. 2006). The merging of the soil moisture tension data for the 299-E29-22 well and borehole C4297 at several elevations (e.g., ~186 and ~178 m), and concomitant spikes of higher water content at these elevations, may indicate the potential for lateral flow at the interfaces between both the backfill and H1 units, and between the H1 and H2 units under the tank farm. A similar effect is also seen at an elevation of ~168 m. Higher water contents at the interface between the backfill and H1 units could also be primarily associated with compacted sediments found at the base of the pit that the tanks were constructed on prior to backfilling around them. The variability in water content data is less than the soil moisture tension data, but several high-value water content spikes in the data set are notable. These thin zones of higher water content usually indicate areas of finer-textured sediment.

For comparison with Figure 4.5, in situ measurements of soil moisture tension in backfill sediments from the upper 10 m of an interim surface barrier demonstration site at the T tank farm in the 200 West Area range from near zero up 342 cm of tension, with this variability reflecting seasonal fluctuations in weather. Temporally-averaged values from the T tank farm site range from 118 to 316 cm of tension, depending on the location of the instrument nest (Zhang et al. 2009). These measurements at the T tank farm would be in the equivalent of what is backfill material at WMA C. Either set of hydraulic parameters noted above for WMA C produces this approximate range of soil moisture tension values for the backfill portion of the sediment profile for recharge rates that should be representative of conditions inside the tank farm. It should be evident from this discussion that the in situ water content distribution in the subsurface reflects both the physical and hydraulic properties of the sediment, as well as the predominant water flux conditions.

Using uniform hydraulic properties for each of the three major units that are represented here (i.e., backfill, H1, and H2 units) produces relatively smooth predicted soil moisture tension and water content profiles. Figure 4.6 shows plots of the PTF-based water retention and unsaturated hydraulic conductivity curves that are produced from the van Genuchten (1980) water retention and Mualem (1976) unsaturated hydraulic conductivity models for the parameters used in the analytical solution (Table 4.1). The curves representing the adjusted parameters are also shown. The horizontal lines shown in Figure 4.6 represent different assumed recharge rates. The intersection points of these horizontal lines with the unsaturated hydraulic conductivity curves can be used to estimate the soil moisture tension and corresponding water content values that would be expected for each recharge rate under unit hydraulic gradient conditions. Parameter adjustments (“adj.” in Table 4.1) were made by comparing predicted water content and soil moisture tension values with observed data for both borehole/well locations. The process of adjusting model parameters to achieve closer correspondence to the field data results in a set of “effective” parameters. These effective parameters capture the average character of the observed water content and soil moisture tension data for assumed steady vertical flow conditions over the profile. However, possible lateral flow is not considered in these calculations.

With the hydraulic parameters that are shown, the analytical solution produces travel time estimates from ground surface to the water table for a recharge rate of 100 mm/yr of ~57 years. The travel time increases if the assumed values of  $K_s$  are decreased. The estimated travel time also increases to several hundred years when the recharge rate is reduced from 100 to 10 mm/yr. Given the multi-dimensional nature of the problem, there are obvious limitations to the use of a 1-D model for interpreting these field data. Diversion of water above and around finer-grained sequences of sediments would likely result in increased travel times to the water table relative to the 1-D calculations owing to increased transport

distance. However, a waste loss event of any significant volume could easily shorten the travel time by preferential downward flow through larger pore channels.

The soil moisture tension data reported by Brown et al. (2006) clearly show that the soil water energy status is different between the borehole located adjacent to the C-105 tank (C4297), and the borehole/well located outside the fence line (299-E27-22). However the accuracy of the soil moisture tension data is uncertain. These measurements are susceptible to error associated with sample handling. Specifically, if a sample is not handled and sealed quickly during placement of the filter paper, and/or if the filter paper is not processed quickly following opening of the sealed sample after it equilibrates, evaporative drying may occur. This could lead to higher calculated soil moisture tension values than are actually present in the in situ sediment. A number of soil moisture tension data values reported by Brown et al. (2006) were greater than what is theoretically possible for zero-flux conditions (data omitted from Figure 4.5). Therefore it was assumed that there is some error associated these data and alternative estimates of average soil moisture tension were used to represent each major geologic unit.

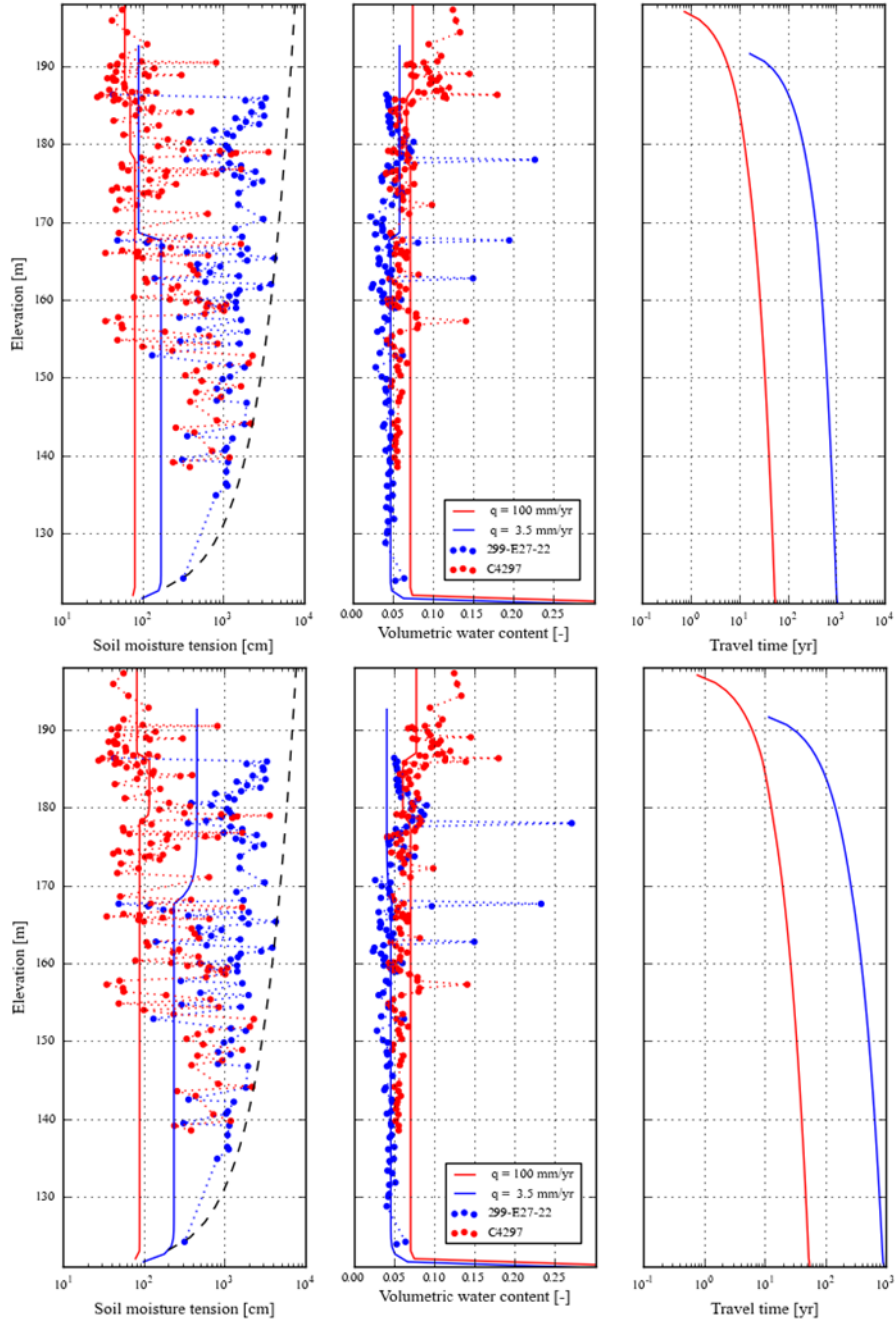


**Figure 4.5.** Analytical solution results for 1-D steady vertical flow using PTF-based hydraulic parameters (top), and adjusted parameters (bottom). Symbols represent data from Brown et al. (2006). The dashed line shows theoretical soil moisture tension results for zero flux conditions.

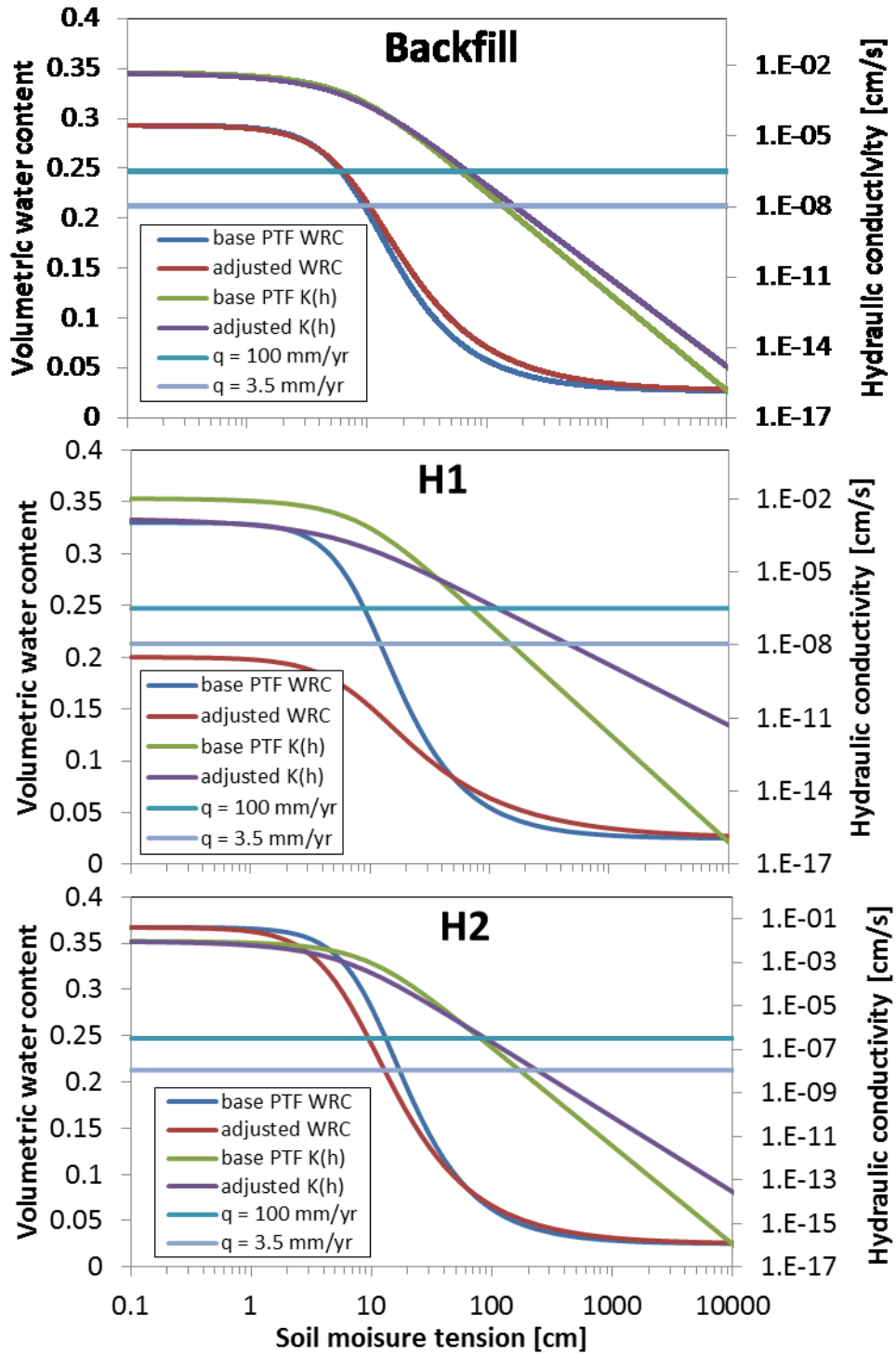


**Figure 4.6.** Water retention (WRC) and unsaturated hydraulic conductivity (K(h)) curves generated with parameters developed from PTFs using grain size distribution metrics, and parameters adjusted to provide better matches to water content and soil moisture tension data from Brown et al. (2006). Horizontal lines represent different recharge rates.

#### 4.5.4 Scaling

Select water content data from WMA C and the A-AX tank farms were used to generate stochastic conditional simulations of water content distributions over the 95 to 210 m elevation interval. The conditional simulations were performed using uniform 5-m spacing in the x-y directions, and 0.5-m spacing the vertical direction using the variogram model parameters from Appendix A. Volume averaging was used to compute water content values for each grid block in the non-uniform STOMP model grid. Hydraulic parameters for individual model grid blocks were then estimated from water content using the method described below.

Reference hydraulic parameters and soil moisture tension values were defined for each major geologic unit, based in part on the data from Brown et al. (2006) and results from the 1-D analytic solution. The reference hydraulic parameters are denoted  $K_{szz}^*$ ,  $\theta_s^*$ ,  $\theta_r^*$ ,  $\alpha^*$ ,  $n^*$ , and  $\ell_{zz}^*$ , and the reference soil moisture tension is,  $h_{ref}$  (Table 4.2). Ideally,  $h_{ref}$  would be determined by field measurements, but as shown in Figure 4.5 and discussed earlier, such measurements are typically noisy and are notoriously prone to error. Therefore values of  $h_{ref}$  were estimated in part based on the field observations, and in part based on expert judgement (similar to the approach used by Khaleel (2004) for estimating the tension value used in calculating parameters for the Polmann model of anisotropy). Subscripts  $xx$ ,  $yy$ , and  $zz$  denote the principal components of tensor variables in the horizontal and vertical directions. The parameterization method proceeds as follows.

A scale factor for soil moisture tension,  $f_h$ , is defined as

$$f_h = \frac{h^*}{h_{ref}} \quad (4.2)$$

where  $h^*$  is the soil moisture tension predicted for any given field-measured (or stochastically simulated) water content using the reference hydraulic parameters. The value of  $h^*$  is calculated from water content using van Genuchten's equation:

$$h^* = \frac{1}{\alpha^*} (S_e^{-1/m} - 1)^{1/n^*} \quad (4.3)$$

where  $S_e$  is the effective saturation defined as

$$S_e = \frac{(\theta - \theta_r)}{(\theta_s - \theta_r)} \quad (4.4)$$

and  $m = 1 - 1/n^*$ . The van Genuchten (1980) model  $\alpha$  parameter and  $K_{szz}$  are estimated as

$$\alpha = f_h \cdot \alpha^* \quad (4.5)$$

and

$$K_{szz} = K_{szz}^* \cdot f_h^2 \quad (4.6)$$

based on similar media scaling theory (Miller and Miller 1956; Rockhold et al. 1996). The parameters  $\theta_s^*$ ,  $\theta_r^*$ ,  $n^*$ , and  $\ell_{zz}^*$  are assumed constant for each of the major geologic units (backfill, H1, H2, H3). Values of  $\ell_{xx}^*$  and  $\ell_{yy}^*$  were adjusted for the backfill and H2 units to yield anisotropy ratios for unsaturated conditions that are comparable to those determined for the IDF site (Rockhold et al. 2015). Separation into more hydrologically distinct units for vadose zone flow and transport modeling might also be accomplished by applying thresholds to the conditionally simulated water content fields, to better distinguish between regions with different texture and hydraulic properties (e.g., higher water content for fine sand and silt, and lower water content for coarser sand and gravel). However, using the major geologic units provides a tie to the interpreted stratigraphy that was used for development of the geologic framework model.

**Table 4.2.** Reference hydraulic parameters for water content-based parameterization of WMA C model.

Reference parameters	Geologic unit			
	Backfill	H1	H2	H3 <sup>†</sup>
$\theta_s^*$	0.293	0.2	0.367	0.2
$\theta_r^*$	0.027	0.025	0.025	0.025
$\alpha^*$ [1/cm]	0.114	0.12	0.14	0.12
$n^*$	1.74	1.6	1.8	1.6
$K_{sxx}^*$ [cm/s]	5.07e-3	4.79e-3	9.4e-3	4.79e-3
$K_{syy}^*$ [cm/s]	5.07e-3	4.79e-3	9.4e-3	4.79e-3
$K_{szz}^*$ [cm/s]	5.07e-3	1.6e-3	9.4e-3	1.6e-3
$\ell_{xx}^*$	0.1	-1.2	-1.0	-1.2
$\ell_{yy}^*$	0.1	-1.2	-1.0	-1.2
$\ell_{zz}^*$	0.5	-1.2	-0.2	-1.2
$h_{ref}$ [cm]	180	446	245	446

<sup>†</sup>Parameters for H3 assumed to be the same as those for H1.

After determining  $K_{szz}$  as described above,  $K_{sxx}$  (and  $K_{syy}$ ) were estimated from

$$K_{sxx} = K_{szz} \frac{K_{sxx}^*}{K_{szz}^*} \quad (4.7)$$

Values of  $K_{sxx}$ ,  $K_{syy}$ ,  $\ell_{xx}$  and  $\ell_{yy}$  shown in Table 4.2 were selected to produce anisotropy ratios that are similar to what was estimated for the sandy and gravelly sediments at the IDF site (Rockhold et al. 2015).

Ideally, the parameterization steps in Equations (4.2-4.6) should be applied to water content values generated on a very high-resolution grid, with grid spacing comparable to the vertical spacing of borehole measurements (15 cm or less), and using reference hydraulic parameters determined at the core scale. In lieu of actual hydraulic property data for core samples from WMA C, the PTF-based parameter estimates could be used. The resulting parameters should then be upscaled to the model grid block scale using an approach like that described Rockhold et al. (2015) that was used at the IDF site, but over each model grid block, or a similar alternative method. This intermediate upscaling step was omitted here owing to complications associated with the water content data (discussed in Appendix A) and the adjusted parameters were used directly with the upscaled water content values.

Figure 4.7 shows a reference water retention curve for the H2 unit (blue line) and scaled water retention curves. For the reference curve, a value of  $h_{ref} = 245$  cm yields a volumetric water content value of  $\theta \approx 0.046$ , which is consistent with the water content data from the H2 unit in well 299-E27-22 (Brown et al. 2006). The reference value used here for the soil moisture tension is less than the filter paper data, but we assume the filter paper data may be biased toward the dry side. The scaled curves in Figure 4.7 correspond to volumetric water content values of  $\theta = 0.08$ , and  $\theta = 0.03$ . The scaling process determines the value of  $\alpha$  required to yield any given value of  $\theta$  at  $h_{ref}$ . The  $K_s$  values are also scaled accordingly. This procedure was used to estimate spatially distributed model parameters for the WMA C model domain based on stochastic conditional simulation of selected field-measured volumetric water content data (Appendix A).

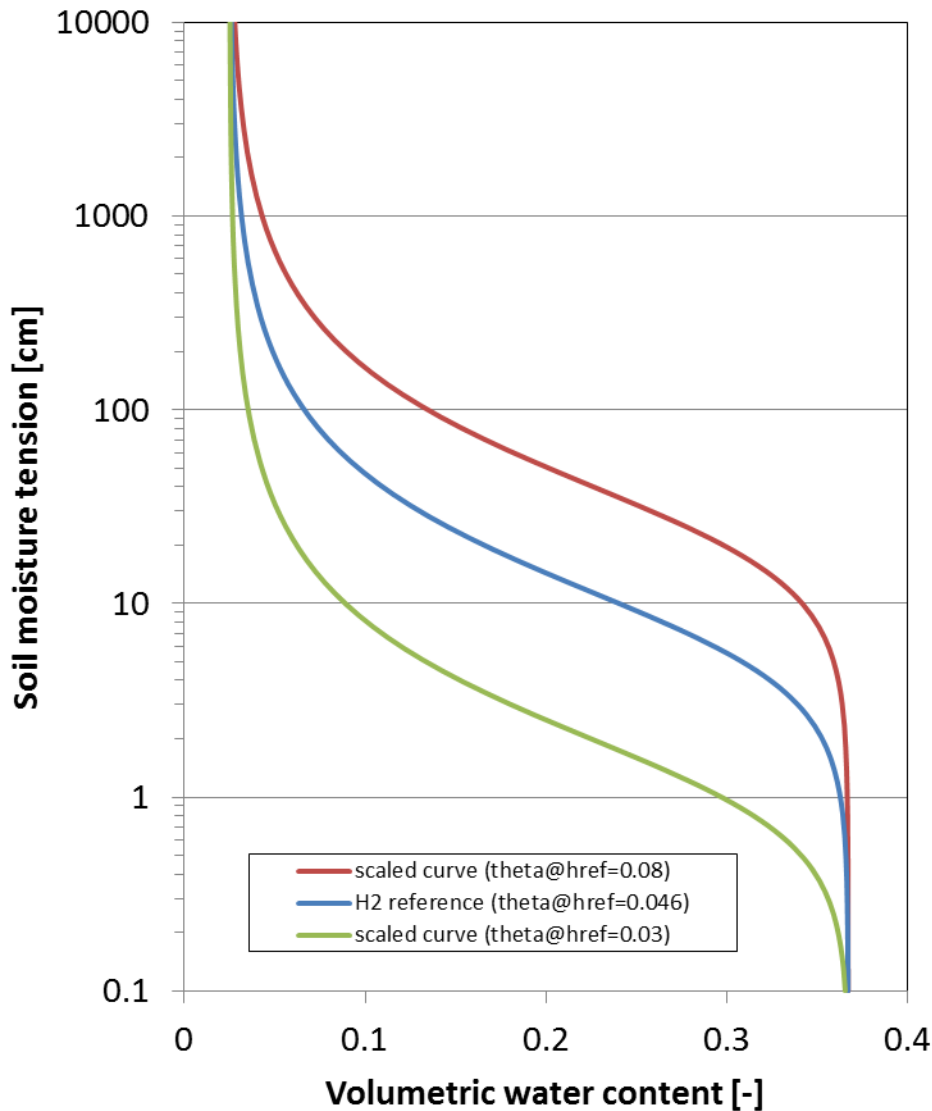


**Figure 4.7.** Reference water retention curve for unit H2 and scaled curves required to obtain the given values of water content at the reference soil moisture tension.

#### 4.5.5 Parameterization of Facies Models

Hou et al. (2015) grouped the Hanford fm sediments underlying WMA C into three primary facies classes based on clustering of spectral gamma log data. Facies 1 was described as mixed sediments consisting of both sandy and gravelly materials, and is the predominant facies within the H2 coarse sand subunit of the Hanford fm. Facies 2 was described as being gravel dominated, and is the predominant facies within the H1 gravelly subunit of the Hanford fm. Facies 3 is sand dominated and is the predominant facies within the H2 sandy subunit of the Hanford fm (see Figures 3.2 and 4.9). Hydraulic parameters for the facies-based models were based initially on parameter estimates from Rockhold et al. (2015) for sediments at the IDF site. Manual adjustments were then made to better match the water content data from Brown et al. (2006).

Figure 4.8 shows data from Brown et al. (2006) with computed steady state pressure head and water content profiles generated with the analytical solution of Rockhold et al. (1997) using the manually adjusted parameters. The hydraulic parameters assigned to the backfill and facies for the facies-based models are listed in Table 4.3. The hydraulic parameters assigned to the backfill were the same as those assigned to facies 1 (mixed sandy and gravelly sediments). A lower recharge rate of 0.3 mm/yr was used to represent undisturbed area outside the tank farm with the analytical solution.

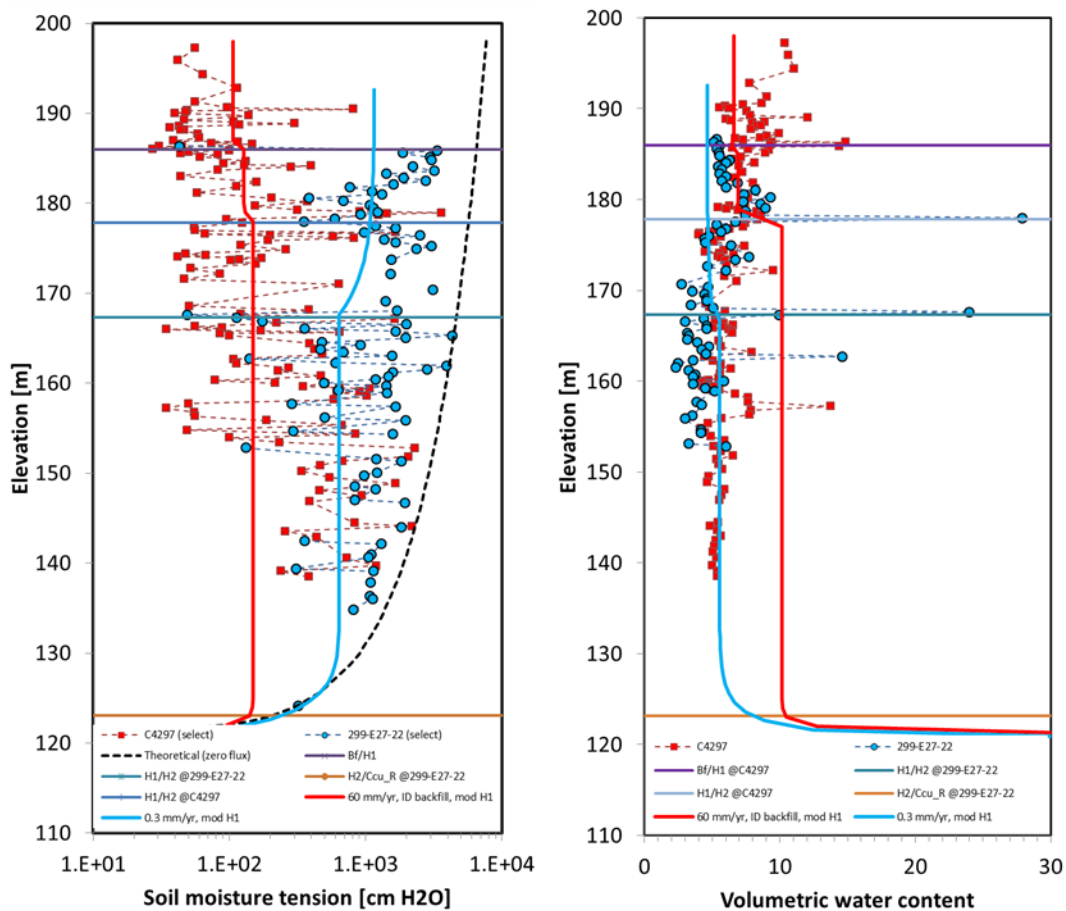


**Figure 4.8.** Soil moisture tension and water content profiles computed using a steady-state analytical solution and data from Brown et al. (2006).

**Table 4.3.** Hydraulic parameters for facies-based parameterization of WMA C models.

Parameter	Geologic unit			
	Backfill	Facies 1	Facies 2	Facies 3 <sup>†</sup>
$\theta_s$	0.34	0.34	0.178	0.284
$\theta_r$	0.03	0.03	0.03	0.029
$\alpha$ [1/cm]	0.081	0.081	0.178	0.03
$n$	2.18	2.18	1.4	1.898
$K_{sxx}$ [cm/s]	1.56e-3	1.56e-3	7.71e-3	6.2e-3
$K_{syy}$ [cm/s]	1.56e-3	1.56e-3	7.71e-3	6.2e-3
$K_{szz}$ [cm/s]	1.56e-3	1.56e-3	7.71e-3	6.2e-3
$\ell_{xx}$	0.8	0.8	-0.54	-0.6
$\ell_{yy}$	0.8	0.8	-0.54	-0.6
$\ell_{zz}$	0.5	0.5	-1.0	-0.5

<sup>†</sup>Parameters for backfill assumed to be the same as those for Facies 1.

The lower recharge rate of 0.3 mm/yr used in the analytical solution is consistent with rates reported by Fayer and Szecsody (2004) for relatively undisturbed areas with native shrub-steppe vegetation around the IDF site. The higher rate of 3.5 mm/yr used for flow and transport simulations with the base case PA and alternative models was intended to provide conservative transport results within the range of uncertainty in recharge rates.

Both the facies- and water content-based models used a TCT model for tension-dependent anisotropy (Zhang et al. 2003; Rockhold et al. 2015), for which the directional pore-interaction terms  $\ell_{xx}$ ,  $\ell_{yy}$ , and  $\ell_{zz}$  are used. The values of  $\ell$  listed in Table 4.3 were selected to yield anisotropy ratios for unsaturated hydraulic conductivity that are similar to those calculated for the IDF site (Rockhold et al. 2015). As noted previously, although some degree of heterogeneity is incorporated into the facies and water content based models, the scales of model grid blocks that are grouped into facies regions, as well as the scales of individual model grid blocks, are large relative to the scale of some heterogeneities in the subsurface (e.g. thin layers or lenses), and to the scales of the core and grab sample and geophysical log data that form the initial basis for model parameterization. Therefore the TCT model of anisotropy was used with the facies and water content based models to account for anisotropy induced by smaller (than grid block) scale heterogeneities.

## 4.6 Overview of Conceptual Models

Flow and transport simulations were performed with eSTOMP using three different types of conceptual models of the subsurface at WMA C. The first model represents the deterministic PA base case generated in the WMA C PA effort and documented in RPP-ENV-58782 (2106). The second model represents lithofacies that were generated by stochastic conditional simulation of clustered spectral gamma log data from boreholes and wells in and around WMA C (Hou et al. 2015). Results from two realizations of the lithofacies distributions are presented. The third model utilizes continuously variable parameter fields estimated from the conditionally simulated water content data from both WMA C and A-AX tank farms. Additional information on geostatistical analysis of water content data is provided in Appendix A.

The facies- and water content-based models were both generated using stochastic methods. Multiple realizations with equal probability of being drawn have been generated and can be used to produce an ensemble of results for use in uncertainty analysis. However, uncertainty assessment was beyond the scope of the current effort.

The PA base case model and one realization of a facies-based model are depicted in Figure 4.9. A total of 100 realizations of the facies-based model were generated by Hou et al. 2015, but results from just two realizations are presented here. Note that for the facies based models, facies distributions were produced only for the Hanford formation sediments because of insufficient geophysical log data at deeper depths. Therefore the same layering structure and material property assignments used for the PA base case model were used in the facies model for the deeper (non-Hanford fm) units. The material distributions shown in Figure 4.8 were used for steady-state (pre-Hanford) simulations. All three conceptual models assumed the tanks were not present in the steady state simulation. Backfill properties were assumed for this region.

The hydraulic parameters for the water content-based model (Figure 4.10) were generated using conditional simulation of water content and the scaling method described previously. Note that the material regions for the water content-based model cannot be displayed like those shown in Figure 4.9. Each grid block in the upper two-thirds of the domain for the water content-based models has different properties and is effectively a different material type.

All models used the same grid, upper boundary conditions, and source terms. All models also used the same properties for the regions named “aquifer” and “H3 gravelly sand” in the PA base case model (see lower two green-colored units in Figure 4.10), since this region of the domain has very sparse data. The “aquifer” unit is the lowest unit of the PA base case model that overlies the (inactive) basalt. The “H3 gravelly sand” is the layer immediately above it. Both of these regions are located below the water table. The models were run for the same time sequences: pre-Hanford (steady state), operational (1945.5-2020), and post-closure (2020-12020). Steady state results were used as initial conditions for operational period simulations. Results from the end of the operational period simulations were used as initial conditions for post-closure period simulations.

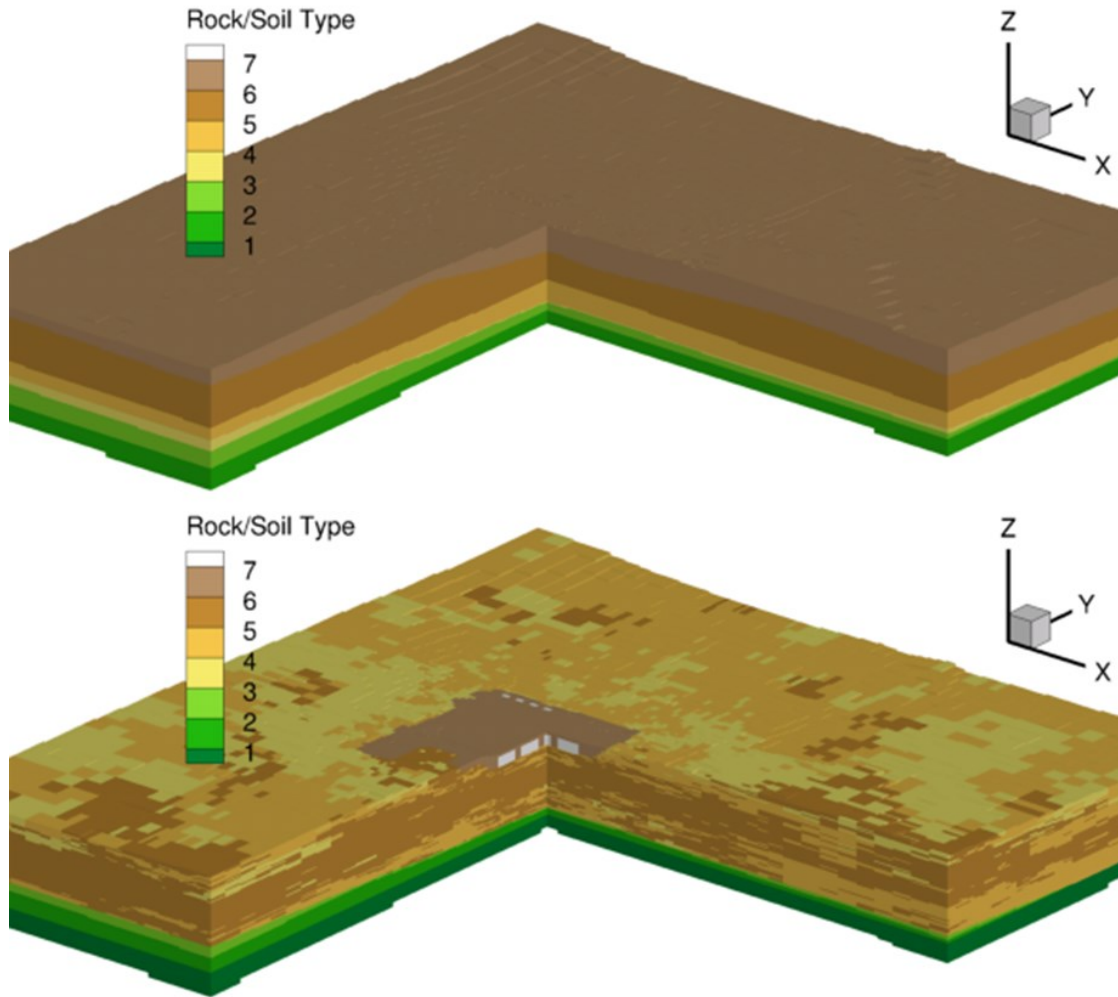


**Figure 4.9.** Cutaway view showing material regions for the PA base case model (top) and one realization of a lithofacies model (bottom) for WMA C.

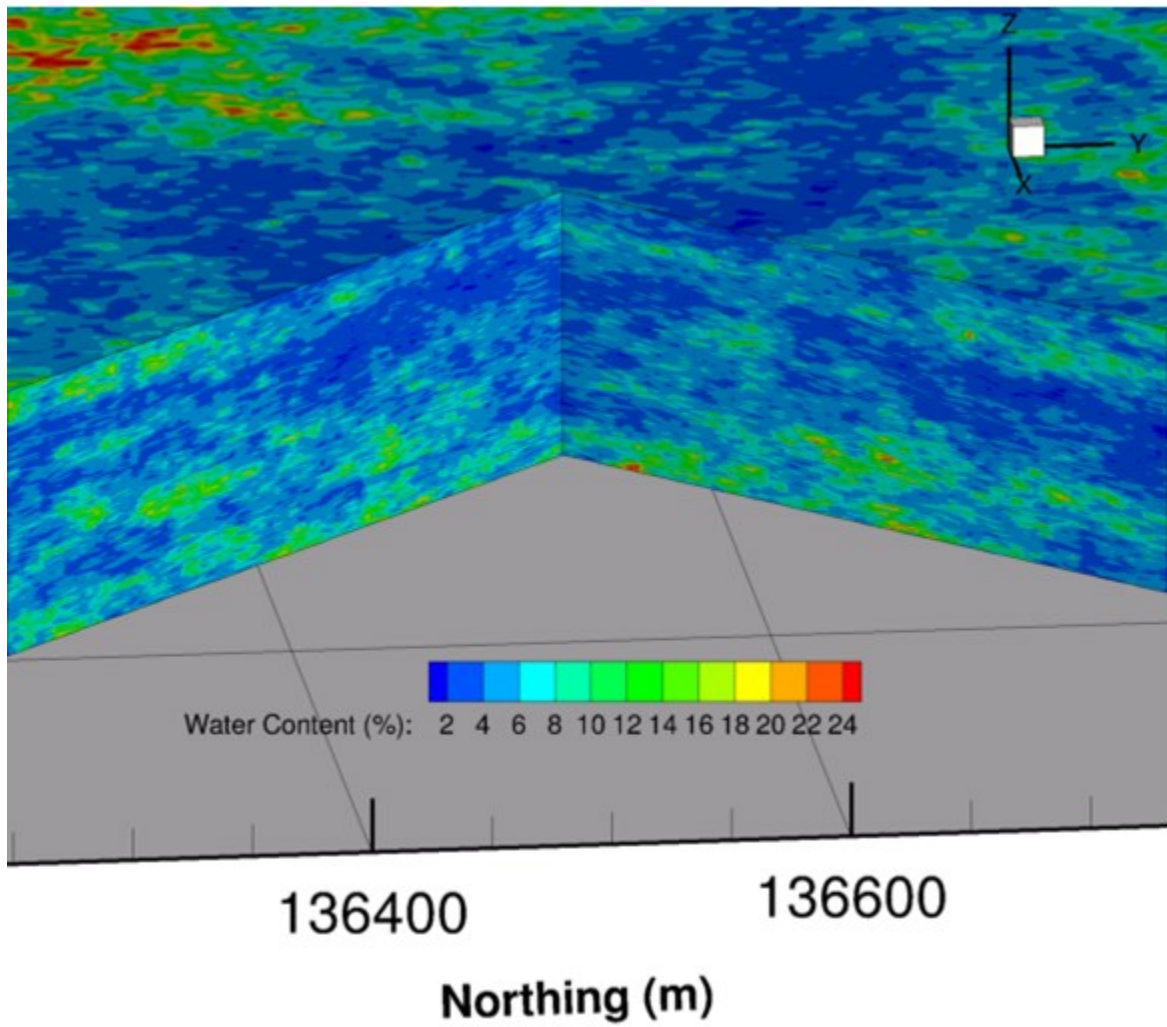


**Figure 4.10.** Zoomed image of one water content realization (001) used for parameterization of the WMA C model domain. The vertical elevation extent shown is 95-210 m.

## 5.0 Simulation Results

### 5.1 Simulations of Releases from Tank Residuals

Figure 5.1 shows oblique views of the aqueous saturation distributions at year 2020 (end of operational period) for the four conceptual models; i.e., the PA base case model, two realizations of the facies-based model (facies 003 and 004), and the water content-based model (theta 001). All four sets of water content results that are shown are similar to field measurements in terms of the magnitude of the water content values which range from  $\sim 4 - 8$  volume percent for most of the profile (Brown et al. 2006). The spatial variability of simulated water contents is greatest for the water content-based model and lowest for the base case PA model owing to different representations of heterogeneity (grid block vs hydrostratigraphic unit scales). Differences in water content and saturation distributions in the vicinity of the tanks are a result, in part, of the tank regions being treated as inactive cells in the base case PA model, and as active but very low permeability ( $K_s=1 \times 10^{-16}$  cm/s) cells in the two other models.

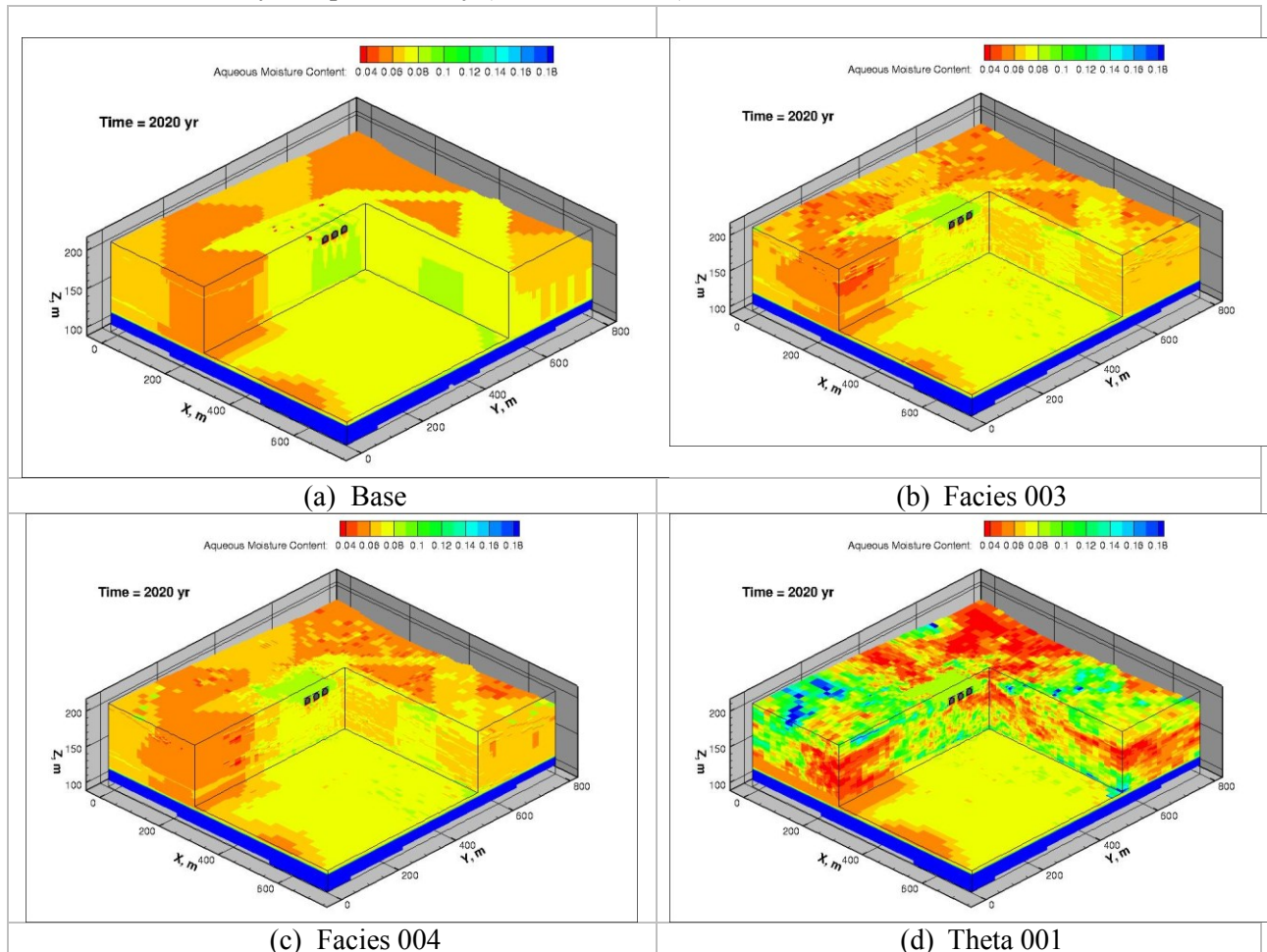


**Figure 5.1.** Oblique cutaway views of moisture content distributions at year 2020 for the four conceptual models of WMA C tank residual.

For the post-closure period, simulations were performed for transport of Tc-99 from release of tank waste residuals in C-105, with Tc-99 being modeled as a conservative tracer. Figure 5.2 and Figure 5.3 show the cutaway view of the concentration distribution of Tc-99 from C-105 in (arbitrarily chosen) years 3280 and 3680, respectively.

Figure 5.4 shows the flux-averaged concentration breakthrough curves and Table 5.1 shows the peak concentration and arrival time for different positions along a 100-m down-gradient monitoring plane for the four conceptual models. The lines shown in Figure 5.4 represent different locations, or points of calculation (PoC), along the 100-m down-gradient monitoring plane.

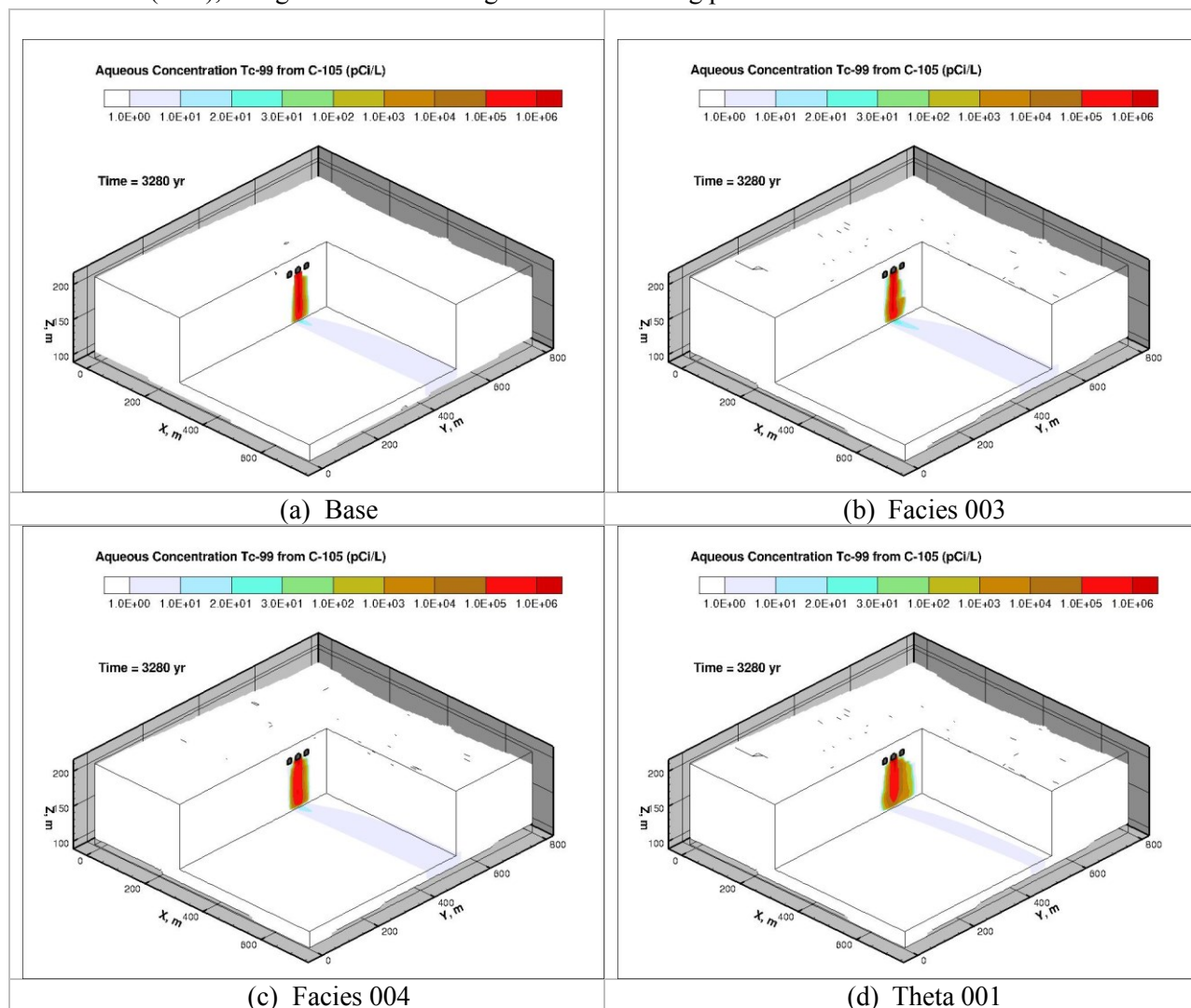


**Figure 5.2.** Oblique cutaway views of the distributions of aqueous Tc-99 from C-105 at year 3280 for the four conceptual models of WMA C tank residual.

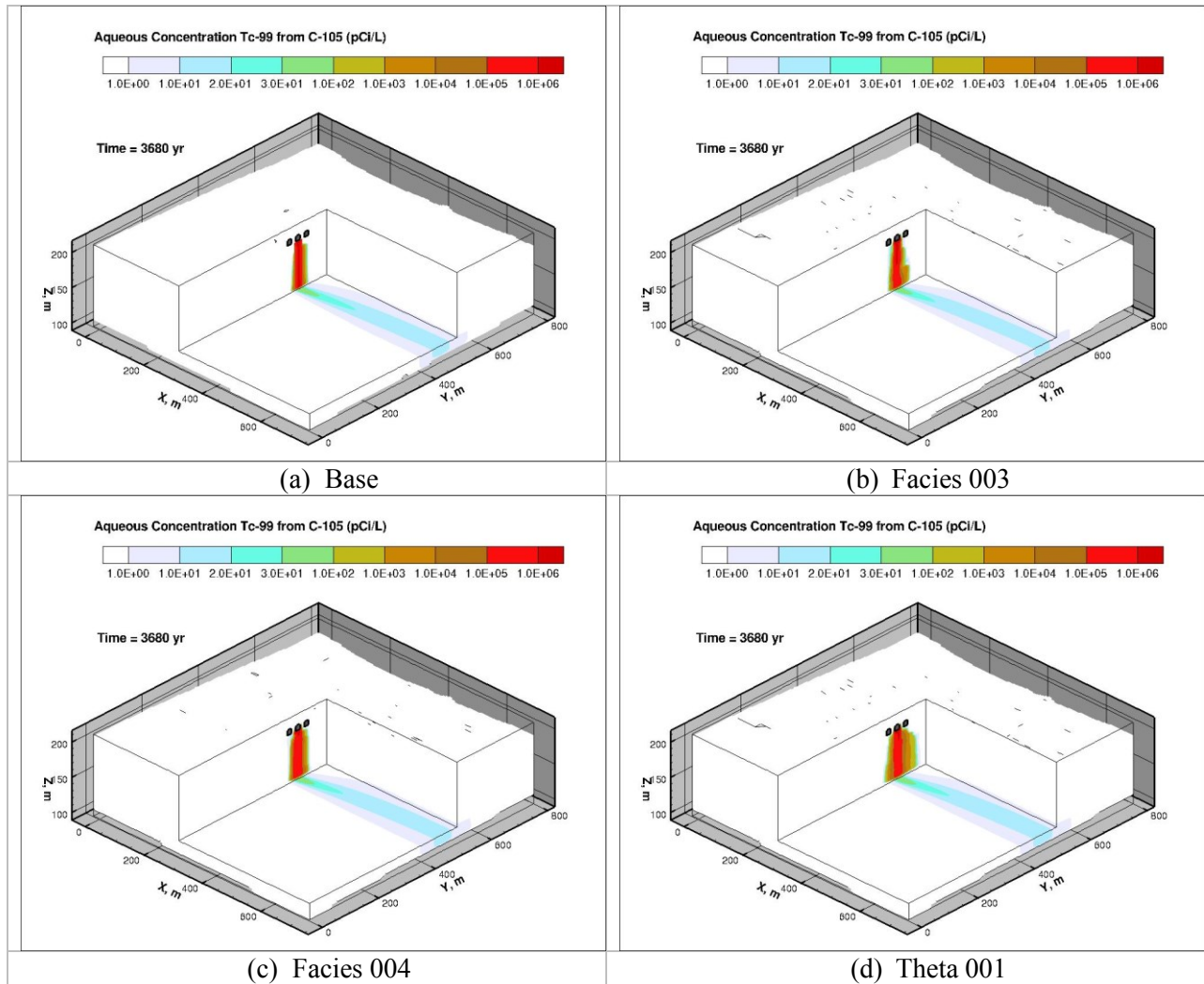


**Figure 5.3.** Oblique cutaway views of the distributions of aqueous Tc-99 from C-105 at year 3680 for the four conceptual models of WMA C tank residual.

The maximum or peak concentration occurred at PoC04 for all the cases. The predicted times for Tc-99 to reach peak concentrations in groundwater 100-m down-gradient of the WMA C fence-line are similar for all cases, ranging from year 3519 (1499 years after closure for facies realization 003) to year 3692 (1672 years after closure) for theta-based realization 001. The peak (maximum) concentrations range from 18.9 pCi/L for the Theta001 case to 19.9 pCi/L for the base (layered) case. All simulation cases that were evaluated yield predicted peak concentrations that are a factor of 45 or more below the maximum contaminant level (MCL) for Tc-99 (MCL=900 pCi/L).

Differences between the PA base case model and the alternative conceptual model results stem not only from differences in how material types are distributed, but also in how hydraulic parameters were estimated. Some of the differences may also be attributed to different process models used to represent tension-dependent anisotropy in unsaturated hydraulic conductivity. Based on the available data and simulation results, it is clear that hydraulic parameter estimates for this site are non-unique. Multiple sets of plausible hydraulic parameters can be developed that provide results which are consistent with field data. The stochastic methods used for generation of the facies- and water content-based models can be

readily used to generate ensembles of material type and parameter distributions that could be used for a more complete assessment of uncertainty associated with the conceptual model and its impact on the simulated fate and transport of residual tank wastes. The developed models can also be applied to assess impacts associated with the transport and fate of contaminants in the subsurface that resulted from past tank leaks and losses.

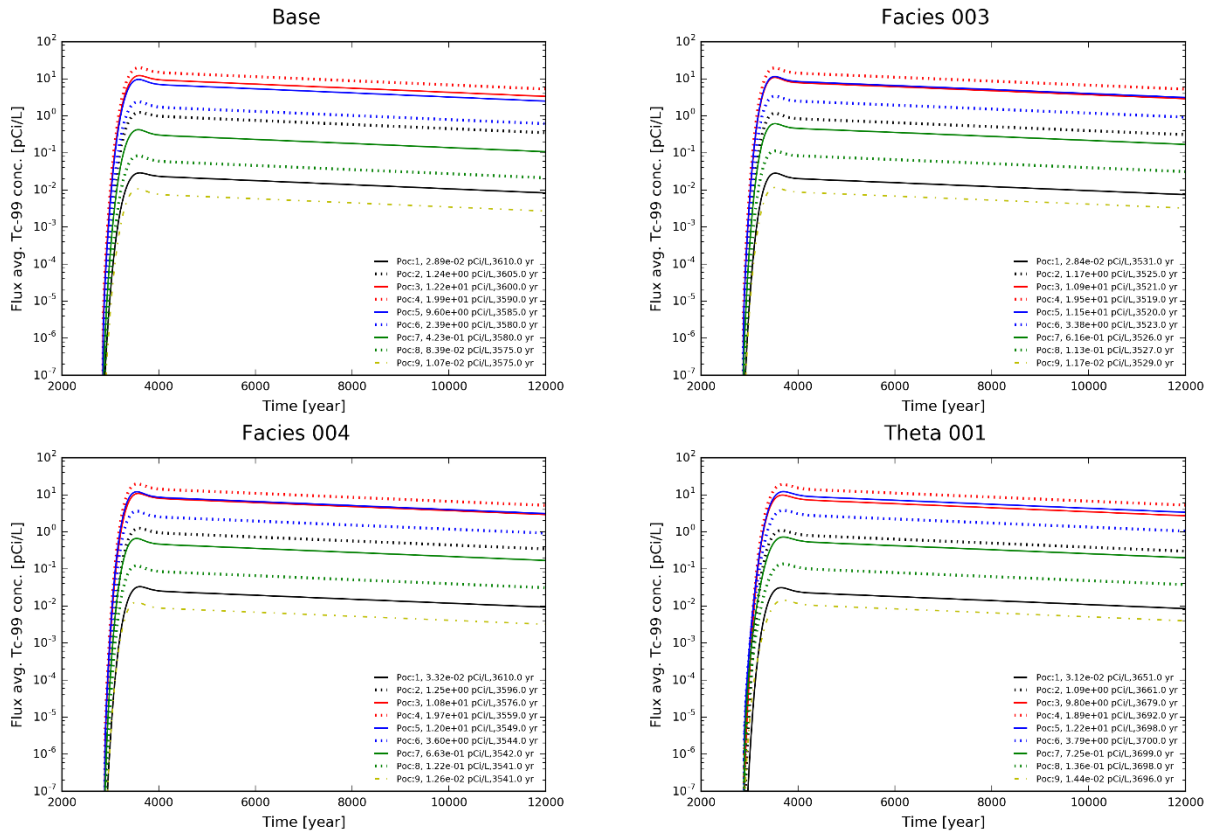


**Figure 5.4.** Flux-averaged concentrations in the top 5 m of the unconfined aquifer at different locations along a plane located 100-m down-gradient of the WMA C fence line for the simulations of tank residuals. PoC refers to points of calculation used in RPP-ENV-58782, Rev A Draft.

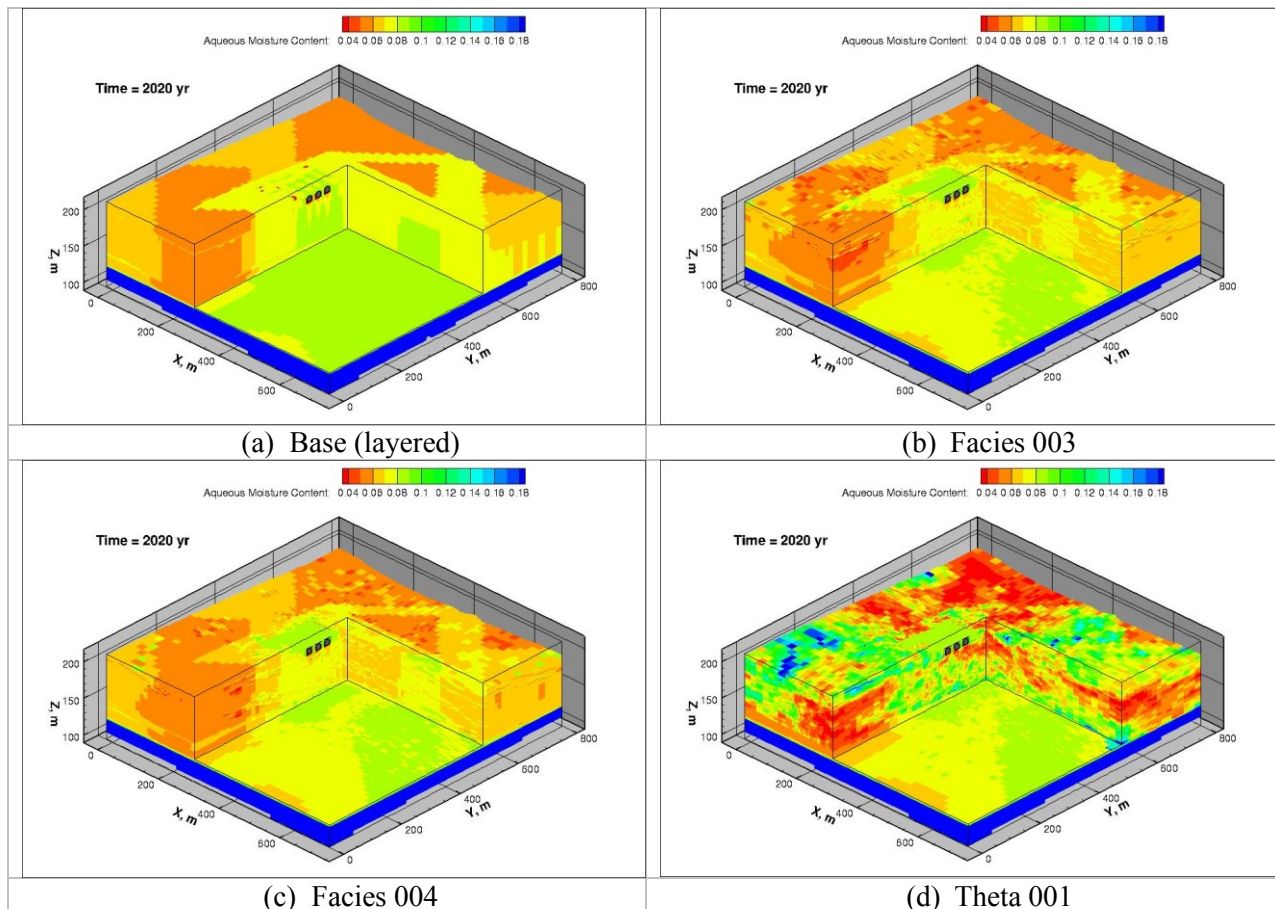
**Table 5.1.** Flux-averaged peak concentrations and arrival time in the top 5 m of the unconfined aquifer at different locations along a plane located 100-m down-gradient of the WMA C fence line for simulations of tank residuals. PoC refers to points of calculation used in RPP-ENV-58782, Rev Rev. 0.

	Base		Facies003		Facies004		Theta001	
	Time (yr)	Peak C (pCi/L)						
PoC:01	3610.0	2.89E-02	3531.0	2.84E-02	3610.0	3.32E-02	3651.0	3.12E-02
PoC:02	3605.0	1.24E+00	3525.0	1.17E+00	3596.0	1.25E+00	3661.0	1.09E+00
PoC:03	3600.0	1.22E+01	3521.0	1.09E+01	3576.0	1.08E+01	3679.0	9.80E+00
PoC:04	3590.0	1.99E+01	3519.0	1.95E+01	3559.0	1.97E+01	3692.0	1.89E+01
PoC:05	3585.0	9.60E+00	3520.0	1.15E+01	3549.0	1.20E+01	3698.0	1.22E+01
PoC:06	3580.0	2.39E+00	3523.0	3.38E+00	3544.0	3.60E+00	3700.0	3.79E+00
PoC:07	3580.0	4.23E-01	3526.0	6.16E-01	3542.0	6.63E-01	3699.0	7.25E-01
PoC:08	3575.0	8.39E-02	3527.0	1.13E-01	3541.0	1.22E-01	3698.0	1.36E-01
PoC:09	3575.0	1.07E-02	3529.0	1.17E-02	3541.0	1.26E-02	3696.0	1.44E-02

## 5.2 Simulations of Past Tank Waste Releases

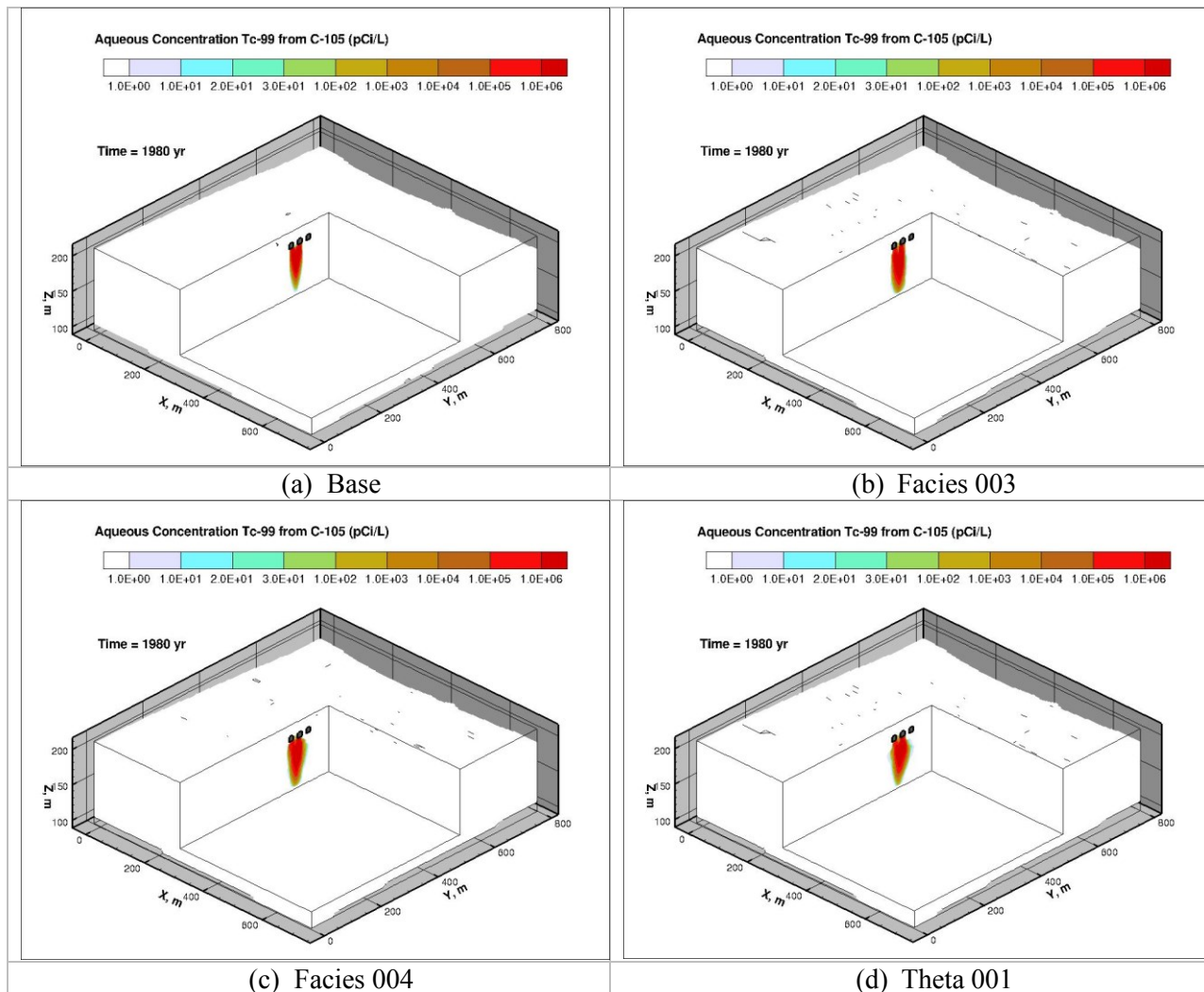
Two alternative inventories were evaluated in the WMA C PA for the C-105 tank leak. The larger of those inventories was used for the simulations reported here because the lower bound Tc-99 inventory estimate of 1 Ci did not produce concentrations in groundwater that were close to what has been observed in monitoring wells (private communication with Bill McMahon, CHPRC). For the simulations reported here, the simulated volume of the leak was 77,592.5 L (20,500 gal) with 9.8 Ci (576.4706 g) of Tc-99, and the leak occurred from 1963-1968.

Figure 5.5 shows oblique views of the aqueous saturation distributions for the four conceptual models at year 1980 (several years after the past tank releases). In spite of the tank waste releases, the aqueous saturation is nearly the same as the scenario in which past releases were not considered (Figure 5.1) except very close to the groundwater. This indicates that the water from the past tank releases migrated relatively fast to groundwater.



**Figure 5.5.** Oblique cutaway views of moisture content distributions at year 1980 for the four conceptual models of WMA C past tank releases.

Figure 5.6 and Figure 5.7 show the cutaway view of the concentration distribution of Tc-99 from C-105 in years 1980 when the plume was approaching the groundwater and 2020 when the plume has spread in the groundwater, respectively.



**Figure 5.6.** Oblique cutaway views of the distributions of aqueous Tc-99 from C-105 at year 1980 for the four conceptual models of WMA C past tank releases.

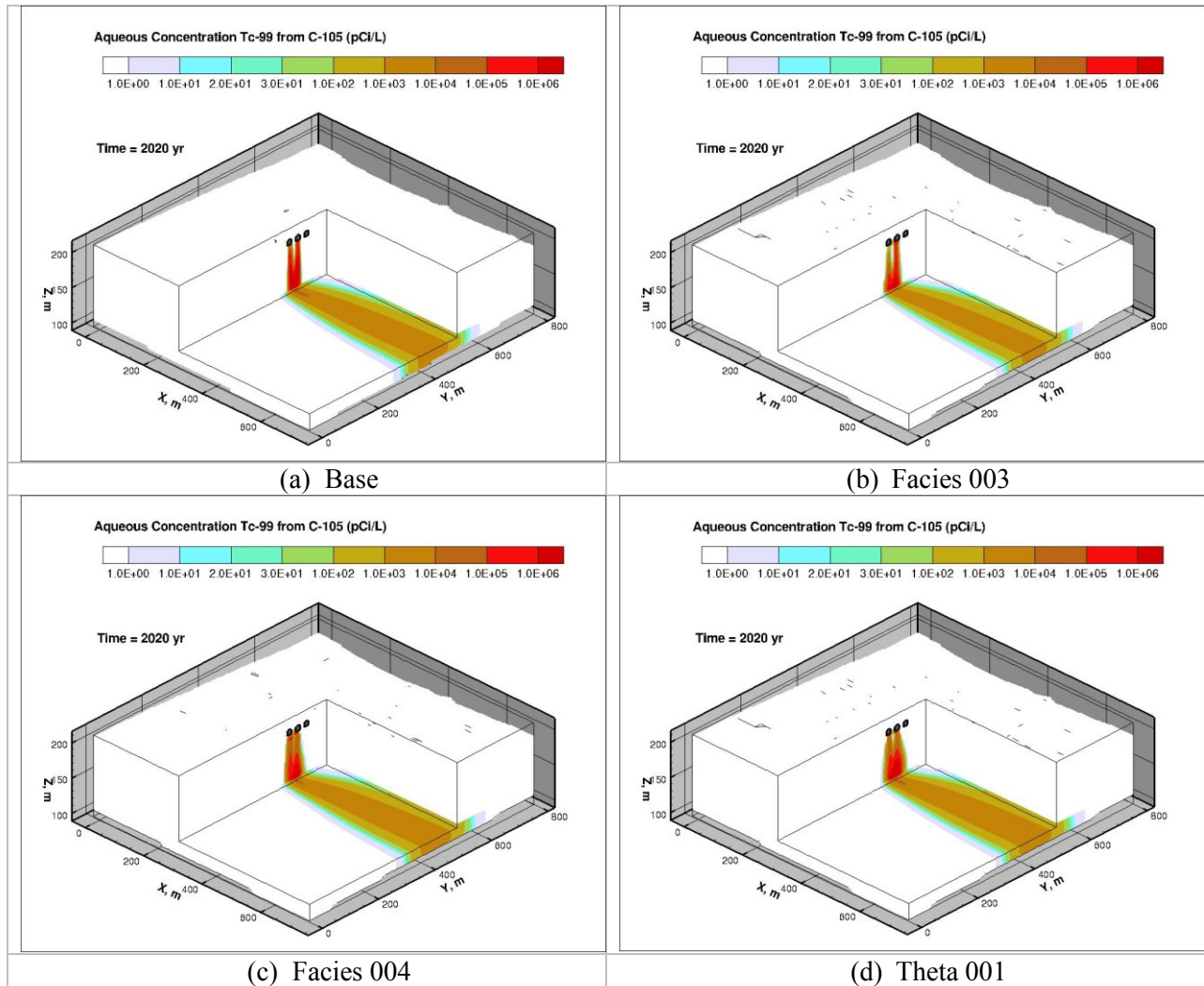


**Figure 5.7.** Oblique cutaway views of the distributions of aqueous Tc-99 from C-105 at year 2020 for the four conceptual models of WMA C past tank releases.

Figure 5.8 shows the flux-averaged concentration breakthrough curves and Table 5.2 shows the peak concentration and arrival time for different positions along a 100-m down-gradient monitoring plane for the four conceptual models. The peak (maximum) concentrations occurred at PoC06 for all cases. The peak concentrations for the three alternative cases differ from that of the base by -14% to 26%. The predicted times for Tc-99 to reach peak concentrations in groundwater 100-m down-gradient of the WMA C fence-line are similar for all cases, ranging from year 2008 for facies realization 003 to year 2019 for theta-based realization 001. The peak concentrations range from 4690 pCi/L for the case Theta001 and 6850 pCi/L for the Facies003 case. All simulation cases that were evaluated yield predicted peak concentrations that are 5.2 to 7.6 times the MCL of 900 pCi/L for Tc-99.

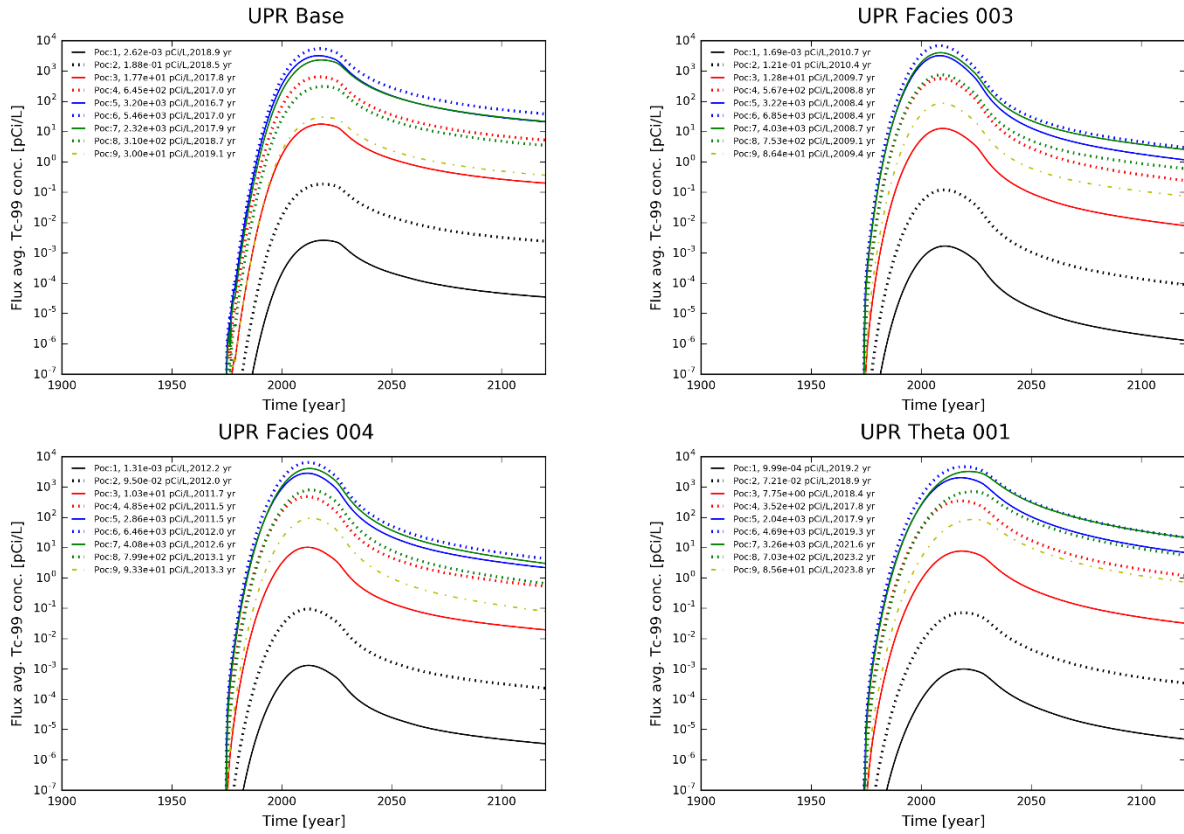


**Figure 5.8.** Flux-averaged concentrations in the top 5 m of the unconfined aquifer at different locations along a plane located 100-m down-gradient of the WMA C fence line for the four conceptual models of WMA C past tank releases. PoC refers to points of calculation used in RPP-ENV-58782, Rev A draft. (Note that the distances in the direction parallel to the fence line of these PoCs are not the same as those used in the simulations of tank residual in Fig. 5.4).

**Table 5.2.** Flux-averaged peak concentrations and arrival time in the top 7.5 m of the unconfined aquifer at different locations along a plane located 100-m down-gradient of the WMA C fence line for simulations of past tank releases. PoC refers to points of calculation used in RPP-ENV-58782, Rev A Draft. (Note that the distances in the direction parallel to the fence line of these PoCs are not the same as those used in the simulations of tank residual in Table 5.1).

	<b>Base</b>		<b>Facies003</b>		<b>Facies004</b>		<b>Theta001</b>	
	Time (yr)	Peak C (pCi/L)	Time (yr)	Peak C (pCi/L)	Time (yr)	Peak C (pCi/L)	Time (yr)	Peak C (pCi/L)
PoC:01	2018.9	2.62E-03	2010.7	1.69E-03	2012.2	1.31E-03	2019.2	9.99E-04
PoC:02	2018.5	1.88E-01	2010.4	1.21E-01	2012.0	9.50E-02	2018.9	7.21E-02
PoC:03	2017.8	1.77E+01	2009.7	1.28E+01	2011.7	1.03E+01	2018.4	7.75E+00
PoC:04	2017.0	6.45E+02	2008.8	5.67E+02	2011.5	4.85E+02	2017.8	3.52E+02
PoC:05	2016.7	3.20E+03	2008.4	3.22E+03	2011.5	2.86E+03	2017.9	2.04E+03
PoC:06	2017.0	5.46E+03	2008.4	6.85E+03	2012.0	6.46E+03	2019.3	4.69E+03
PoC:07	2017.9	2.32E+03	2008.7	4.03E+03	2012.6	4.08E+03	2021.6	3.26E+03
PoC:08	2018.7	3.10E+02	2009.1	7.53E+02	2013.1	7.99E+02	2023.2	7.03E+02
PoC:09	2019.1	3.00E+01	2009.4	8.64E+01	2013.3	9.33E+01	2023.8	8.56E+01

## 6.0 Summary and Conclusions

Neutron moisture, spectral gamma, and grain-size distribution data were used in conjunction with a geologic framework model to develop alternative conceptual models of the subsurface at WMA C. The development of these models was motivated, in part, by concerns raised during the PA development process about the representation of the subsurface using an EHM approach in the PA base case model. One goal of this work was to evaluate the potential impact of smaller-scale heterogeneities on simulated subsurface flow and transport behavior relative to the EHM-based numerical model being used for WMA C performance assessment calculations.

The spatial distributions and parameters assigned to the smaller-scale heterogeneities were estimated using borehole spectral gamma, neutron moisture, and grain size distribution data. The field-measured water content data determined from neutron moisture logging was used as a proxy for sediment texture and associated hydraulic properties in a parameterization method based on similar media scaling. Although application of this parameterization method to WMA C was successful, the effort was complicated by the possible impacts of past tank leaks in and around the tank farms.

Simulations of tank waste residuals and past tank waste releases were performed. The results from this study showed very similar predictions of flow and transport behavior for different representations of heterogeneity inferred from borehole spectral gamma, neutron moisture, and sediment texture data.

For the tank residual simulations, the four models evaluated in this study produced simulated peak concentrations at 100-m down-gradient calculation planes used in the analysis that ranged from 18.9 pCi/L for the Theta001 case, to 19.9 pCi/L for the PA base case. For the past tank release simulations, the peak concentrations ranged from 4690 pCi/L for the case Theta001, to 6850 pCi/L for the Facies003 case. For simulations of tank waste residual impacts from the four models, the simulated peak concentrations were a factor of 45 or more below the maximum concentration limit for Tc-99 (MCL = 900 pCi/L). For the simulations of past tank release impacts using the alternative models, the peak concentrations are a factor of 5.2 or more above the MCL.

Although the results from the heterogeneous models for both the tank residuals and the past leaks were very similar in both the magnitude and timing of peak Tc-99 concentrations, a better understanding of the range of heterogeneous model predictions could possibly be developed by examining a larger ensemble of realizations. This can be accomplished by conducting additional simulations using more realizations of stochastic material type and property fields. Analysis of an ensemble of results produced with multiple realizations of alternative models would provide a more complete picture of the potential variability in simulated contaminant transport behavior stemming from conceptual model and parameter uncertainty.

Finally, the alternative conceptual models discussed herein did not include an assessment case that contains sloping thin layers that have been suggested in WMA C workshops. While such features may exist, available field-measured water content data arguably do not allow thin, continuous sloping layers to be unambiguously identified (Appendix A). Uncertainty in the timing, locations, and rates of past releases and the sparse nature of the available characterization and monitoring data are also such that inverse modeling or history matching efforts may be of limited value.



## 7.0 References

- Arya LM and JF Paris. 1981. A physicoempirical model to predict the soil moisture characteristic from particle-size distribution and bulk density data. *Soil Science Society of America Journal*. 45:1023-1030.
- Arya LM, FJ Leij, and M Th van Genuchten. 1999. Relationship between Particle-Size Distribution and Soil Water Retention. In M Th van Genuchten, FJ Leij, and L Wu (eds.), *Proceedings of the International Workshop on Characterization and Measurement of the Hydraulic Properties of Unsaturated Porous Media*. October 22-24, 1997, University of California, Riverside, USA
- Bear J. 1972. *Dynamics of Fluids in Porous Media*. Dover, New York.
- Bergeron MP, GV Last, and AE Reisenauer. 1987. *Geohydrology of a Commercial Low-Level Radioactive Waste Disposal Facility near Richland, Washington*. Technical Report, Prepared for U.S. Ecology, Inc. by Battelle Pacific Northwest Laboratories, Richland, Washington.
- Bjornstad B. 2006. *On the Trail of the Ice Age Floods: A Geological Field Guide to the Mid-Columbia Basin*. Keokee Co. Publishing, Inc., Sandpoint, Idaho.
- Brooks RH and AT Corey. 1964. *Hydraulic Properties of Porous Media*. Hydrology Paper 3, Colorado State University, Fort Collins.
- Brown CF, RJ Serne, BN Bjornstad, DG Horton, DC Lanigan, ER Clayton, MM Valenta, TS Vickerman, IV Kutnyakov, KN Geiszler, SR Baum, KE Parker, and MJ Lindberg. 2006. *Characterization of Vadose Zone Sediments Below the C Tank Farm: Borehole C4297 and RCRA Borehole 299-E27-22*. PNNL-15503, Pacific Northwest National Laboratory, Richland, Washington.
- Campbell GS. 1985. *Soil Physics with Basic – Transport Models for Soil-Plant-Systems*, Developments in Soil Science 14, Elsevier, New York.
- Connelly MP. 2009. *Sampling and Analysis Plan for Phase 2 Characterization of Vadose Zone Soil in Waste Management Area C*. RPP-PLAN-38777, Rev. 1. Washington River Protection Solutions, LLC, Richland, Washington.
- Connelly MP, JV Borghese, CD Delaney, BH Ford, JW Lindberg, and SJ Trent. 1992. *Hydrogeologic Model for the 200 East Groundwater Aggregate Area*. WCH-SD-EN-TI-019, Westinghouse Hanford Company, Richland, Washington.
- Connelly MP, PW Cabbage, and MP Bergeron. 2014. *Development of Alternative Digital Geologic Models for Waste Management Area C*. RPP-RPT-56356, Rev. 0., Washington River Protection Solutions, LLC, Richland, Washington.
- DOE. 2002. *Standardized Stratigraphic Nomenclature for the Post-Ringold-Formation Sediments Within the Central Pasco Basin*. DOE/RL-2002-39, Rev. 0, U.S. Department of Energy Richland Operations Office, Richland, Washington.

- DOE. 2014. Hanford Site Groundwater Monitoring Report for 2013. DOE/RL-2014-32, Rev. 0. U.S. Department of Energy, Richland Operations Office, Richland, Washington.
- EMDT-OB-0009. 2015. WMA C Vadose Zone Moisture Content for Handheld Neutron Moisture Gauges, Rev. 0. Washington River Protection Solutions, LLC, Richland, Washington.
- Fayer MJ, RE Lewis, RE Engelman, AL Pearson, CJ Murray, JL Smoot, RR Randall, WH Wegener, and AH Lu. 1995. *Re-Evaluation of a Subsurface Injection Experiment for Testing Flow and Transport Models*. PNL-10860, Pacific Northwest National Laboratory, Richland, Washington.
- Fayer MJ and JE Szecsody. 2004. *Recharge Data Package for the Integrated Disposal Facility 2005 Performance Assessment*. PNNL-14744, Pacific Northwest National Laboratory, Richland Washington.
- Gee GW, M Oostrom, MD Freshley, ML Rockhold, and JM Zachara. 2007. "Hanford Site Vadose Zone Studies." *Vadose Zone Journal* 6(4):899-905.
- Gee GW and D Or. 2002. Particle-Size Analysis, In JH Dane and GC Topp (eds.), *Methods of Soil Analysis, Part 4 – Physical Methods*. Number 5 in Soil Science Society of America Book Series, Soil Science Society of America, Madison, Wisconsin.
- Gee GW, MJ Fayer, ML Rockhold, MD Campbell. 1992. "Variations in Recharge at the Hanford Site." *Northwest Science* 66:237-250.
- Hanford Federal Facility Agreement and Consent Order. 1989 (amended 1990). Washington State Department of Ecology, U.S. Environmental Protection Agency, and U.S. Department of Energy. 89-10, Rev. 1.
- Hou Z, CJ Murray, and Y Bott. 2015. *Geostatistical Realizations of WMA-C Lithofacies*. PNNL-24698, Pacific Northwest National Laboratory, Richland, Washington.
- Khaleel R. 2004 *Far-Field Hydrology Data Package for Integrated Disposal Facility Performance Assessment*. RPP-20621, Rev. 0, CH2M Hill Hanford Group, Richland, Washington.
- Khaleel R and EJ Freeman. 1995. *Variability and Scaling of Hydraulic Properties for 200 Area Soils, Hanford Site*. WHC-EP-0883, Westinghouse-Hanford Company, Richland, Washington.
- Lotspeich FB and FH Everest. 1981. *A New Method for Reporting and Interpreting Textural Composition of Spawning Gravel*. USDA Forest Service, Pacific Northwest Forest and Range Experiment Station Research Note.
- Miller EE and RD Miller. 1956. "Physical Theory for Capillary Flow Phenomena." *Journal of Applied Physics* 27:324-332.
- Mualem Y. 1976. "A New Model for Predicting the Hydraulic Conductivity of Unsaturated Porous Media." *Water Resources Research* 12:513:522.
- Pachepsky Y and WJ Rawls. 2004. *Development of Pedotransfer Functions in Soil Hydrology, Developments in Soil Science – Volume 30*, Elsevier, New York.

Polmann DJ. 1990. Application of Stochastic Methods to Transient Flow and Transport in Heterogeneous Unsaturated Soils. Ph.D. Thesis, Massachusetts Institute of Technology.

Rockhold ML, MJ Fayer, and GW Gee. 1988. *Characterization of Unsaturated Hydraulic Conductivity at the Hanford Site*. PNL-6488, Pacific Northwest National Laboratory, Richland, Washington.

Rockhold ML, MJ Fayer, and PR Heller. 1993. *Physical and Hydraulic Properties of Sediments and Engineered Materials Associated with Grouted Double-Shell Tanks Waste Disposal at Hanford*. PNL-8813, Pacific Northwest National Laboratory, Richland, Washington.

Rockhold ML, RE Rossi, and RG Hills. 1996. "Application of Similar Media Scaling and Conditional Simulation for Modeling Water Flow and Tritium Transport at the Las Cruces Trench Site." *Water Resources Research* 32(3):595-609.

Rockhold ML, CS Simmons, and MJ Fayer. 1997. "An Analytical Solution Technique for One-Dimensional, Steady Vertical Water Flow in Layered Soils." *Water Resources Research*. 33(4):897-902.

Rockhold ML, GV Last, and LA Middleton. 2010. *Prototype Data Models and Data Dictionaries for Hanford Sediment Physical and Hydraulic Properties*. PNNL-19817, Pacific Northwest National Laboratory, Richland, Washington.

Rockhold ML, DH Bacon, VL Freedman, KR Parker, SW Waichler, and MD Williams. 2013. *System-Scale Model of Aquifer, Vadose Zone, and River Interactions for the Hanford 300 Area – Application to Uranium Reactive Transport*. PNNL-22886, RPT-DVZ-AFRI-019, Pacific Northwest National Laboratory, Richland, Washington.

Rockhold ML, ZF Zhang, PD Meyer, and JN Thomle. 2015. *Physical, Hydraulic, and Transport Properties of Sediments and Engineered Materials Associated with Hanford Immobilized Low-Activity Waste*. PNNL-23711, RPT-IGTP-004, Rev. 0, Pacific Northwest National Laboratory, Richland, Washington.

RPP-RPT-42294. 2016. Hanford Waste Management Area C Soil Contamination Inventory Estimates, Rev. 2. Washington River Protection Solutions, LLC, Richland, Washington.

RPP-ENV-58782. 2016. Performance Assessment of Waste Management Area C, Hanford Site Washington, Rev. 0. Washington River Protection Solutions, LLC, Richland, Washington.

RPP-RPT-58949. 2016. Model Package Report Flow and Contaminant Transport Numerical Model Used in WMA C Performance Assessment and RCRA Closure Analysis, Rev. 0. Washington River Protection Solutions LLC, Richland Washington.

RPP-CALC-60450. 2016. Process for Determining the Volumetric Moisture Content for the Vadose Zone Geologic Units Underlying Waste Management Area C, Rev. 0, Washington River Protection Solutions, LLC, Richland, Washington.

RPP-CALC-60450. 2016. Heterogeneous Media Models for Waste Management Area C Performance Assessment, Rev. 0. Washington River Protection Solutions, LLC, Richland, Washington.

Schaap MG, PJ Shouse, and PD Meyer. 2003. *Laboratory Measurements of the Unsaturated Hydraulic Properties at the Vadose Zone Transport Field Study Site*. PNNL-14284, Pacific Northwest National Laboratory, Richland, Washington.

Schroth MH, SJ Ahearn, JS Selker, and JD Istok. 1996. "Characterization of Miller-similar sands for laboratory hydrologic studies." *Soil Science Society of America Journal* 60:1331-1339.

Sisson JB and AH Lu. 1994. *Field Calibration of Computer Models for Application to Buried Liquid Discharges: A Status Report*. RHO-ST-46 P, Rockwell Hanford Operations, Richland, Washington.

van Genuchten MT. 1980. "A Closed-Form Equation for Predicting the Hydraulic Conductivity of Unsaturated Soils." *Soil Science Society of America Journal* 44:892-898.

Ward AL, ME Conrad, WD Daily, JB Fink, VL Freedman, GW Gee, GM Hoverston, MJ Keller, EL Majer, CJ Murray, MD White, SB Yabusaki, and ZF Zhang. 2006. *Vadose Zone Transport Field Study Summary Report*. PNNL-15443, Pacific Northwest National Laboratory, Richland, Washington.

Yi AB and N Standish. 1991. Estimation of the porosity of particle mixtures by a linear-mixture packing model. *Industrial and Engineering Chemistry Research* 30:1372-1385.

Zhang ZF, AL Ward, and GW Gee. 2003. "A Tensorial Connectivity-Tortuosity Concept to Describe the Unsaturated Hydraulic Properties of Anisotropic Soils." *Vadose Zone Journal* 2:313-321.

Zhang ZF, CE Strickland, JG Field, and DL Parker. 2009. *T Tank Farm Interim Surface Barrier Demonstration – Vadose Zone Monitoring FY08 Report*. PNNL-18083, Pacific Northwest National laboratory, Richland, Washington.

## **Appendix A**

### **Geostatistical Analysis of Sediment Moisture Content Data from WMA C**



## Appendix A

### Geostatistical Analysis of Sediment Moisture Content Data from WMA C

The original intent of this work was to use field-measured water content data from Waste Management Area (WMA) C as a proxy for sediment texture, and to estimate sediment hydraulic properties from water content data using a parameterization method described by Rockhold et al. (1996). This parameterization method uses similar media scaling theory and relies on the fact that finer-textured sediments retain more moisture and are thus wetter than coarser-textured sediments in the field. Under steady, predominantly vertical flow conditions that would normally exist at undisturbed sites, and with estimates of average hydraulic parameters and upper and lower boundary conditions (e.g., recharge rates and elevation of the water table, respectively), field-measured water content data can be used to estimate spatially distributed hydraulic parameters. Application of this parameterization method to areas around tank farms is problematic, however, owing to past water line and tank waste leaks and losses and other undocumented water additions to the subsurface.

The basic premise for applying the parameterization method noted above to WMA C is that the variability in the existing water content distribution in the field primarily reflects differences in sediment texture and associated hydraulic properties. Indiscriminant use of surface-applied water for operational activities such as dust control at WMA C is thought to have ceased by about the year 2000 (private communication with Marcel Bergeron, Washington River Protection Solutions [WRPS]). Such water additions would likely have been relatively small and the propagation of this water to any significant depth was presumed to be minimal. Variability in natural recharge or net infiltration rates inside and outside the tank farm, resulting from removal of vegetation and alternation of natural sediment layering within the tank farm, is acknowledged. At the outset of this work, it was also assumed that the signatures of past water line or tank waste leaks or losses would have largely dissipated by the time that the more recent water content measurements were made. After examination of the data, this initial assumption does not appear to have been realistic. This potentially impacts the analysis because regions of high water content are implicitly assumed to be indicative of finer textured sediments, rather than caused by non-uniformities in water fluxes.

Sediment moisture content data have been collected from boreholes and wells drilled in the vicinity of WMA C and other tank farms at Hanford using both gravimetric sampling and neutron moisture logging methods. Neutron moisture data are typically reported as (dimensionless) volumetric water content. Gravimetric water content data are usually converted to volumetric water content by multiplying by the sample bulk density (assuming unit mass density for water). Moisture content data have been collected routinely at Hanford for characterization efforts associated with installation of groundwater monitoring wells. Periodic and ongoing monitoring has also been performed using neutron moisture logging of “dry wells” that have been used historically for leak detection around Hanford’s waste storage tanks.

A compilation of water content data from WMA C was obtained from the current Hanford Site performance assessment modeling contractor, INTERA, representing relatively recent water content measurements, most of which were made since 2010 (RPP-CALC-60345, Rev. 0). The data represent

measurements reported in the Hanford Environmental Information System and unpublished neutron moisture logs from direct push boreholes (both provided by Marcel Bergeron and Mike Connelly, WRPS), and from handheld neutron probe measurements made in dry wells for leak detection monitoring (RPP-CALC-60345, Rev. 0). This data set was augmented with neutron moisture data provided by Marcel Bergeron (WRPS) from the A-AX tank farms. Initial inspection of the data from WMA C suggested that much of the temporal variability was limited to the upper 5 to 10 m of the sediment profile, presumably resulting primarily from seasonal variability in precipitation. Therefore, no attempt was made to account for the temporal variability of the water content data, and repeat measurements made at the same locations were averaged.

Variography was performed to evaluate the spatial autocorrelation structure of the water content data. Figure A.1 shows horizontal and vertical experimental and model variograms for the normal score transformed (Deutsch and Journel 1998) field-measured water content data.

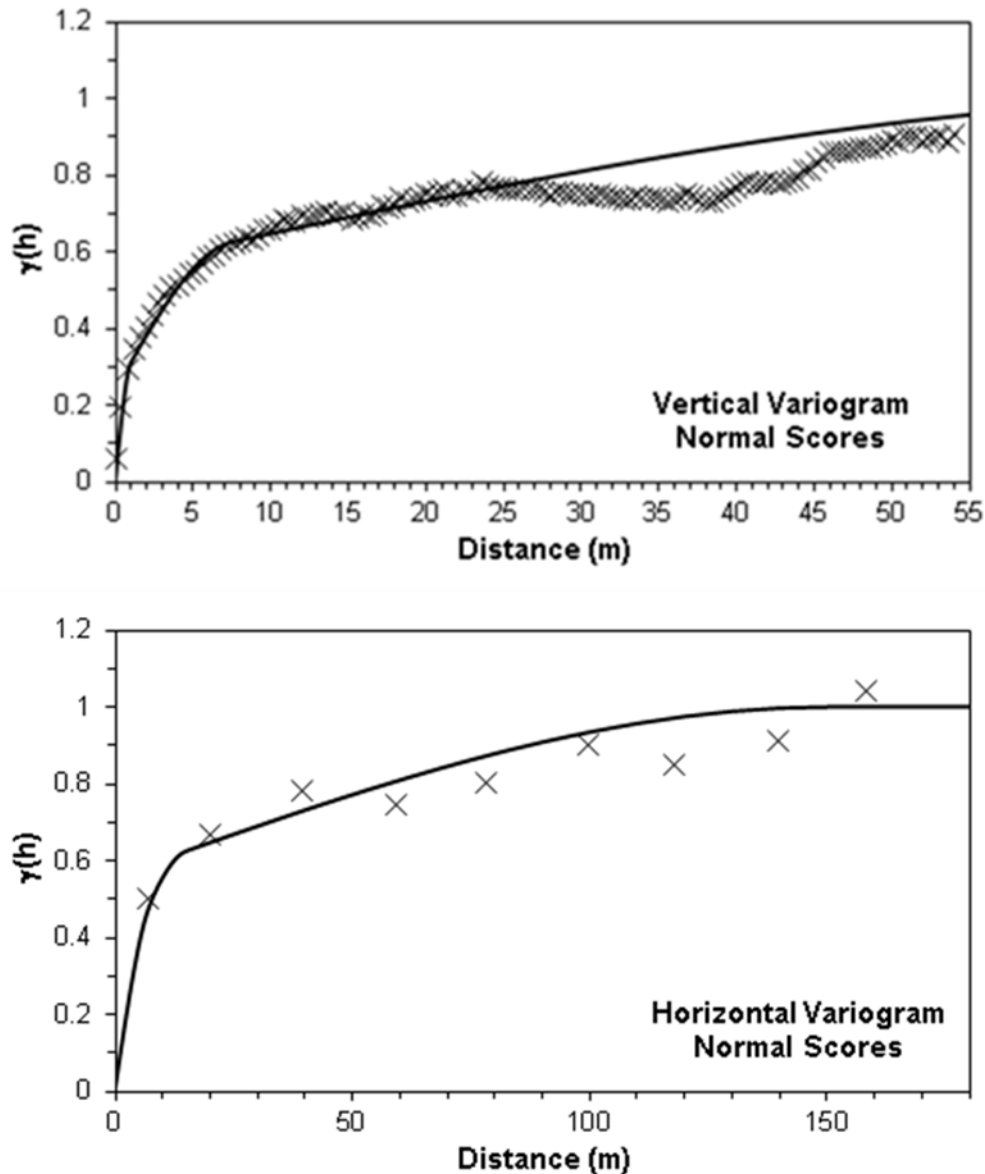


**Figure A.1.** Experimental and spherical model variograms for normal score transformed water content.

Table A.1 lists the parameters for the nested spherical variogram model. The water content data were kriged using ordinary kriging to facilitate visualization and further assessment of the data set. A reduced data set was then identified for use in stochastic conditional simulation using sequential Gaussian simulation. Kriging and sequential Gaussian simulation were performed using GSLIB (Deutsch and Journel 1998).

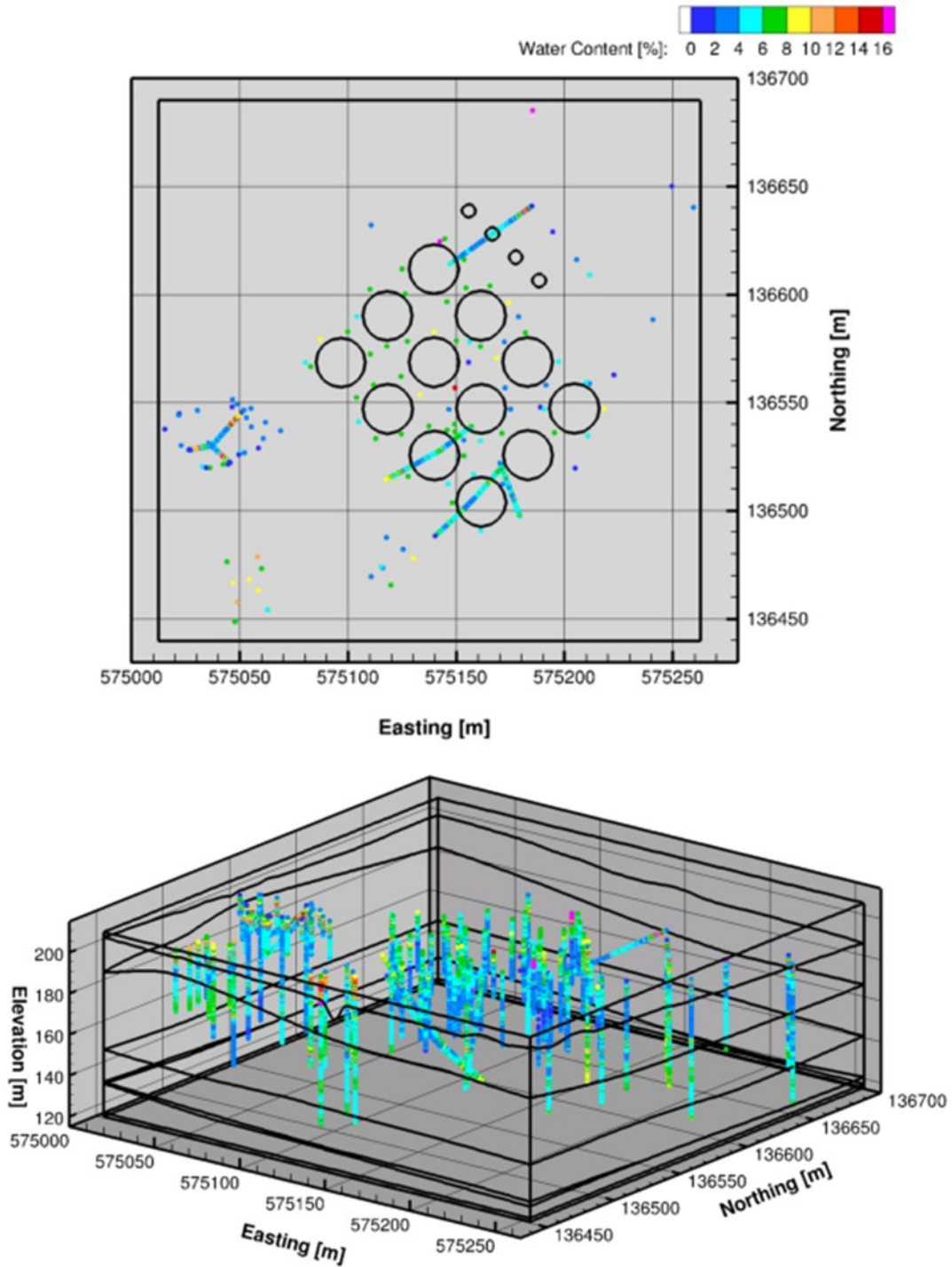
Figure A.2 shows plan and oblique views of the borehole and well locations and the available water content data from the vicinity of WMA C. Figure A.3 shows the same views for the kriged water content field. The kriging results show several areas of elevated water content in the shallow subsurface, which may reflect the localized effects of past waste loss or leak events.

Figure A.3 through Figure A.20 show vertical east-west cross sections of the kriged water content data for the vicinity of WMA C over the elevation range from 120 to ~205 m. The water table underlying WMA C lies at an elevation of ~121 m, so the kriging results extend from approximately the top of the water table up to the ground surface. Note that the regions occupied by tanks and auxiliary equipment are not shown in these figures, but these features were considered when the data were used for parameter estimation and modeling.

The volumetric water content data from WMA C range from near zero to greater than 16% by volume. This range is similar to what was observed over the 3 to 13 m depth interval under ambient conditions prior to water injection at the Sisson and Lu site, located near the southern end of the 200 East Area (Sisson and Lu 1984). Field experiments performed at the Sisson and Lu site have been used for testing and calibrating vadose zone flow and transport models used for performance and risk assessment at Hanford (Zhang and Khaleel 2007). Although the range of water content values for WMA C is similar to the range at the Sisson and Lu site, the spatial patterns of water content data shown in Figure A.3 through Figure A.20 do appear to show evidence of past waste losses or leak discharges, particularly in the shallow subsurface. For example, the localized high water content values shown in red in the upper middle portions of the plots in Figure A.3 through Figure A.6 are from measurements made around a diversion box (UPR-81) where releases of waste and contaminants are known to have occurred (RPP-RPT-42294). In fact, many of the boreholes that have been drilled and logged for moisture around the periphery of the tanks were installed specifically to determine the extent of tank waste leaks and losses.

**Table A.1.** Parameters for the nested spherical variogram models fit to normal score transformed water content data from WMA C and A-AX tank farms.

Nugget	Sill	Vertical Range (m)	Horizontal Range (m)
0.01	0.23	1.0	7.5
	0.32	7.5	15.0
	0.44	75.0	150.0



**Figure A.2.** Plan view (top plot) and oblique view (bottom plot) of water content data measurement locations for WMA C. The circles in the top plot show the outlines (inside diameter) of the 100-series (large circles) and 200-series (small circles) single-shell tanks.

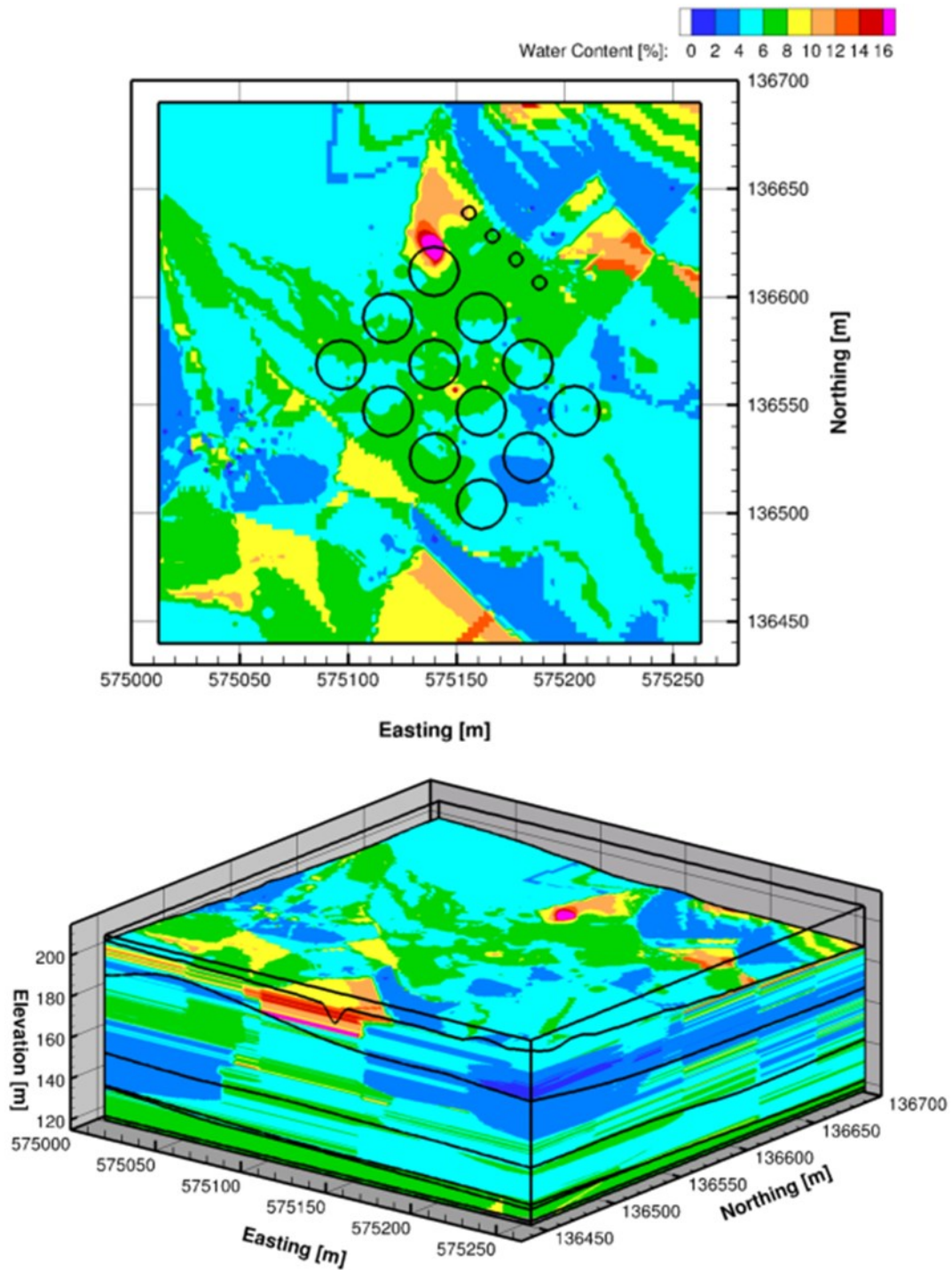


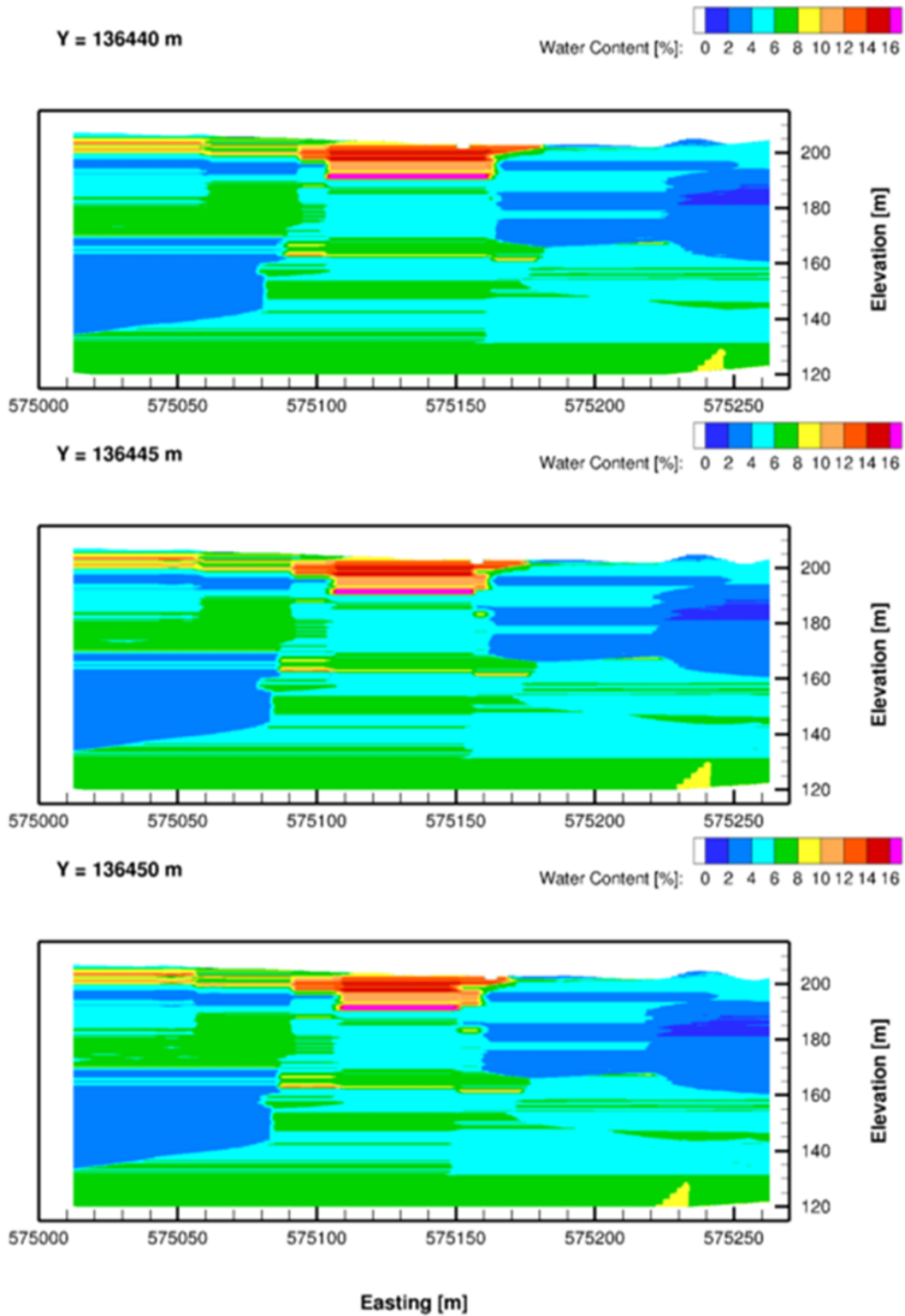
**Figure A.3.** Plan view (top plot) and oblique view (bottom plot) of kriged water content data from WMA C. The circles in the top plot show outlines (inside diameter) of the 100-series (large circles) and 200-series (small circles) single-shell tanks.

Although the patterns of the water content data appear to show evidence of past tank waste leaks and losses, the configuration of these data is such that kriging artifacts are also evident, particularly along the bottom and sides of the domain depicted in Figure A.4 through Figure A.20. In particular, no data existed to inform the northwest and southeast portions of the domain shown in these figures, so caution is warranted in interpreting the kriged results, especially in areas where data are extrapolated. For example, the thin red band of higher water content that appears in the upper left parts of the profiles shown in Figure A.16 through Figure A.20 appears to propagate more to the west with increasing distance to the north. However, based on the configuration of the data shown in Figure A.1, this feature is informed by only a few near surface high-value water content data points to the north of tank C-112. There are no actual data in the area where this thin red band appears. Therefore, this feature is an artifact of extrapolation.

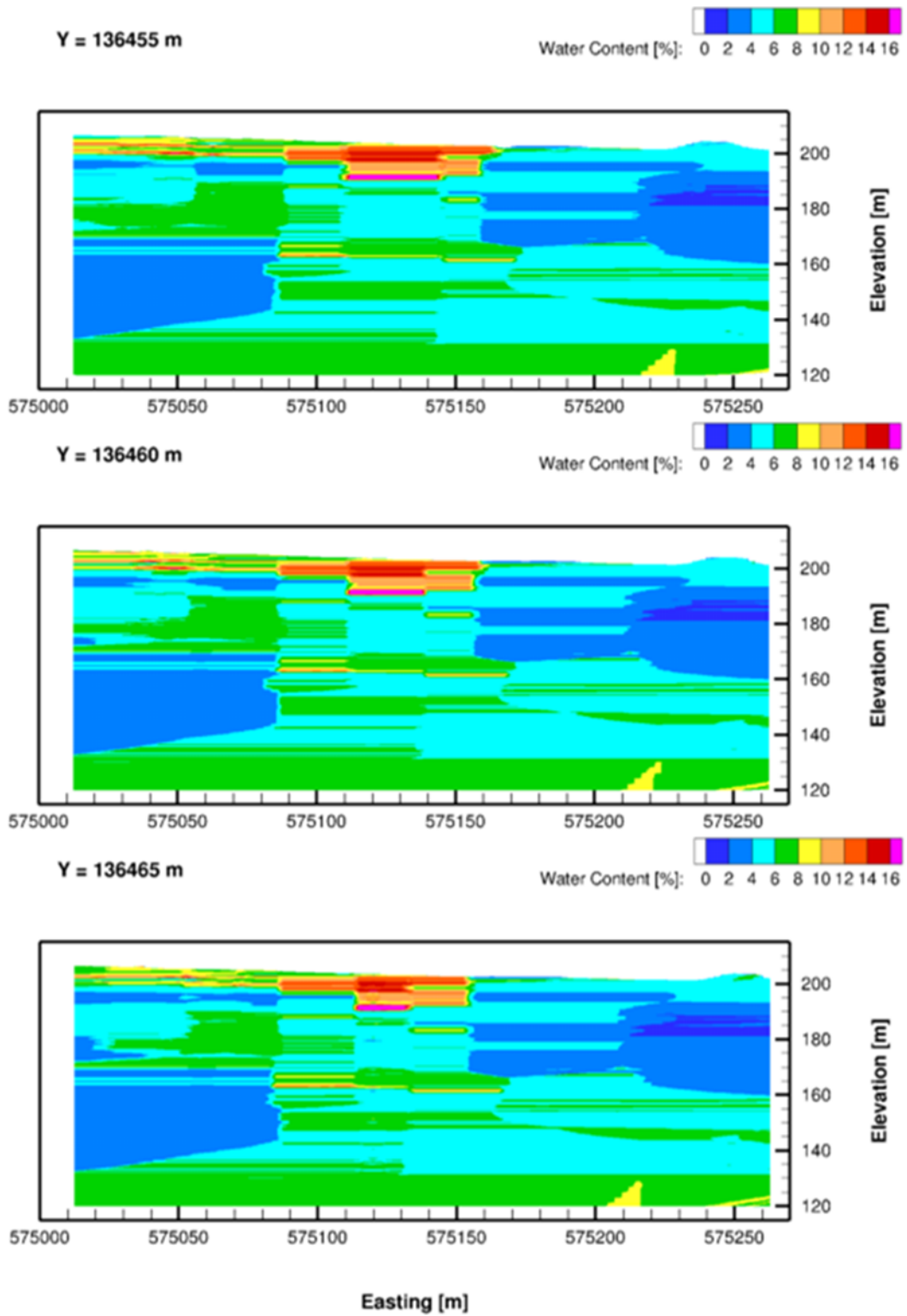
Given the goals of the project, and considering the apparent remaining signatures of localized, near-surface water additions, and the kriging artifacts resulting from the configuration and sparsity of the data set, a subset of the available data was selected. The objectives in selecting the subset of data were threefold: (1) select data from deeper boreholes and wells to provide better representation of the entire vadose zone rather than just the upper half to two-thirds of the domain, (2) to the extent possible, eliminate data that appeared to be influenced by anthropogenic sources of water, and (3) select data for boreholes and wells whose water content profiles are consistent with the major lithology. The second two criteria are subjective.

Table A.2 lists the IDs and coordinates for the selected boreholes and wells from which data were used for stochastic conditional simulation, as discussed in the main body of this report. To provide better control over the larger domain representing the WMA C model, data for an additional 25 pseudo-well locations were also generated, shown in Figure A.21. The pseudo-boreholes are spaced 150 m apart, five boreholes per row for five rows, resulting in 25 pseudo-boreholes. The locations of the 25 pseudo-boreholes are listed in Table A.3. C7681 is the source well for the top two rows of pseudo-boreholes shown in Figure A.21, C7669 for the middle row, and C6393 for the bottom two rows. The source boreholes were also placed by a vertical offset which is the difference of the top of H2 at the location of a given pseudo-well and the source boreholes except for C6393, for which the offset is based on the top of H3 to avoid placing the source well C6393 deeper than the water table. For example, for the first pseudo-well (Well No. 20), the original elevations of the water content data from the source well C6393 are added with an elevation offset of 5.59 m. While for Well No. 24 in Table A.3, the source well was lowered down with an elevation offset of 3.01 m. This approach was also applied in the lithofacies characterization of the site by taking into account the change in elevations of stratigraphic units.

The stochastic conditional simulation results generated using the selected water content data were used for model parameterization. An example of one realization of the stochastic conditional simulation results for the selected water content data are shown in Figure A.22.



**Figure A.4.** East-west cross sections of kriged water content for northing (Y) coordinates of 136440, 136445, and 136450 m.



**Figure A.5.** East-west cross sections of kriged water content for northing (Y) coordinates of 136455, 136460, and 136465 m.

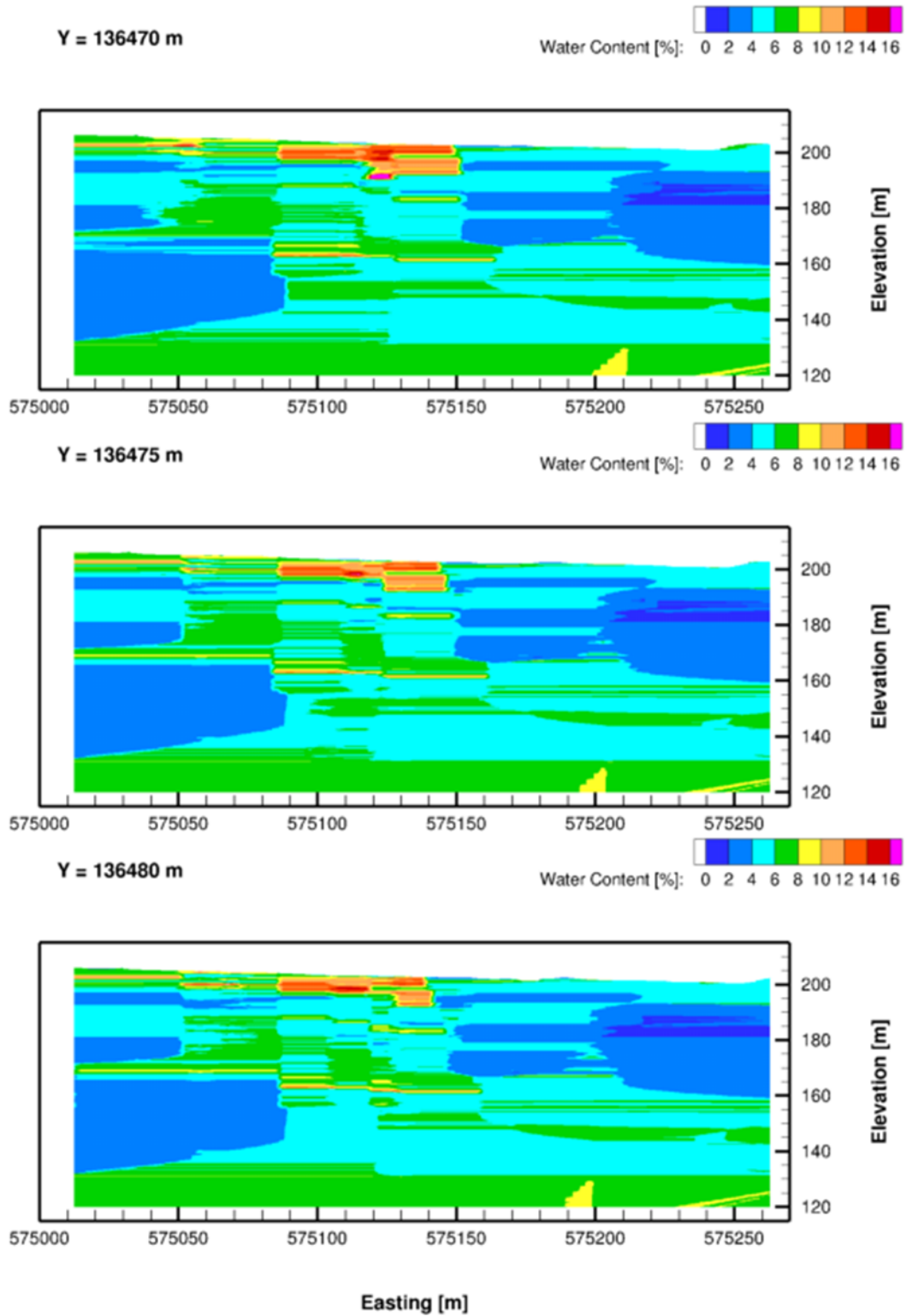


**Figure A.6.** East-west cross sections of kriged water content for northing (Y) coordinates of 136470, 136475, and 136480 m.

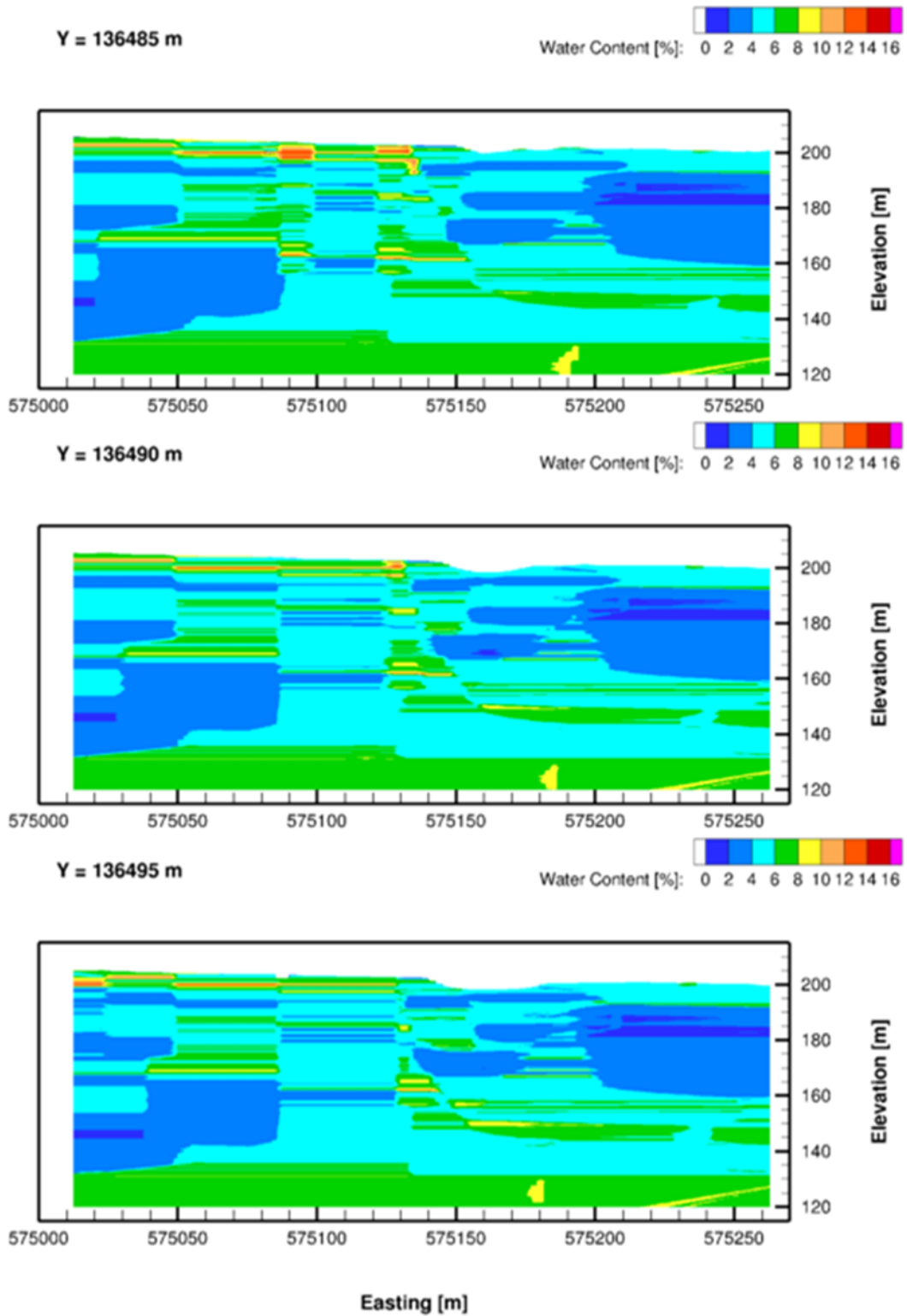


**Figure A.7.** East-west cross sections of kriged water content for northing (Y) coordinates of 136485, 136490, and 136495 m.

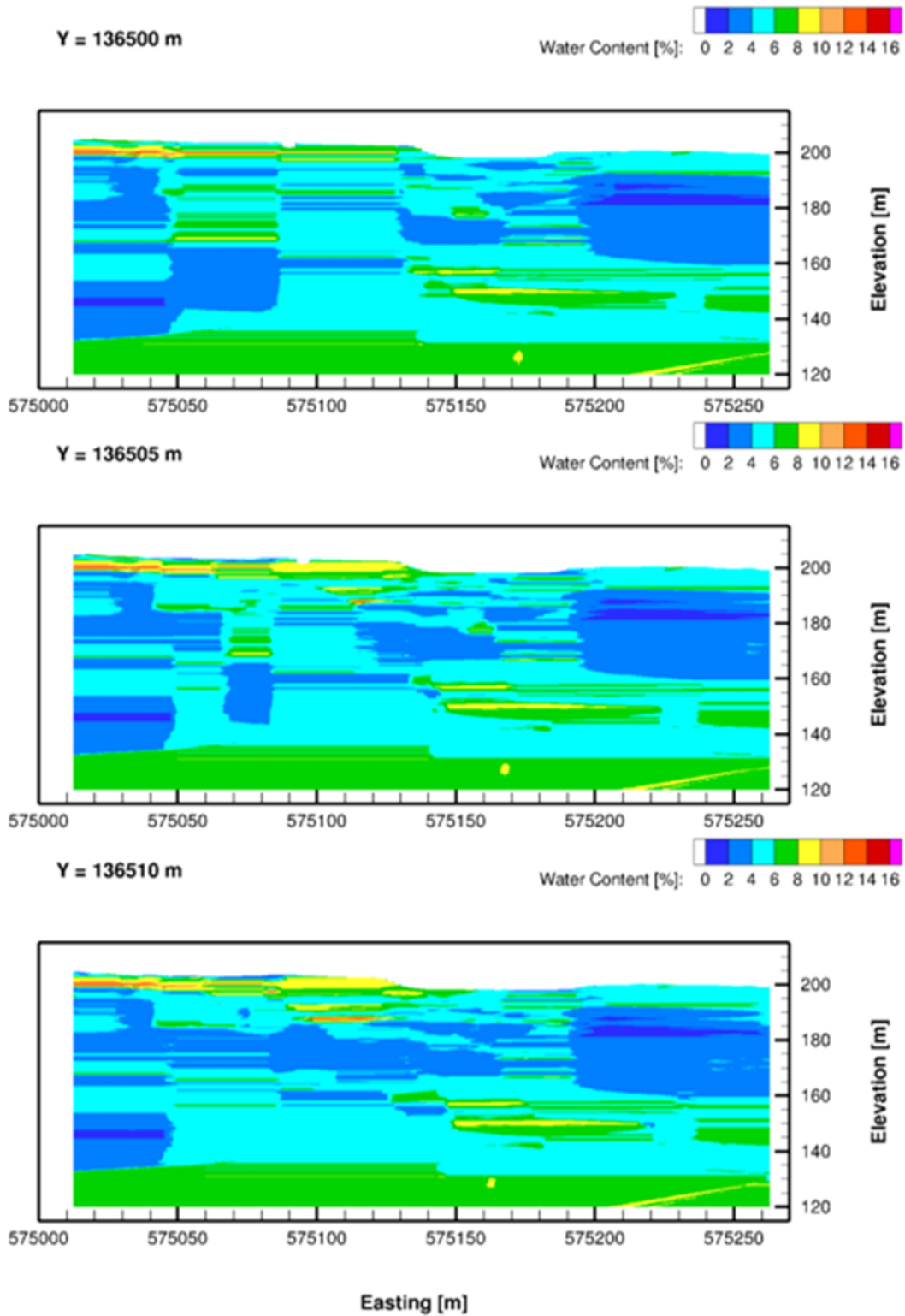


**Figure A.8.** East-west cross sections of kriged water content for northing (Y) coordinates of 136500, 136505, and 136510 m.

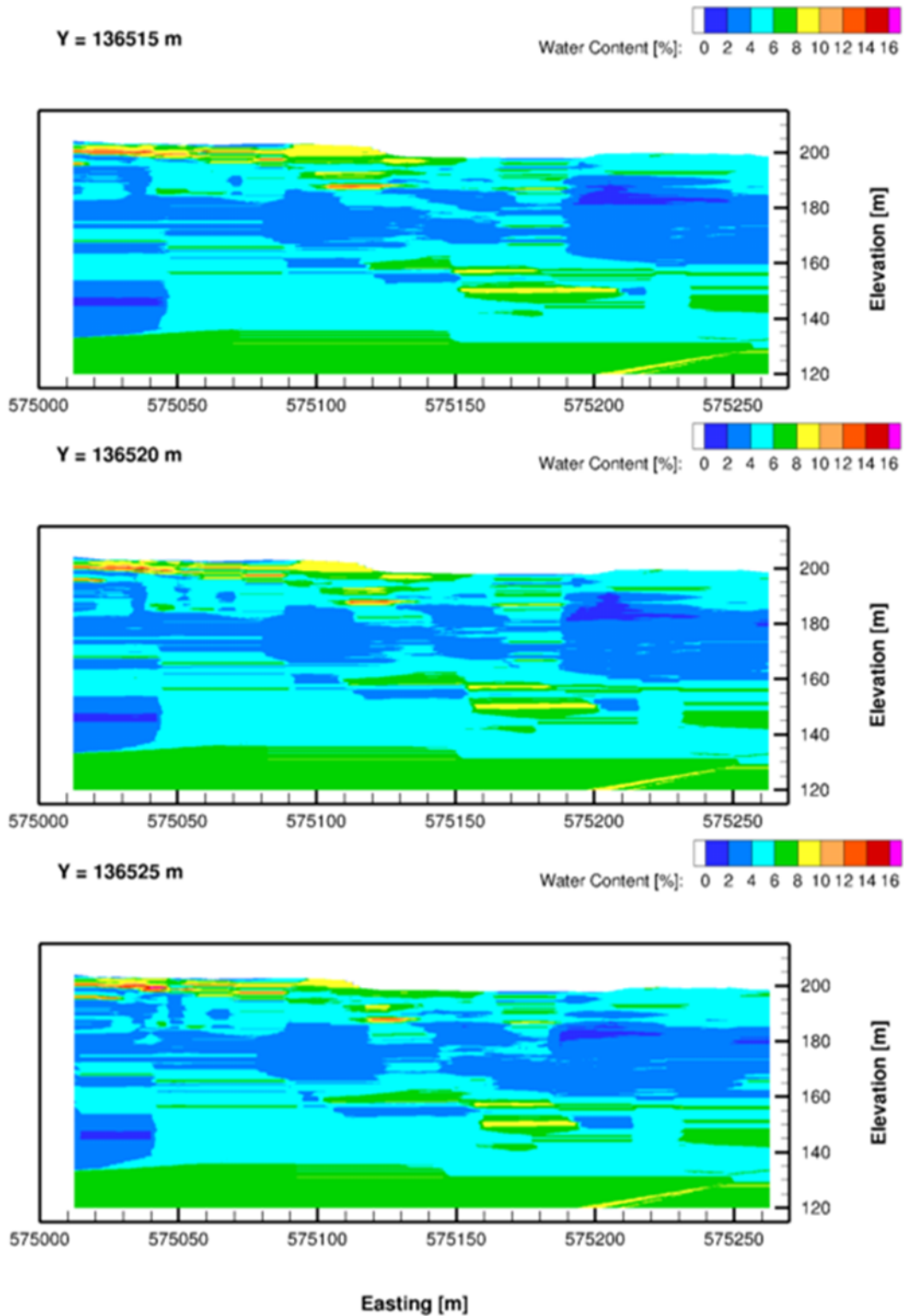


**Figure A.9.** East-west cross sections of kriged water content for northing (Y) coordinates of 136515, 136520, and 136525 m.

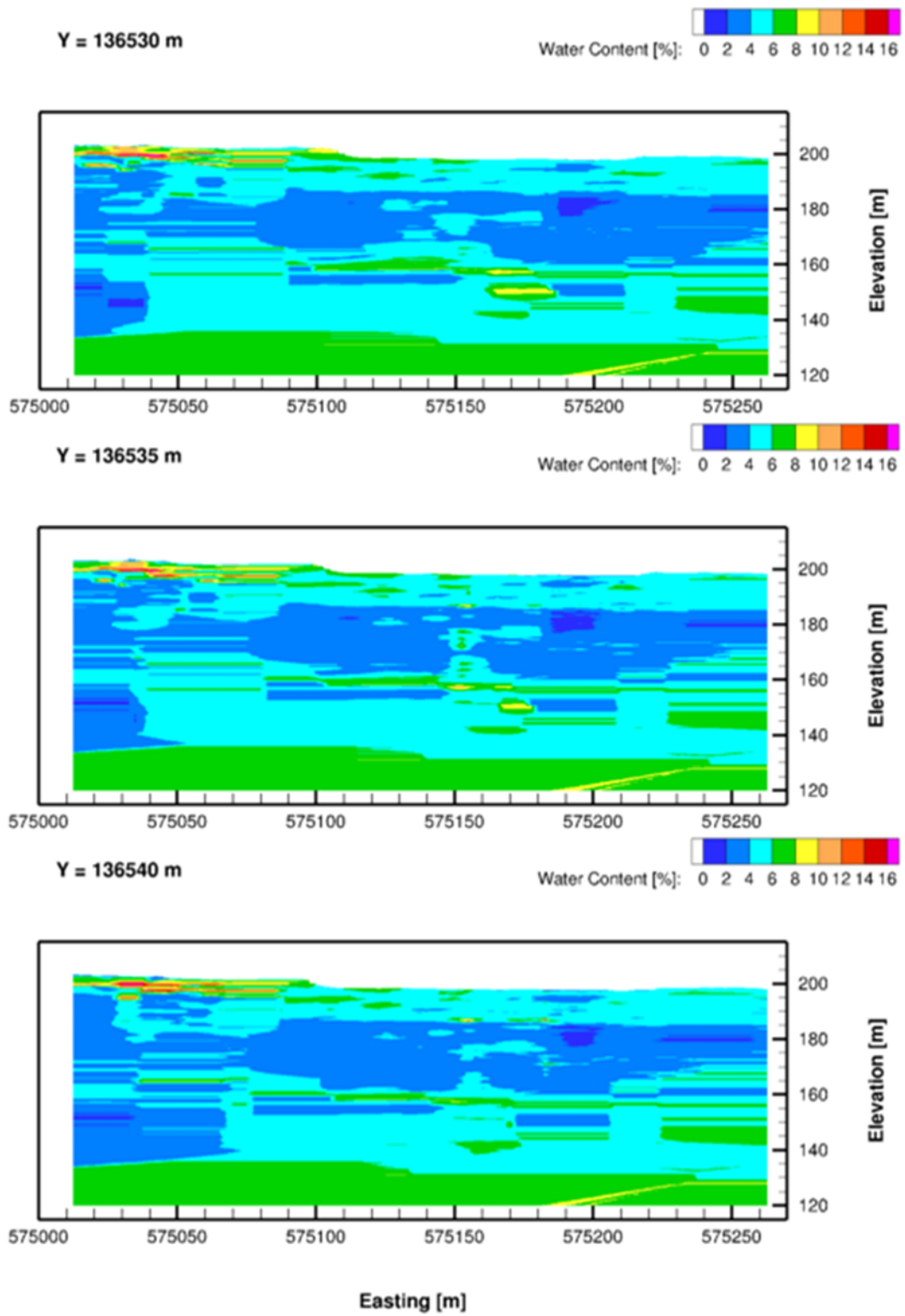


**Figure A.10.** East-west cross sections of kriged water content for northing (Y) coordinates of 136530, 136535, and 136540 m.

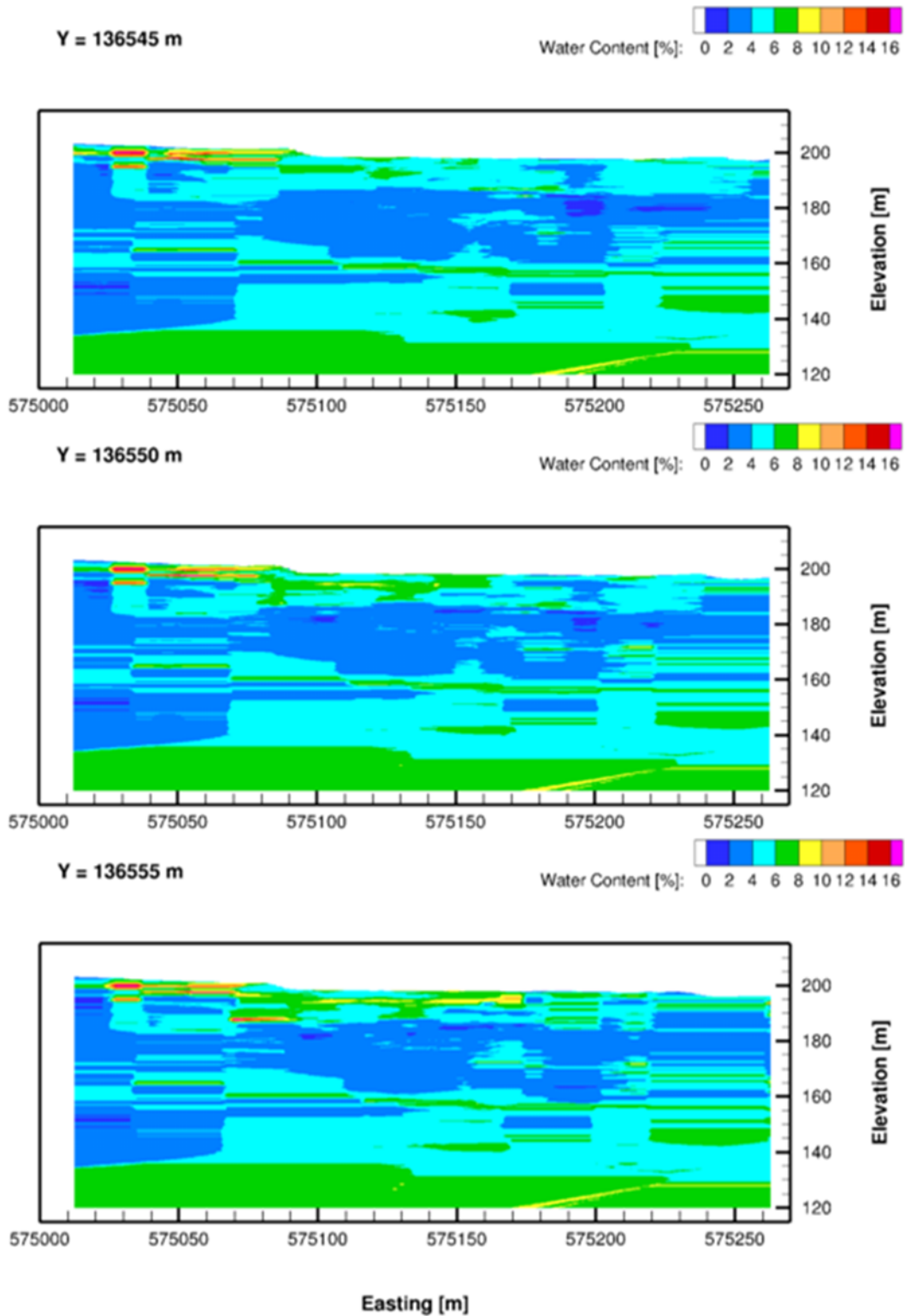


**Figure A.11.** East-west cross sections of kriged water content for northing (Y) coordinates of 136545, 136550, and 136555 m.

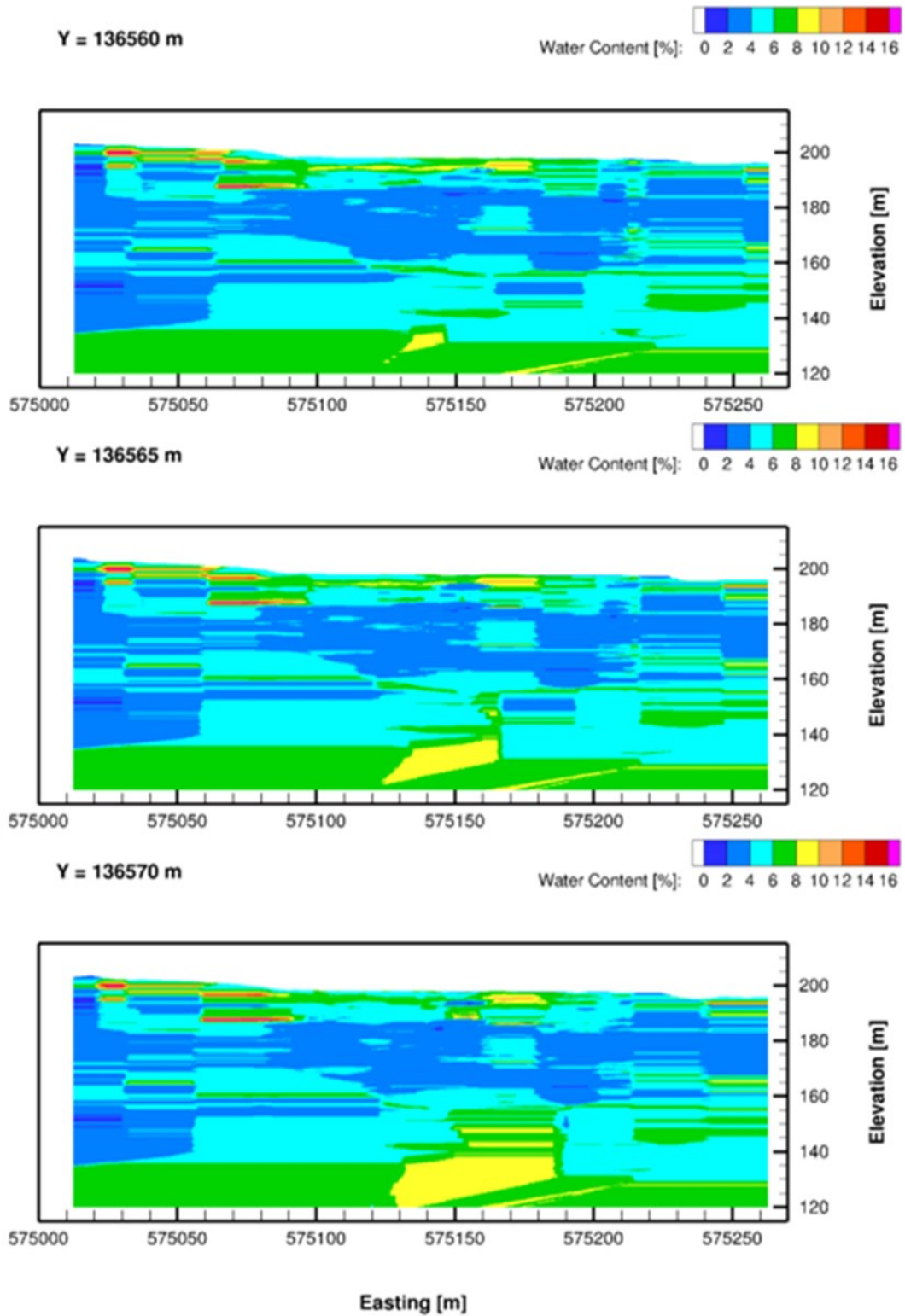


**Figure A.12.** East-west cross sections of kriged water content for northing (Y) coordinates of 136560, 136565, and 136570 m.

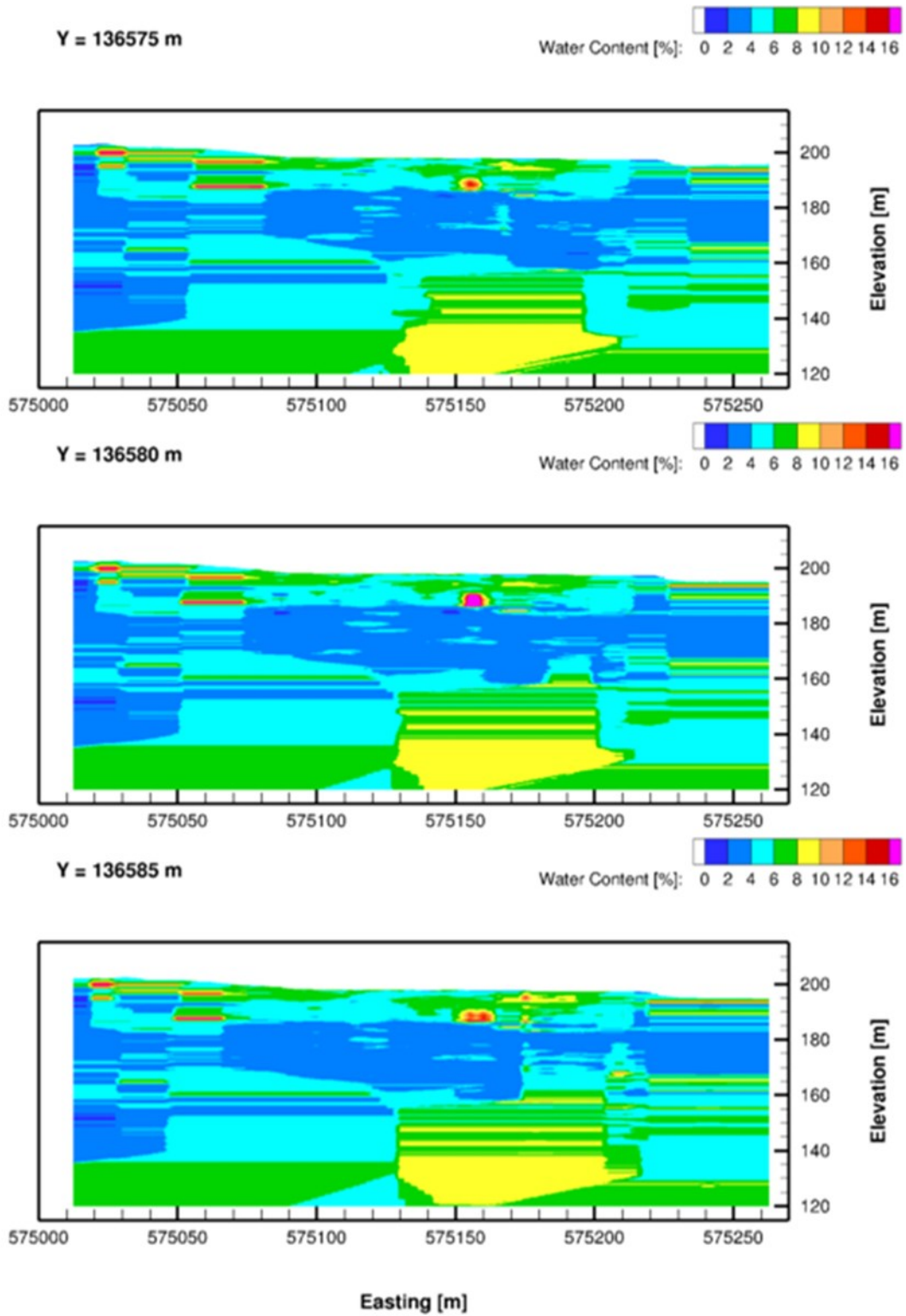


**Figure A.13.** East-west cross sections of kriged water content for northing (Y) coordinates of 136575, 136580, and 136585 m.

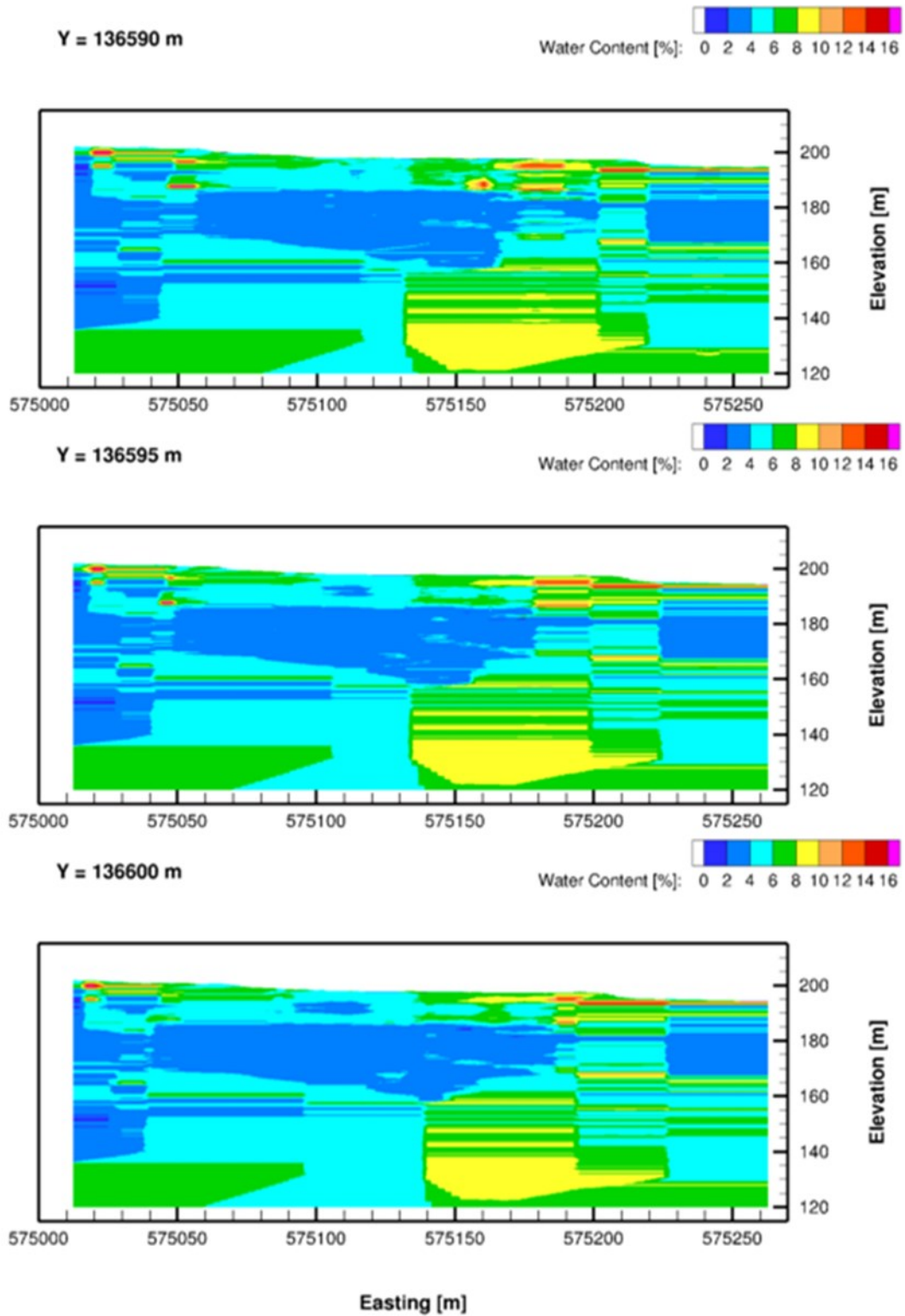


**Figure A.14.** East-west cross sections of kriged water content for northing (Y) coordinates of 136590, 136595, and 136600 m.

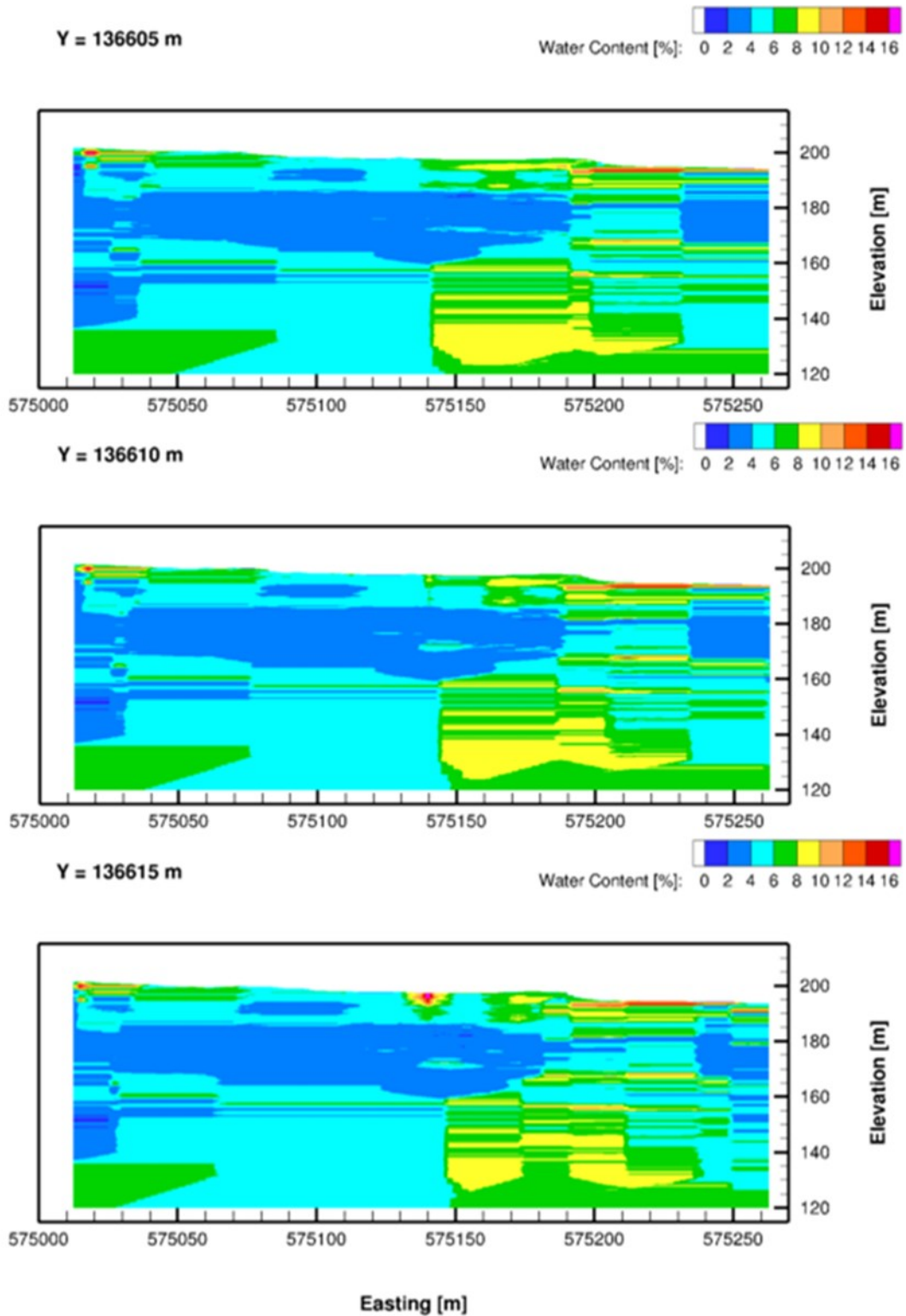


**Figure A.15.** East-west cross sections of kriged water content for northing (Y) coordinates of 136605, 136610, and 136615 m.

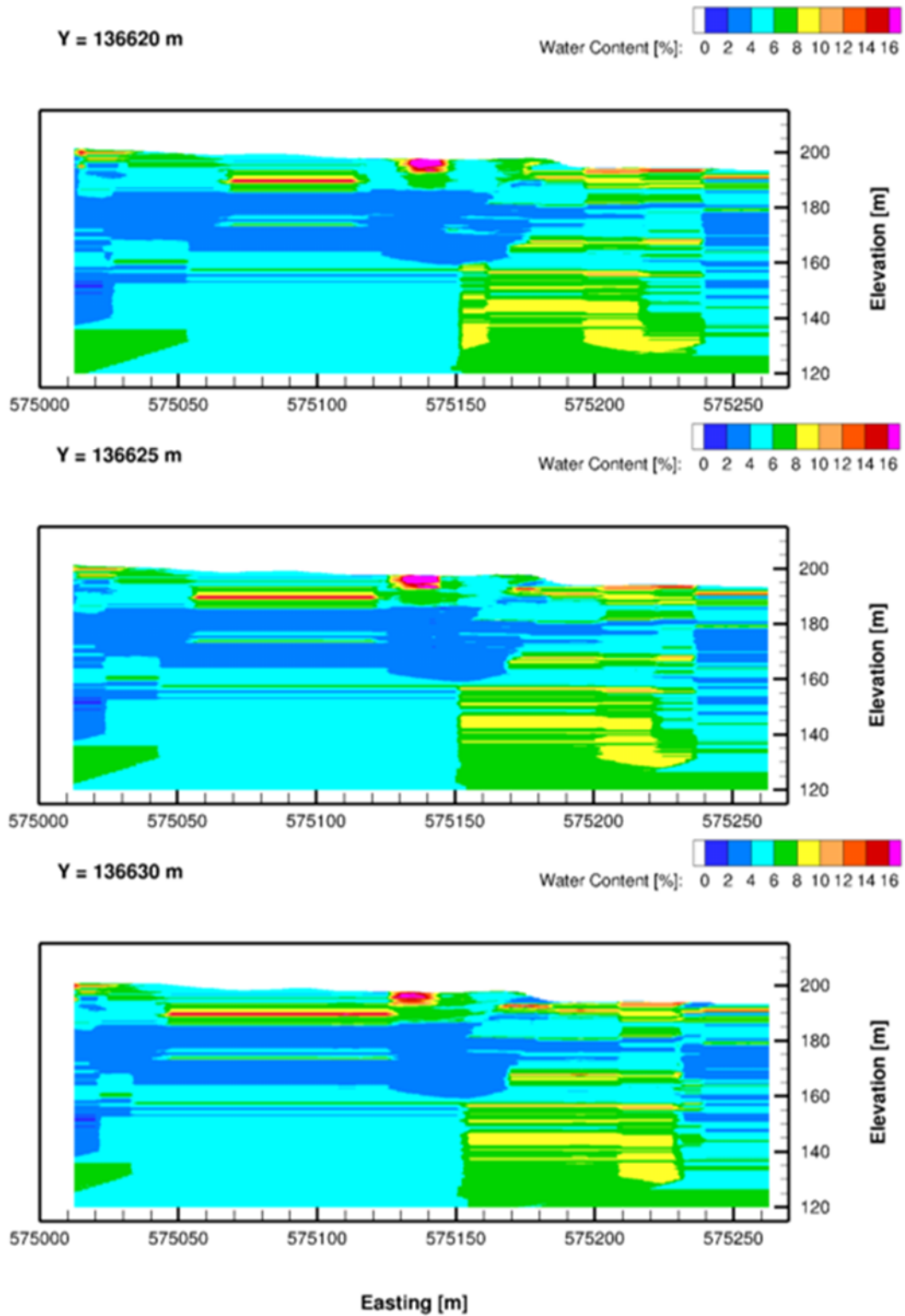


**Figure A.16.** East-west cross sections of kriged water content for northing (Y) coordinates of 136620, 136625, and 136630 m.

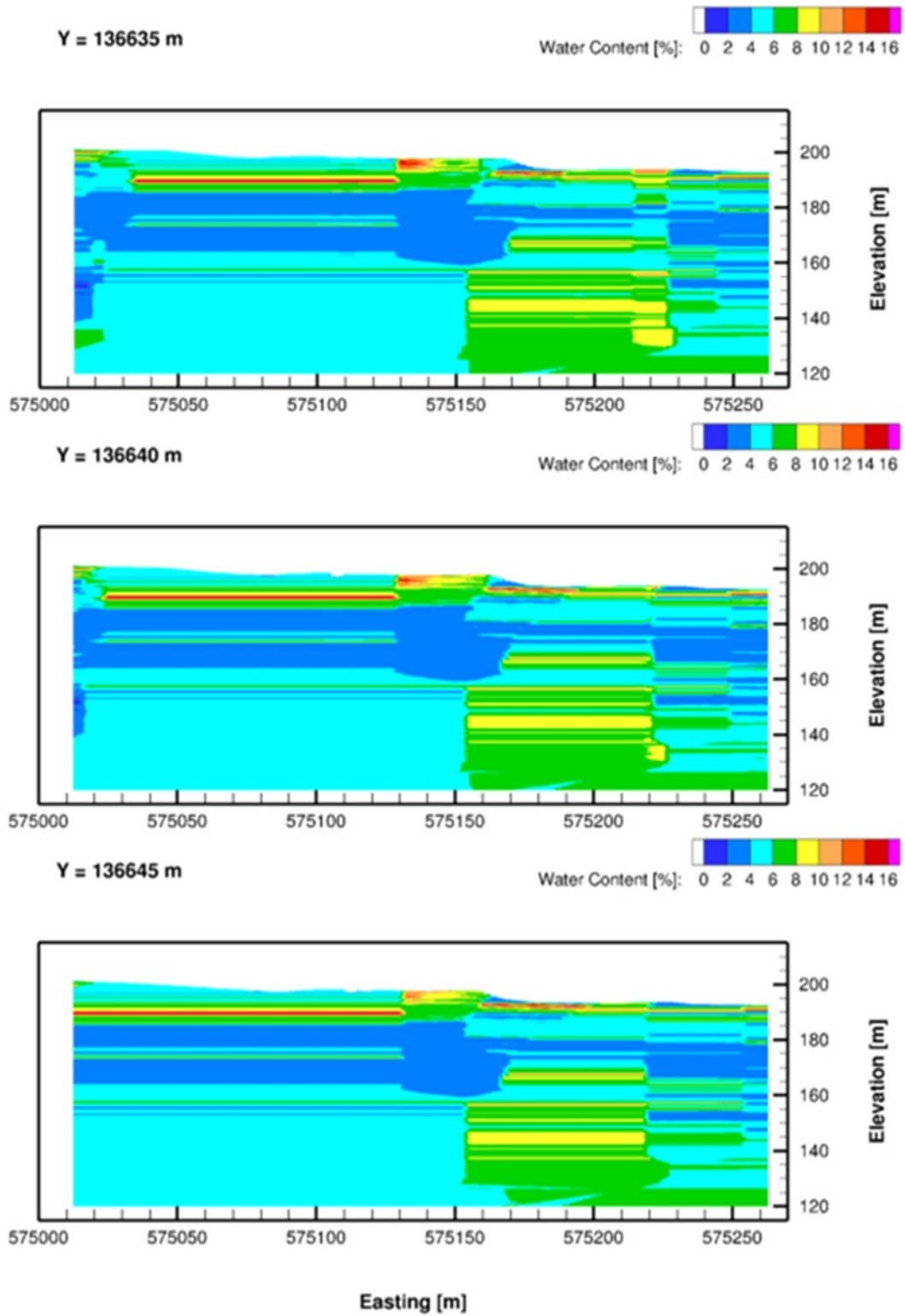


**Figure A.17.** East-west cross sections of kriged water content for northing (Y) coordinates of 136635, 136640, and 136645 m.

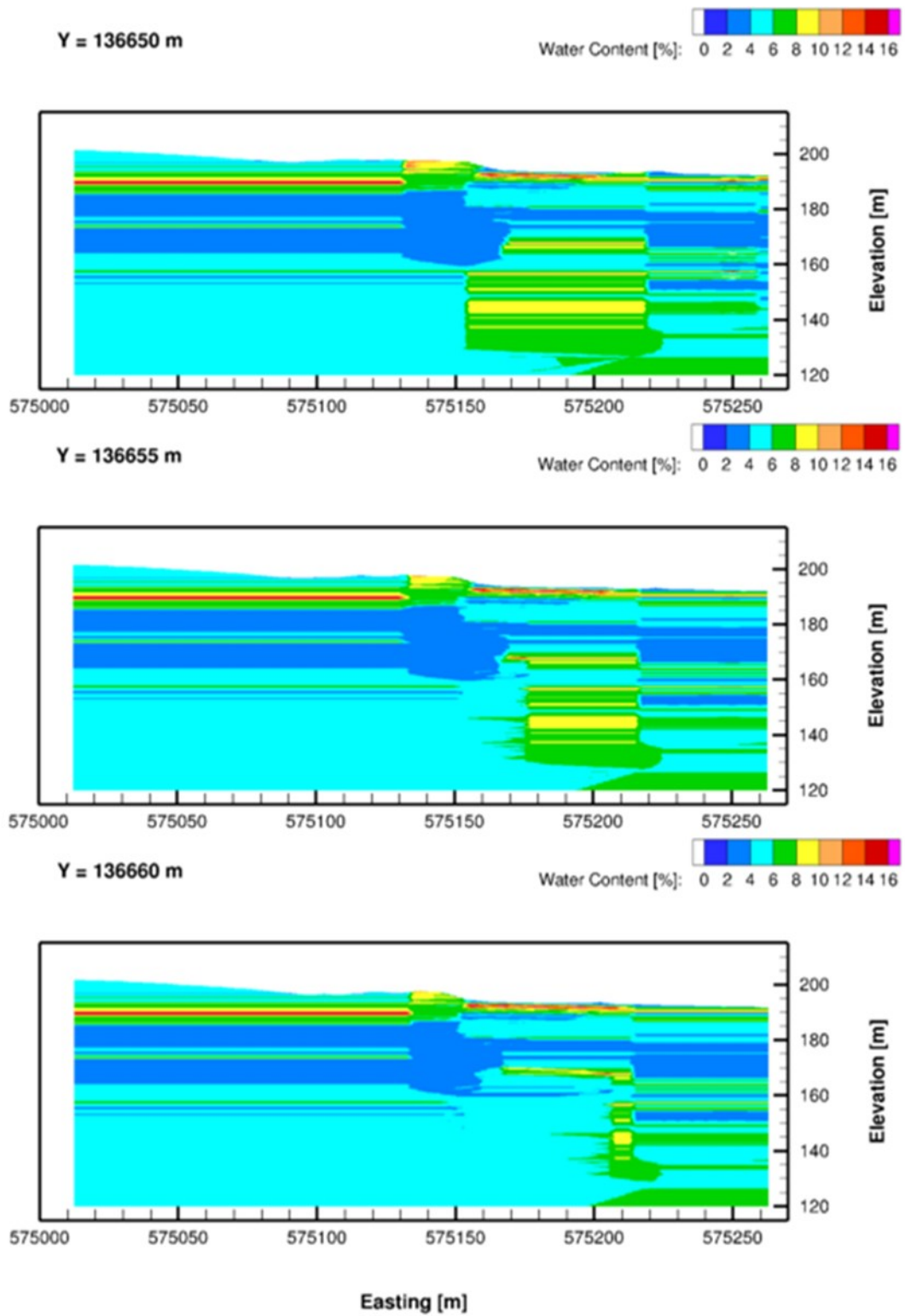


**Figure A.18.** East-west cross sections of kriged water content for northing (Y) coordinates of 136650, 136655, and 136660 m.

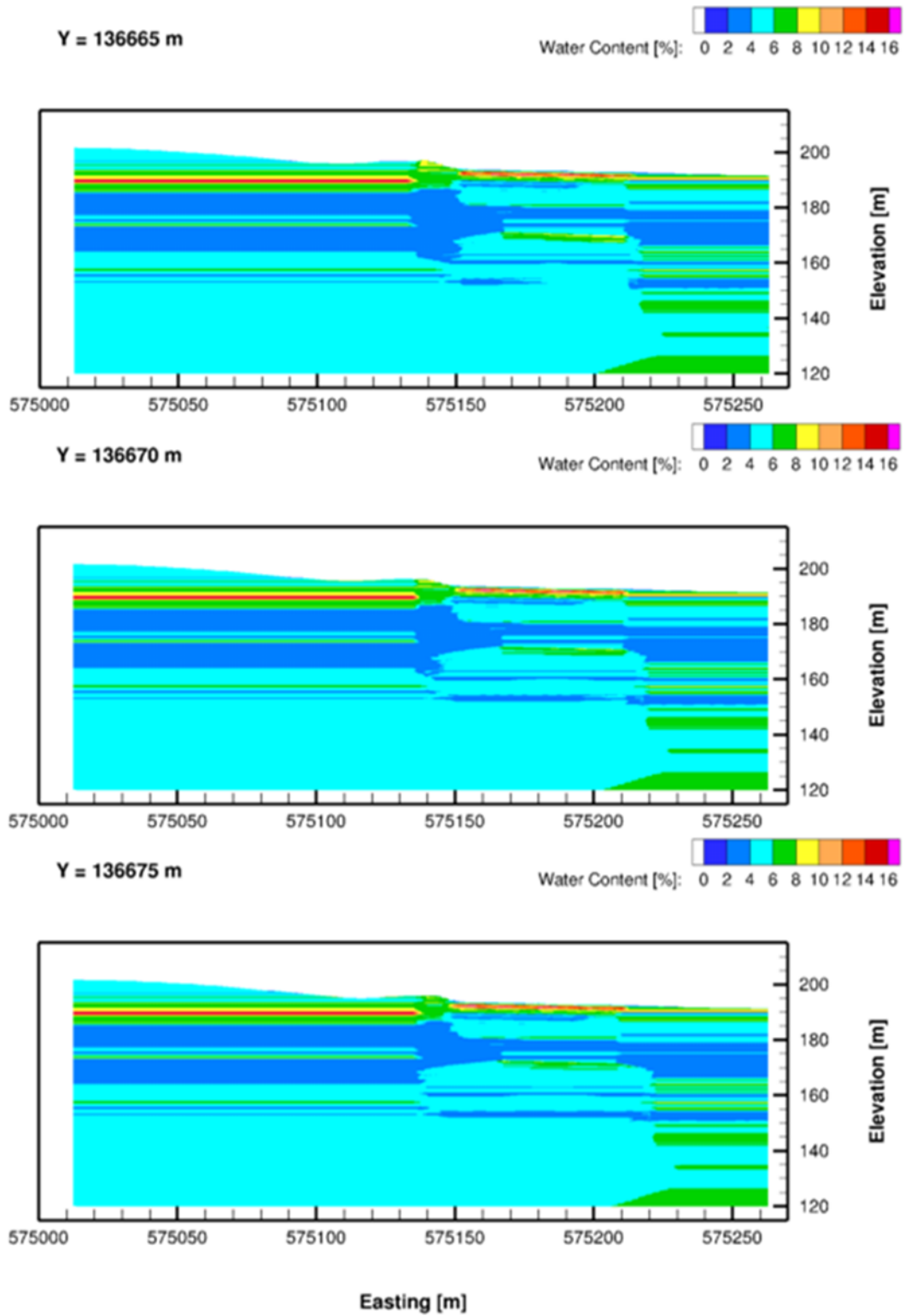


**Figure A.19.** East-west cross sections of kriged water content for northing (Y) coordinates of 136665, 136670, and 136675 m.

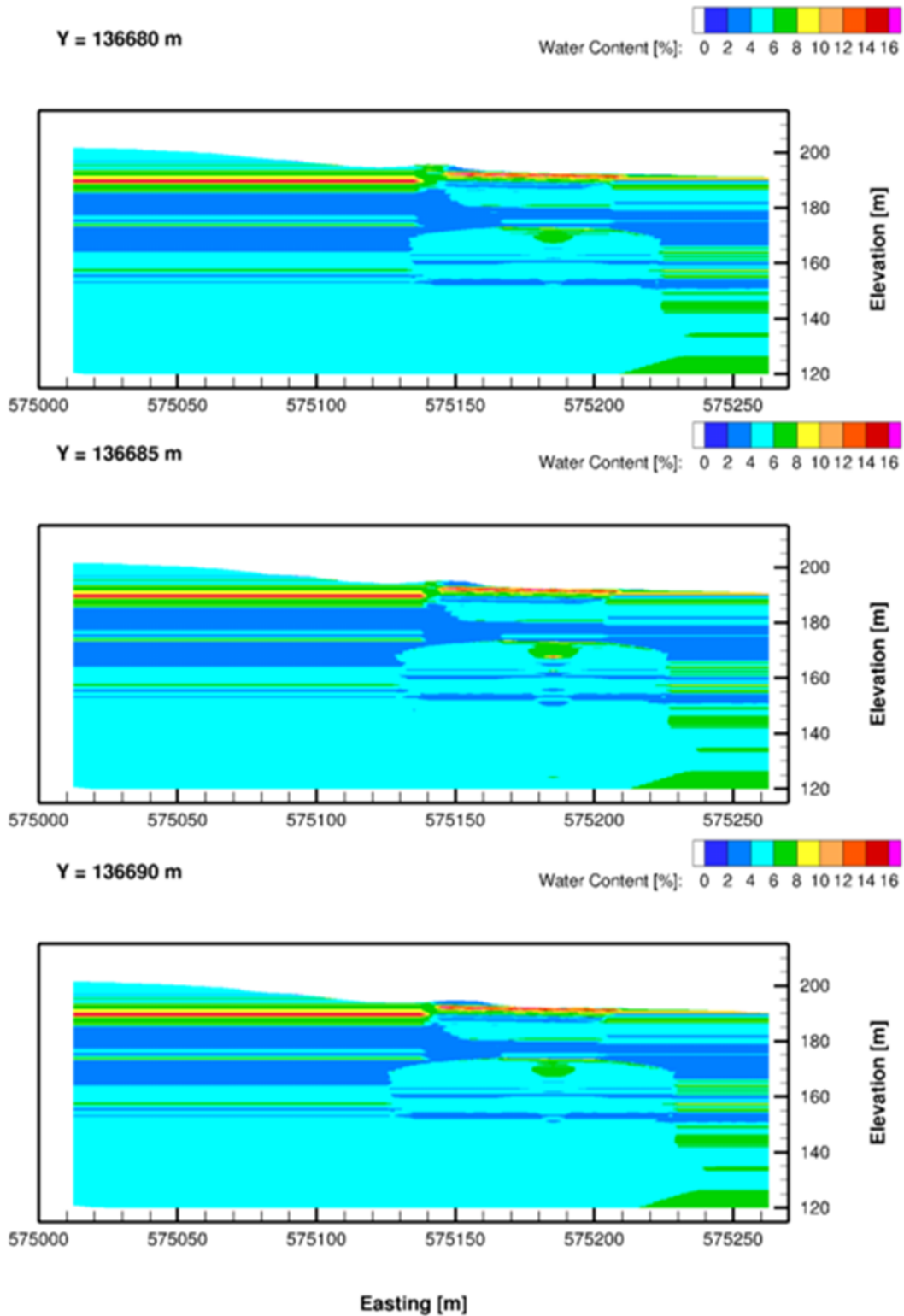


**Figure A.20.** East-west cross sections of kriged water content for northing (Y) coordinates of 136680, 136685, and 136690 m.

**Table A.2.** Selected Boreholes of Volumetric Water Content Data. C6393, C7669 and C7681 are used as source wells for placing pseudo-boreholes.

Well No.	Borehole Name	Easting (m)	Northing (m)	Rotated Easting (m)	Rotated Northing (m)	Bottom Elevation (m)	Top Elevation (m)
1	C4124	575185.13	136685.33	574873.65	136994.65	123.87	167.61
2	C4297	575151.19	136534.78	574956.10	136864.20	138.64	177.96
3	<b>C6393</b>	575119.68	136465.78	574982.62	136793.14	131.48	203.42
4	C6399	575130.10	136478.00	574981.36	136809.16	130.56	202.72
5	C6405	575117.70	136487.80	574965.64	136807.29	129.96	202.88
6	C7465	575211.40	136559.00	574981.53	136923.88	136.10	197.44
7	C7471	575240.60	136588.60	574981.29	136965.49	127.36	194.87
8	C7667	575110.60	136632.30	574858.46	136904.47	130.48	197.99
9	<b>C7669</b>	575188.70	136548.10	574973.20	136900.13	130.13	197.72
10	C7679	575249.30	136650.30	574943.80	137015.27	138.27	192.38
11	<b>C7681</b>	575259.40	136640.50	574957.85	137015.45	125.66	192.56
12	C9359	575407.10	136221.38	575358.68	136823.57	146.74	208.31
13	C9361	575432.93	136185.81	575402.09	136816.67	147.05	208.62
14	C9363	575411.03	136151.67	575410.71	136777.02	147.37	208.94
15	C9365	575378.43	136190.98	575359.89	136781.79	147.02	208.90
16	C9369	575371.06	136087.06	575428.16	136703.09	143.52	205.40
17	C9377	575403.56	136047.56	575479.07	136698.14	143.67	205.54
18	C9381	575363.06	136030.24	575462.69	136657.25	144.73	206.00
19	C9383	575332.63	136087.26	575400.84	136676.05	144.16	205.66

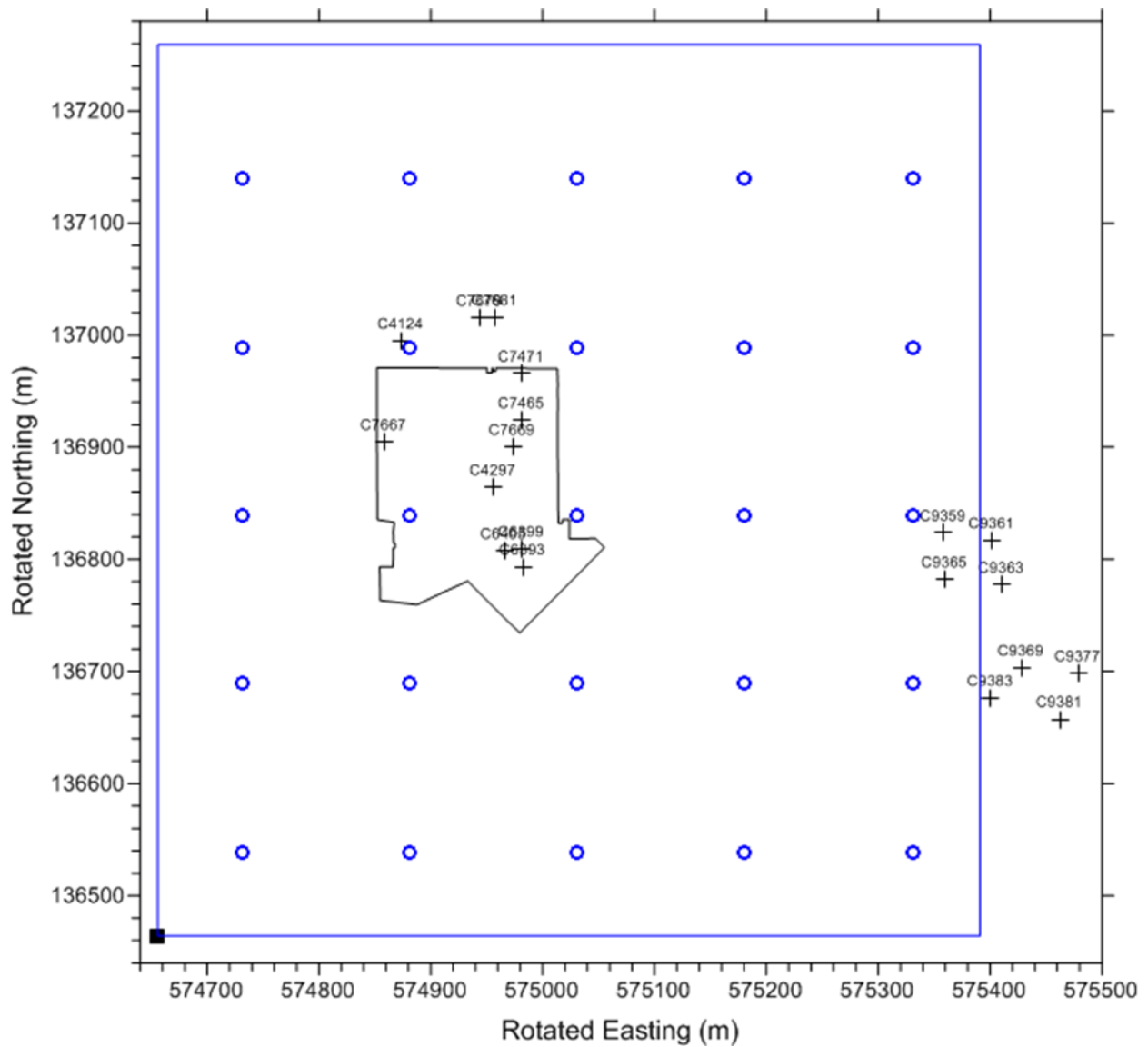


**Figure A.21.** Locations of 19 selected boreholes with volumetric water content data (black crosses) and 25 pseudo-boreholes (blue circles) in rotated coordinates used for STOMP modeling. The blue boundary is the outline of the modeling domain.

**Table A.3.** Locations of pseudo-boreholes and elevation offsets used to conform with surfaces of major geologic units.

	Rotated Easting (m)	Rotated Northing (m)	Easting (m)	Northing (m)	Source Well	Borehole No.	Elevation Offset (m)
1	574731.00	136539.00	574762.06	136464.00	C6393	20	5.59
2	574881.00	136539.00	574868.13	136357.94	C6393	21	5.12
3	575031.00	136539.00	574974.19	136251.88	C6393	22	2.70
4	575181.00	136539.00	575080.25	136145.80	C6393	23	0.19
5	575331.00	136539.00	575186.31	136039.73	C6393	24	-3.01
6	574731.00	136689.00	574868.13	136570.06	C6393	25	3.71
7	574881.00	136689.00	574974.19	136464.00	C6393	26	4.44
8	575031.00	136689.00	575080.25	136357.94	C6393	27	1.38
9	575181.00	136689.00	575186.31	136251.88	C6393	28	-2.31
10	575331.00	136689.00	575292.38	136145.80	C6393	29	-3.43
11	574731.00	136839.00	574974.19	136676.13	C7669	30	15.37
12	574881.00	136839.00	575080.25	136570.06	C7669	31	13.15
13	575031.00	136839.00	575186.31	136464.00	C7669	32	6.16
14	575181.00	136839.00	575292.38	136357.94	C7669	33	12.35
15	575331.00	136839.00	575398.44	136251.88	C7669	34	9.61
16	574731.00	136989.00	575080.25	136782.20	C7681	35	7.87
17	574881.00	136989.00	575186.31	136676.13	C7681	36	-1.16
18	575031.00	136989.00	575292.38	136570.06	C7681	37	1.61
19	575181.00	136989.00	575398.44	136464.00	C7681	38	7.71
20	575331.00	136989.00	575504.50	136357.94	C7681	39	6.70
21	574731.00	137139.00	575186.31	136888.27	C7681	40	5.02
22	574881.00	137139.00	575292.38	136782.20	C7681	41	0.17
23	575031.00	137139.00	575398.44	136676.13	C7681	42	-1.59
24	575181.00	137139.00	575504.50	136570.06	C7681	43	-0.58
25	575331.00	137139.00	575610.63	136464.00	C7681	44	-2.27

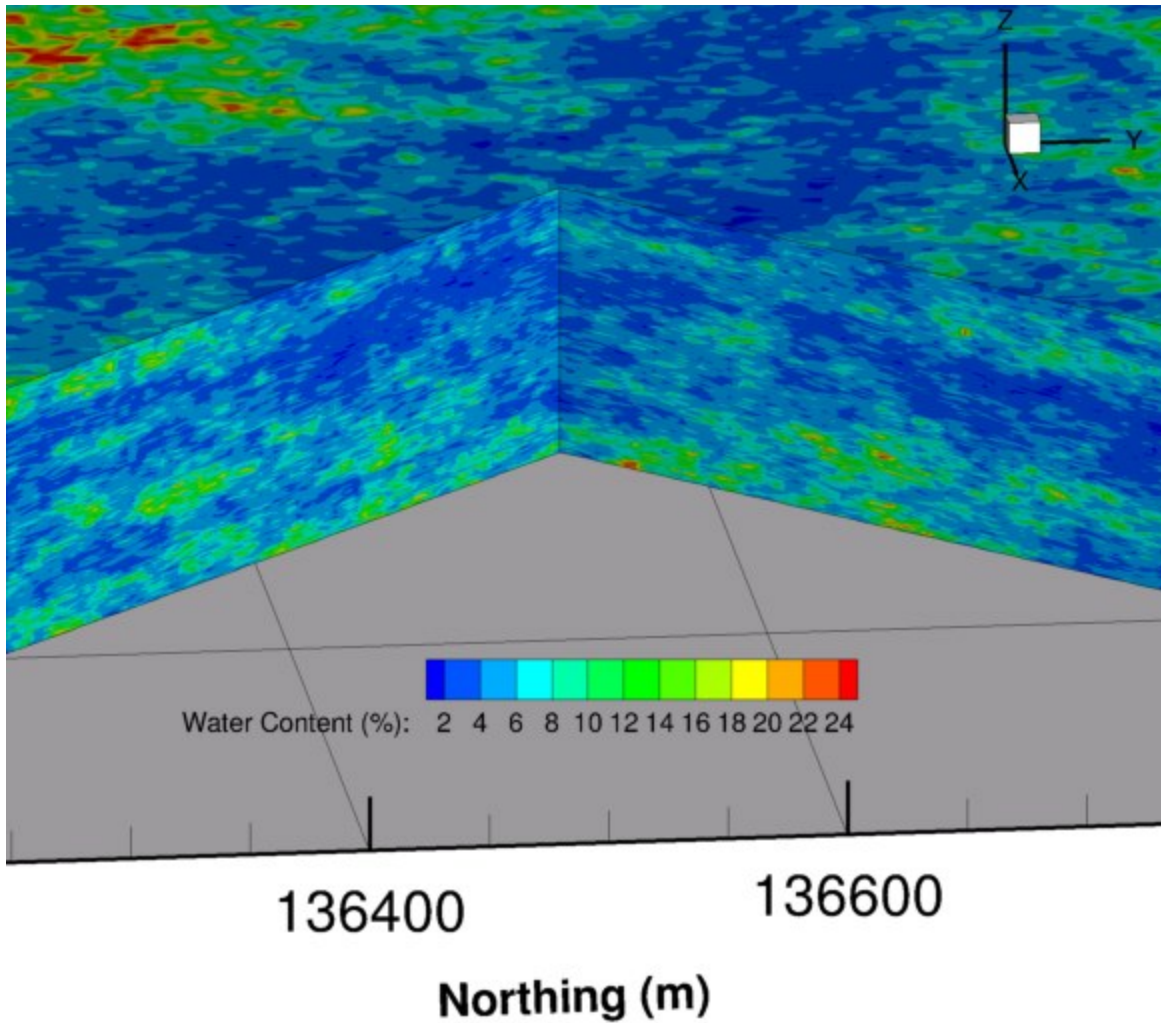


**Figure A.22.** Image showing one realization of stochastic conditional simulation results for water content distribution in WMA C model domain (vertical elevation extent shown is 95-210 m).

## References

Deutsch CV and AG Journel. 1998. *GSLIB – Geostatistical Software Library and User’s Guide*, 2<sup>nd</sup> Ed., Oxford University Press, New York.

Rockhold ML, RE Rossi, and RG Hills. 1996. “Application of Similar Media Scaling and Conditional Simulation for Modeling Water Flow and Tritium Transport at the Las Cruces Trench Site.” *Water Resource Research* 32(3):595-609.

Zhang ZF and R Khaleel. 2007. *Comparison of Models of Saturation-Dependent Anisotropy in Unsaturated Hydraulic Conductivity*. PNNL-16886, Pacific Northwest National Laboratory, Richland, Washington.

## Distribution

**No. of  
Copies**

**No. of  
Copies**

**OFFSITE**

**ONSITE**

**Washington River Protection Solutions**

**Pacific Northwest National Laboratory**

Marcel Bergeron

Yi-Ju Bott  
Mike Fayer  
Vicky Freedman  
Mark Rockhold  
Fred Zhang

\*All distribution will be made electronically.







**Pacific Northwest**  
NATIONAL LABORATORY

*Proudly Operated by **Battelle** Since 1965*

902 Battelle Boulevard  
P.O. Box 999  
Richland, WA 99352  
1-888-375-PNNL (7665)

U.S. DEPARTMENT OF  
**ENERGY**

---

[www.pnnl.gov](http://www.pnnl.gov)